Sunrise Wind Farm Project

Appendix J1
Offshore EMF Assessment

Prepared for:

Sunrise Wind | Powered by Ørsted & Eversource

August 23, 2021

Revision 1 – October 28, 2021

Revision 2 – August 19, 2022

Sunrise Wind

Powered by Ørsted & Eversource

Offshore DC and AC Electric- and Magnetic-Field Assessment

Sunrise Wind Farm Project

Prepared for: Sunrise Wind LLC

Prepared by: Exponent Engineering, P.C.

August 2022

REVISION HISTORY

Date	Revision	Note	Prepared	Reviewed	Approved
9/1/2020	1	Prepared for Orsted & Eversource	Exponent Engineering P.C.		
11/25/2020	2	Prepared for Orsted & Eversource	Exponent Engineering P.C.		
12/10/2020	3	Prepared for Orsted & Eversource	Exponent Engineering P.C.		
6/01/2021	4	Prepared for Orsted & Eversource	Exponent Engineering P.C.		
10/20/2021	5	Prepared for Orsted & Eversource	Exponent Engineering P.C.		
8/12/2022	6	Prepared for Orsted & Eversource	Exponent Engineering P.C.		

Contents

List of Tables

List of Figures

Acronyms and Abbreviations

3D	Three-dimensional
µT	Microtesla
A	Ampere
AC	Alternating current
BOEM	Bureau of Ocean Energy Management
cm/s	Centimeter per second
COP	Construction and Operations Plan
DC	Direct current
EMF	Electric and magnetic fields
Eversource	Eversource Investment LLC
Exponent	Exponent Engineering PC
FEA	Finite element analysis
ft	Feet
ft/s	Feet per second
HDD	Horizontal directional drilling
HVAC	High-voltage alternating current
Hz	Hertz
IAC	Inter-Array Cable (AC)
ICD	Implantable cardioverter defibrillator
ICES	International Committee on Electromagnetic Safety
ICNIRP	International Commission on Non-Ionizing Radiation Protection
IEEE	Institute of Electrical and Electronics Engineers
km	Kilometer
kV	Kilovolt
kV/m	Kilovolt per meter
Lease Area	Renewable Energy Lease Area OCS–0487
m	Meter
MRE	Marine Renewable Energy
mi	Mile
mG	Milligauss
mm	Millimeter
m/s	Meters per second
mT	Millitesla
mV/m	Millivolts per meter
MW	Megawatt
nT	Nanotesla
nV/cm	Nanovolts per centimeter
nV/m	Nanovolts per meter
NY	New York
NYSERDA	New York State Energy and Research Development Authority
NYSPSC	New York State Public Service Commission
OCS–DC	Offshore Converter Station (AC→DC conversion)
OD	Outer diameter
OnCS–DC	Onshore Converter Station (DC→AC conversion)
Orsted NA	Orsted North America, Inc.
OREC	Offshore Wind Renewable Energy Certificate
PDE	Project design envelope
Project	Sunrise Wind Farm Project
ROW	Right of way
SRWEC	Sunrise Wind Export Cable (DC)
SRWF	Sunrise Wind Farm
Sunrise Wind	Sunrise Wind LLC
T	Tesla
TJB	Transition joint bay

TRC	TRC Environmental Corporation
WHO	World Health Organization
WTG	Wind turbine generator

Limitations

At the request of TRC Environmental Corporation (TRC) and Sunrise Wind LLC (Sunrise Wind), Exponent Engineering PC (Exponent) calculated the alternating current and direct current magnetic fields and induced electric fields associated with the operation of the submarine cables proposed for the Sunrise Wind Offshore Wind Farm Project (the Project).

This report summarizes the analysis performed to date and presents the findings resulting from that work. In the analysis, we have relied on cable design geometry, usage, specifications, and various other types of information provided by TRC and Sunrise Wind. We cannot verify the correctness of this input data and rely on TRC and Sunrise Wind for the data's accuracy. Although Exponent has exercised usual and customary care in the conduct of this analysis, the responsibility for the design and operation of the Project remains fully with the client. TRC has confirmed to Exponent that the data contained herein are not subject to Critical Energy Infrastructure Information restrictions.

The analyses presented herein are made to a reasonable degree of engineering and scientific certainty. Exponent reserves the right to supplement this report and to expand or modify opinions based on review of additional material as it becomes available, through any additional work, or review of additional work performed by others.

The scope of services performed during this investigation may not adequately address the needs of other users of this report, and any re-use of this report or its findings, conclusions, or recommendations presented herein for purposes other than for project permitting are at the sole risk of the user. The opinions and comments formulated during this assessment are based on observations and information available at the time of the investigation. No guarantee or warranty as to future life or performance of any reviewed condition is expressed or implied.

Benjamin R.T. Cotts, Ph.D., P.E. (Licensed Electrical Engineer, New York, #103209), employed by Exponent, performed and reviewed calculations of the electric and magnetic fields associated with the operation of the proposed Project.

_____

Benjamin Cotts, Ph.D., P.E.

Executive Summary

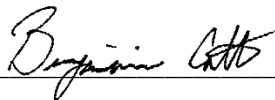At the request of TRC Environmental Corporation (TRC) and Sunrise Wind LLC (Sunrise Wind), Exponent calculated the magnetic fields and induced electric fields associated with the operation of the submarine cables proposed to convey electricity generated by the Sunrise Wind Offshore Wind Farm Project (the Project).

The alternating current (AC) electricity generated by individual wind turbine generators (WTG) will flow on Inter-Array Cables (IAC) buried below the seabed to an Offshore Converter Station (OCS–DC). The AC electricity carried over the IAC will produce AC magnetic fields and AC electric fields induced in the seawater above these cables. The AC fields from these cables are calculated to be lower than reported thresholds for effects on the behavior of local magnetosensitive fish and below detection thresholds of local electrosensitive fish.

Electricity transmitted by the IACs is converted from AC to DC at the OCS–DC. The Sunrise Wind Export Cable (SRWEC) is designed to carry electricity as direct current (DC) from the OCS–DC to shore. The SRWEC will be a source of a static magnetic field that will modify the ambient static geomagnetic field, and very weak electric fields will be caused by the movement of electric charges in a static magnetic field around the cable. At peak loading, the magnetic fields produced by the DC cables at the overlying seabed are projected to be well below the levels detectable by finfish, and slightly above levels documented to elicit minor changes in the behaviors of crustaceans and elasmobranchs. Similarly, electric fields associated with DC cables at peak loading are expected to be detectable by elasmobranchs, but based on available field studies, will not result in adverse effects to species.

At foundations and where the cables are covered with protective concrete mattresses or rock, the physical structures of those elements are expected to attract some species to this habitat (i.e., a reef effect) and as a result these species will spend a relatively greater period at these structures than over buried cables. The assessment at these structures therefore focused on the potential for extended exposure to magnetic fields and induced electric fields to cause harmful biologic effects. Neither exposures to AC nor DC magnetic fields from the Project at these structures were found to harm fish. This conclusion is supported by the 2020 comprehensive review by the US Pacific Northwest National Laboratory of the ecological impacts of Marine Renewable Energy development, which concluded that *"the ecological impacts of EMFs … are likely to be limited, and marine animals living in the vicinity of MRE [Marine Renewable Energy] devices and export cables are not likely to be harmed by emitted EMFs".* (Copping et al., 2020). This conclusion also is supported by years of biological surveys conducted at wind farm sites, the result of which indicate that their presence does not reduce the abundance or diversity of marine species in the region.

Note that this Executive Summary does not contain all of Exponent's technical evaluations, analyses, conclusions, and recommendations. Hence, the main body of this report is at all times the controlling document.

1.0   Introduction

1.1 Project Description

Sunrise Wind LLC (Sunrise Wind), a 50/50 joint venture between Orsted North America Inc. (Orsted NA) and Eversource Investment LLC (Eversource), proposes to construct, own, and operate the Sunrise Wind Farm Project (the Project). The wind farm portion of the Project (i.e., the SRWF) will be located on the Outer Continental Shelf in the designated Bureau of Ocean Energy Management (BOEM) Renewable Energy Lease Area OCS-A 0487 (Lease Area)[1]. The Lease Area is approximately 18.9 statute miles (mi) (16.4 nautical miles [nm], 30.4 kilometers [km]) south of Martha's Vineyard, Massachusetts, approximately 30 mi (26.1 nm, 48.2 km) east of Montauk, New York (NY), and 16.7 mi (14.5 mi, 26.8 km) from Block Island, Rhode Island. The Lease Area contains portions of areas that were originally awarded through the BOEM competitive renewable energy lease auctions of the Wind Energy Areas (WEAs) off the shores of Rhode Island and Massachusetts. Components of the Project will be located in federal waters on the Outer Continental Shelf, in state waters of New York, and onshore in the Town of Brookhaven, Long Island, NY. The proposed interconnection location for the Project is the Holbrook Substation, which is owned and operated by Long Island Power Authority (LIPA). Sunrise Wind has a contract with the New York State Energy Research and Development Authority (NYSERDA) for a 25-year Offshore Wind Renewable Energy Certificate (OREC) Agreement in October 2019.

The Project involves the use of a direct current (DC) export cable to transmit power to shore as well as alternating current (AC) inter-array cables (IAC) interconnecting wind turbine generators (WTGs) and connecting WTGs to the offshore converter station (OCS–DC). Offshore project infrastructure includes:

- up to 94 wind turbine generators (WTGs) at 102 potential positions;

- up to 180 mi (290 km) of (66-kilovolt [kV]) Inter-Array Cables (IAC);

- one Offshore Converter Station (OCS–DC); and

- one DC submarine export cable bundle (SRWEC) comprised of two cables (±320 kV) located within an up to 104.6-mi (168.4-km)-long corridor.

    o Along the majority of the route traversed by the export cable the bundle will be buried beneath the seabed to a minimum target burial depth of 3.3 ft (1 m) and 6 ft (1.8 m) in New York State waters.

    o Near landfall, the export cable bundle will be installed in a bore hole at depths between 46 ft (14 m), and 6 ft (1.8 m) by horizontal directional drilling (HDD).[2]

The WTGs, OCS–DC, and IAC are collectively referred to as the Sunrise Wind Farm (SRWF). Figure 1 provides the proposed location of the SRWF and SRWEC.

---

[1] A portion of Lease Area OCS-A 0500 (Bay State Wind LLC) and the entirety of Lease Area OCS-A 0487 (formerly Deepwater Wind New England LLC) were assigned to Sunrise Wind LLC on September 3, 2020, and the two areas were merged and a revised Lease OCS-A 0487 was issued on March 15, 2021. Thus, when using the term *"Lease Area"* within this COP, Sunrise Wind is referring to the new merged Lease Area OCS-A 0487.

[2] For a distance of up to approximately 3,200 ft (975 m), each of the two DC cables of the SRWEC will be placed within separate 16-inch conduits and placed together within a single 55-inch bore hole installed by HDD.
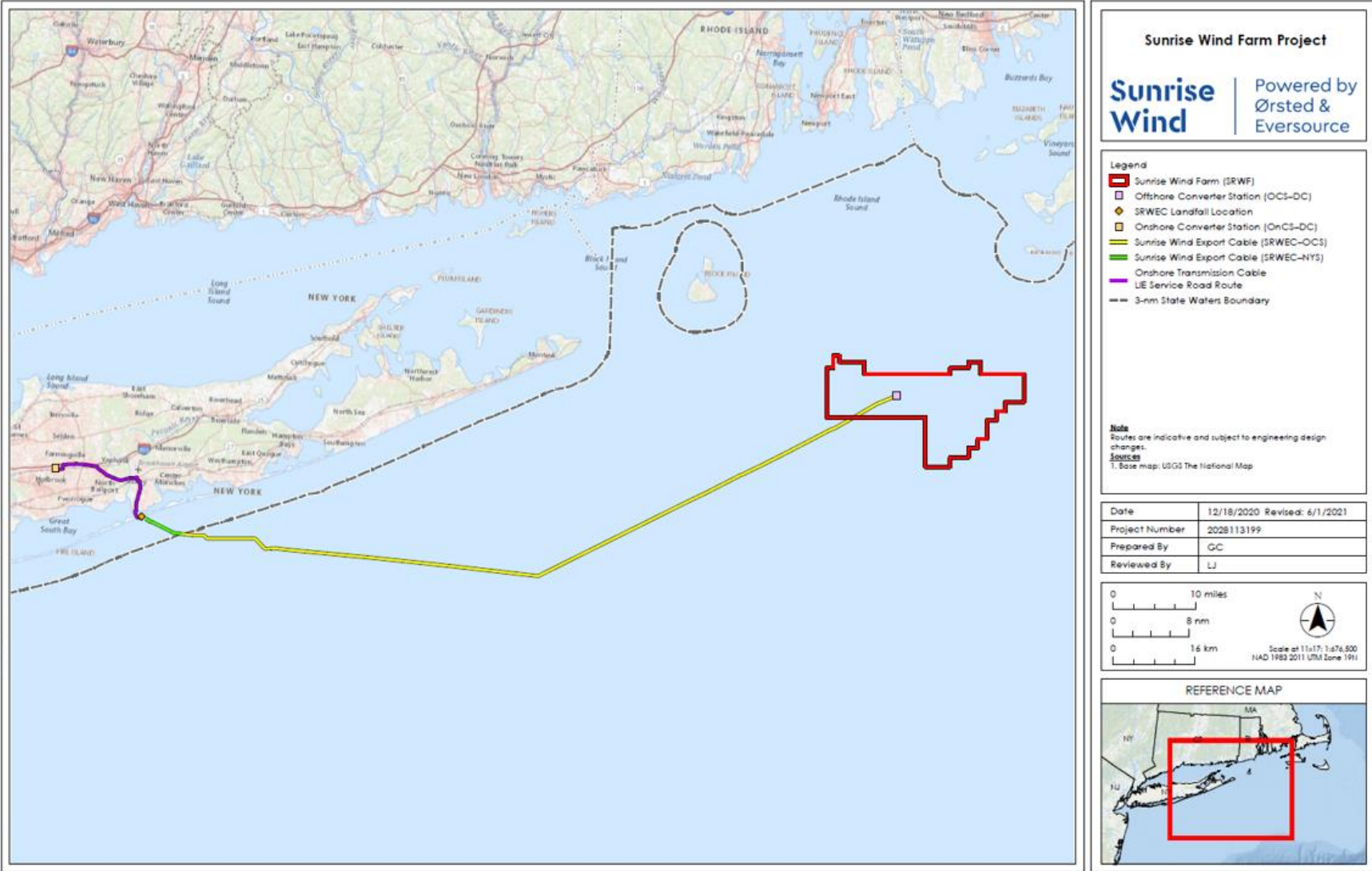
Figure 1.   Overview of the proposed SRWF and SRWEC route.

AC electricity generated by the WTGs will be carried by IACs to the OCS–DC where the voltage will be increased and converted from AC to DC. A pair of SRWEC cables (bundled together) will transfer power to shore; one cable will have positive polarity and the other will have negative polarity, much like the cables from a car battery. At landfall, the SRWEC will be installed via horizontal directional drilling (HDD) to a transition joint bay (TJB) within the Landfall Work Area and subsequently connected to an onshore converter station (OnCS–DC) via underground duct banks.

Each of the electrical elements for the Project, including the IAC and SRWEC—where buried, or protected by concrete mattresses or rock berms, and at the WTGs and OCS–DC—will be sources of magnetic fields and induced electric fields. This report summarizes the 60-Hertz (Hz) magnetic fields and induced 60-Hz electric fields associated with the AC cables and the 0-Hz (i.e., static) magnetic fields associated with the DC cables in the offshore portion of the proposed SRWEC route, as well as at representative structure foundations.

A range of offshore Project designs are being considered to allow for assessments of proposed activities and the flexibility to make development decisions prior to construction. The Project design envelope (PDE) includes several scenarios for which electric and magnetic fields associated with offshore Project infrastructure were evaluated. This offshore electric- and magnetic-field DC and AC assessment for the Project considers the information available at this time; the precise locations and specifications of offshore infrastructure may be subject to change as the engineering design progresses.

The assessment of magnetic fields associated with the Onshore Transmission Cables between the end of the HDD installation and the new OnCS–DC is provided in the companion report titled *Onshore DC and AC Magnetic-Field Assessment* (Exponent, 2022).

1.2 Magnetic Fields and Induced Electric Fields

Magnetic fields are associated with electricity flowing through the submarine cables and are reported as magnetic flux density in units of milligauss (mG), where 1 Gauss is equal to 1,000 mG. Magnetic fields also may be reported as microtesla (µT), where 1 mG is equal to 0.1 µT. Each of the electrical elements for the Project, including the offshore IAC connecting to each WTG or OCS–DC, and the SRWEC, will be sources of magnetic fields. Both humans and marine life may respond differently to AC or DC magnetic and electric fields. As such, both the DC and AC fields were modeled and assessed.

The Earth's natural geomagnetic field (used for compass navigation) is ubiquitous everywhere on earth, including the marine environment. The earth's geomagnetic field is a static (i.e., DC) magnetic field, meaning that it does not vary substantially in strength or direction with time. The DC magnetic field generated by the SRWEC will combine via vector addition with the geomagnetic field, i.e., the DC field from the SRWEC may affect both the magnitude and direction of the local DC field near to the cable. The AC IACs associated with the Project also will produce magnetic fields due to the flow of electric charge along the cables, but instead of being constant with time, the AC magnetic field associated with the Project's AC IACs will change strength and direction in a continuous cycle that repeats 60 times each second (i.e., a frequency of 60 Hz).

While an electric field is created by the voltage applied to the conductors inside the cable, it is entirely shielded from the marine environment by grounded metallic sheaths and steel armoring around the cable (Snyder et al., 2019). The AC magnetic field will induce a weak electric field in the seawater around the AC cables and in nearby marine species. AC magnetic fields from the IACs with a frequency of 60 Hz will induce 60-Hz AC electric fields in the surrounding seawater and organisms. No such induction occurs for DC magnetic fields; a static electric field is only produced when electric charges (such as in ocean currents or marine species) *move* through a DC magnetic field. Electric fields in the marine environment are measured in units of millivolts per meter (mV/m).

The magnetic fields and induced electric fields around the conductors will vary depending on the magnitude of the electrical current—expressed in units of amperes (A)—that flows through the cables. Since current on the conductors will vary with varying power generation (dependent upon the speed of the wind and operational status), measurements or calculations of these fields represent only a snapshot of conditions at one moment in time. On a given day, throughout a week, or over the course of months or years, the magnetic- and induced electric-field levels will also vary. To account for this variability, calculations were performed for annual average load and peak load generated by the Project, which will produce the average and maximum field levels expected for the proposed Project.

1.3 Human Exposure to EMF

1.3.1 Human Exposure to DC Magnetic Fields

While there are no federal standards for magnetic fields produced by DC transmission lines, the International Commission on Non-Ionizing Radiation Protection (ICNIRP) recommends a limit of 4,000,000 mG for general public exposure (ICNIRP 2009). For individuals with implanted medical devices, the standard from the Association for the Advancement of Medical Instrumentation (ISO/ANSI/AAMI 14117:2019) specifies that pacemaker and Implantable cardioverter defibrillator (ICD) functions should not be affected when exposed to DC magnetic fields less than 10,000 mG. Exposure of these devices to magnetic fields up to 500,000 mG should not affect functions after discontinuation of exposure (ISO 2019).

1.3.2 Human Exposure to AC EMF

While land-based exposure to AC electric and magnetic fields from transmission line and distribution lines, and AC devices is relatively common, marine-based submarine cables provide very limited opportunities for persons to come in close proximity to them, although limited exposure is possible for those who may be scuba diving at the seabed directly over the cables[3] or around structure foundations.

The World Health Organization (WHO) recommends that countries follow limits on human exposure to electric and magnetic fields, such as those developed by two international organizations—the International Committee on Electromagnetic Safety (ICES) and the ICNIRP. ICES operates *"under the rules and oversight of the Institute of Electrical and Electronics Engineers (IEEE) Standards Association Board,"* and developed an exposure reference level limit to 60-Hz magnetic fields of 9,040 mG for the general public (ICES 2019). ICNIRP, an independent organization that is an officially recognized collaborator of the WHO, provides scientific advice and guidance on the health and environmental effects of non-ionizing radiation to the WHO, other agencies, and the public. ICNIRP has recommended a reference level limit of 2,000 mG for whole-body exposure to 60-Hz magnetic fields (ICNIRP 2010). These limits are the result of extensive review and evaluation of relevant research of health and safety issues, and the limits they propose are designed to protect the health and safety of persons in an occupational setting and for the general public. The limits for both ICES and ICNIRP for electric-field exposure are roughly one million times higher than those expected from induced electric fields in the marine environment, so human exposure to electric fields is not addressed further. The European Committee for Electrotechnical Standardization recommends not-to-exceed reference levels of 5 kilovolts per meter (kV/m) for AC electric fields and 1,000 mG for AC magnetic fields (CENELEC 50527-1:2010).

---

[3]   Near shore, the SRWEC cables will be installed via HDD, far below the seabed or beach. As a result, magnetic-field levels near shore will be very low.

1.4 Exposure of Marine Species to EMF

Both magnetic fields and associated electric fields from submarine cables are of environmental and ecological interest because research shows that some marine species have specialized sensory receptors that are capable of detecting magnetic fields or associated electric fields, or both, in the natural environment (e.g., Gill et al., 2009; Hellinger and Hoffmann, 2012; Hutchison et al., 2018, 2020; Klimley ,1993; Lohmann et al., 1995; Normandeau et al., 2011; Taylor, 1986). Generally, marine organisms detect fields that are within a very limited frequency range, which includes the earth's geomagnetic field (i.e., a frequency of ~0 Hz), the near 0-Hz induced electric fields produced by ocean currents and fish movement in the earth's geomagnetic field, and the electric fields produced by biological processes of fish with frequencies from 0 Hz to about 10 Hz (Bedore and Kajiura 2013; Snyder et al., 2019).

1.4.1 Marine Assessment Approach

The evaluation approach uses information regarding the types of marine species within the SRWF and SRWEC and the likelihood of exposure to electric and magnetic fields (EMF) from the cable. These site-specific data were assessed in conjunction with the sensitivity of marine species to EMF reported in the scientific literature (field and laboratory studies) and calculations of the EMF levels produced by the Project cables. The evaluation of EMF exposure of marine species was assessed for the various cable configurations associated with each component of the offshore Project infrastructure.

1.4.1.1 Buried Cables

Where cables are buried to a target burial depth of 3 feet (ft) to 7 ft (1 meter [m] to 2 m), the interaction of interest is whether or not EMF can be detected by sensitive species, and if detected, whether the field levels are likely to affect or alter the behavior of these species in a way that could have potentially deleterious population-level effects. To perform this assessment, the magnetic-field and induced electric-field levels associated with the submarine cables were modeled with a burial depth of 3.3 ft (1 m)[4] and results were calculated both at the seabed and at a height of 3.3 ft (1 m) above the seabed as relevant reference locations for most mobile marine species above the seabed.[5]

Near landfall, for a distance of up to approximately 3,200 ft (975 m), each of the DC cables of the SRWEC will enter a separate conduit, which together will be placed within a single bore hole and installed via HDD. Modeling of this Landfall HDD configuration in this region was performed at the target burial depth of 46 ft (14 m), and at the minimum burial depth of 6 ft (1.8 m), both measured from seabed to the center of the HDD bore and evaluated at the seabed and at 3.3 ft (1 m) above seabed.

The calculated field levels were compared to the detection thresholds of various marine species who could be in the vicinity of the SRWEC and SRWF (e.g., sharks; fish, including key groundfish species; and large invertebrates like squid and crustaceans) to assess the likelihood of detection or alteration of animal behavior. These detection thresholds were identified by a thorough review of the laboratory and field studies that assessed the behavioral effects of EMF on fish (including sturgeon and other anadromous fish), invertebrates (such as crustaceans and cephalopods), and elasmobranchii species (e.g., shark, skate, and ray). While specific emphasis is placed on tested species closely related to those expected to inhabit the site, information

---

[4] The specified minimum burial depth of 1 m was used in modeling. Elsewhere and in the COP references to 1 to 2 m burial depths are rounded to 3 to 7 feet.

[5] This height is consistent with recommendations in international EMF exposure assessments (e.g., ICES, 2019, and ICNIRP, 2010) and is meant to capture species swimming in close proximity to the seabed.

regarding the detection thresholds for other, less closely related species was also evaluated in order to fully characterize the EMF detection abilities of marine organisms.

1.4.1.2   OCS–DC, WTGs, and Cables Covered with Protective Mattresses

In contrast to the buried cables, the OCS–DC and WTGs are relatively large structures and the portion of these structures above the seabed will introduce a new vertical habitat, as will the short segments of cables (IAC, SRWEC) along the Project route that will be covered by protective mattresses or rock berms where burial is not practicable. The PDE is currently considering both concrete mattresses and rock berms. Modeling has been performed for a minimum concrete mattress thickness of 1 ft (0.3 m) which will conservatively evaluate covering either by mattresses or rock berms. The calculated magnetic field and induced electric field above a protective mattress or a rock berm of the same thickness will be the same. This conclusion applies to the ocean above the cable and for distances to either side because calculations are conservative and have not assumed any attenuation of the magnetic field or induced electric field from the cable by any material surrounding the conductors within the cables. Throughout the rest of this report, reference will only be made to the mattress-covered case. These added hardground structures provide new and complex habitat that may be considered beneficial to the marine ecosystem and populations of key marine species, including certain species of fish and crustaceans. These new habitats will attract certain species, regardless of the presence of magnetic and induced electric fields. Because of the attraction of certain species to these habitats, the potential exposure of marine species in these new habitats is therefore expected to occur over longer periods than at other locations.

Since marine species swimming near these features would be expected to move freely throughout the environment around these structures from top to bottom, a conservative estimate of average exposure over a medium term (hours, days) is obtained by calculating the average EMF level in a volume of the water column adjacent to these structures or above the mattress-protected cables.[6] These field levels are compared to those reported in the scientific literature where physiologic responses were measured over longer periods than are typically used for acute behavioral studies. Additional consideration is given to marine mammal species that might use these sites as foraging or resting areas. Overall, the potential increased habitat heterogeneity may be a benefit of the Project for marine communities.

2.0   Cable Configurations and Calculation Methods

The potential effects of EMF from the Project during operation are evaluated for multiple cable transmission cases and configurations, as detailed below. Details of the cable configurations are provided in Attachment A. Additional discussion of modeling assumptions is presented in Attachment B with results presented in Attachment C.

2.1 DC Project Cables

Since the DC magnetic field generated by the SRWEC is combined with the earth's geomagnetic field by vector addition, the relative orientation of these two fields changes the resulting combined field. To assess the range of DC magnetic-field levels that could be associated with the SRWEC when oriented in different

---

[6]   This volume average was conservatively calculated using the peak current on the IACs and SRWEC and small volumes near hard-surface structures. At average loading the calculated fields will be lower.

directions, calculations were performed for three representative cable directions and two cardinal directions (north-south and east-west), as addressed in Attachment A. The SRWEC will consist of two cables strapped together, and both a side-by-side configuration and a configuration with one on top of the other are assessed. Magnetic and electric fields are also assessed for either direction of current flow. In total, offshore SRWEC results were calculated for each of four cable and current flow configurations at both peak and average loading levels, at a minimum target burial depth of 3.3 ft (1 m) and a total of four geographic directions, to determine the upper bound for expected magnetic- and induced electric-field levels.

Modeling of the Landfall HDD was performed for one geographic direction and two directions of current flow at both the target offshore burial depth of 46 ft (14 m), and at the minimum target burial depth of 6 ft (1.8 m), both burial depths measured from seabed to the center of the HDD bore.

2.2 DC Cable Magnetic-Field Modeling Methods

2.2.1 Earth's Geomagnetic Field

The total DC magnetic field near the SRWEC depends on the magnitude and direction of the cables and the strength and direction of the earth's ambient geomagnetic field. The geomagnetic field and its vector components near the center of SRWEC route were estimated from the International Geomagnetic Reference Field (IGRF-13) Model[7] as 506 mG. Further discussion is included in Attachment B.

2.2.2 Magnetic-Field Strength

The static magnetic field from the DC current was calculated by the application of the Biot-Savart Law, which was added to earth's geomagnetic-field vector to obtain the total magnetic field.

2.2.3 Compass Deflection

Evaluating how much the local static magnetic field changes direction as a result of the SRWEC is another way to describe the effect of the DC cable on the local environment. A compass needle typically points along the direction of the earth's geomagnetic field, but a new DC magnetic-field source may cause a local deviation in the apparent direction of magnetic north. Here, this deviation is calculated as the compass deflection, which is the difference in angular direction in degrees between the horizontal component of the ambient geomagnetic field and the horizontal component direction of the combined DC field from the earth and from the SRWEC.

2.2.4 Induced Electric Field

The designed dielectric insulation and metallic sheath of the SRWEC will effectively block the electric field from the voltage applied to the conductors from reaching the marine environment (e.g., Snyder et al., 2019). However, an electric field is produced by the movement of electric charges through the static magnetic field produced by the earth or by SRWEC. This induced electric field is calculated by applying the Lorentz force equation described in Attachment B. The induced electric field in fish and in sea water by movement of electric charges in the total magnetic field was calculated for a representative water flow velocity of 2 feet per second (ft/s) (60 centimeters per second [cm/s]) as well as movement of marine species (1 ft/s [30 cm/s] for sturgeon and 0.7 ft/s [21 cm/s] for dogfish).

---

[7]   https://ccmc.gsfc.nasa.gov/modelweb/models/igrf_vitmo.php

2.3 AC Project Cables

Exponent calculated the 60-Hz fields from the IACs proposed for portions of the Project and compared the calculated levels to assessment criteria to evaluate potential effects on marine species. Two configurations, differing in the burial depth of the IACs, are described as part of the PDE.

2.4 AC Cable Modeling Methods for Magnetic and Induced Electric Fields

Exponent calculated the magnetic- and induced electric-field levels for individual IACs using 3-dimensional (3D) finite element analysis (FEA) models using conservative assumptions designed to ensure that the calculated levels overestimate the field levels that would be measured above the cables at any specified loading. The results of AC calculations are presented at maximum loading (i.e., peak loading, which is the maximum Project capacity) and at the anticipated Project loading (i.e., average loading). Calculations are reported both at the seabed and at 3.3 ft (1 m) above the seabed.

2.5 Modeling Methods at WTGs and OCS–DC

Magnetic-field and induced electric-field calculations for the WTGs and OCS–DC were performed using the same 3D FEA modeling approach applied to the helically-twisting AC cables. For the DC cables, magnetic-field results from the SRWEC were combined by vector addition with the ambient geomagnetic field of the earth. As discussed in Attachments A, B, and D, these models involve the convergence of multiple cables at the WTGs and OCS–DC and their vertical rise through the water column. Monopile foundations were modeled for WTGs, while both jacket foundations and monopile foundations were modeled for the OCS–DC, as both were considered options at the time of modeling. Magnetic and induced electric fields were calculated throughout the entire volume of the 3D model, and field strengths were reported from volumetric averages evaluated over regions of interest for marine species. In the 3D model for monopile structures, the cables were assumed to descend vertically through the water column inside the monopile. Near the foundation the cables exit the monopile at an angle of 45 degrees relative to the vertical and separate radially away from the structure. An illustrative example of the WTG monopile is shown below in Figure 2, wherein the cables travel vertically downward through the water column near the center of the monopile foundation and exit the monopile at a height of approximately 16 ft (5 m) above the seabed.

Although a monopile foundation is not proposed for the OCS–DC and only the jacket lattice structure is now being considered, the convergence of cables at a monopile structure will likely conservatively overestimate volume-averaged DC magnetic fields near the *seabed* compared to a jacket foundation. The smaller volumes over which averages were calculated accounts for the higher field levels at the seabed for the monopile foundations. Thus, calculated magnetic and induced electric fields for the OCS–DC jacket foundation will be similar to or lower than the values presented here. Conversely, in the water column above, the jacket structure will provide a more conservative estimate of the volume-averaged DC magnetic fields compared to the monopile foundation because the separation between cables and marine life is reduced. In all cases, modeling was based upon the configurations of cables and scenarios accounting for the minimum separation between adjacent cables and also for the minimum separation between cables and the marine environment (resulting in the maximum field exposure scenarios).
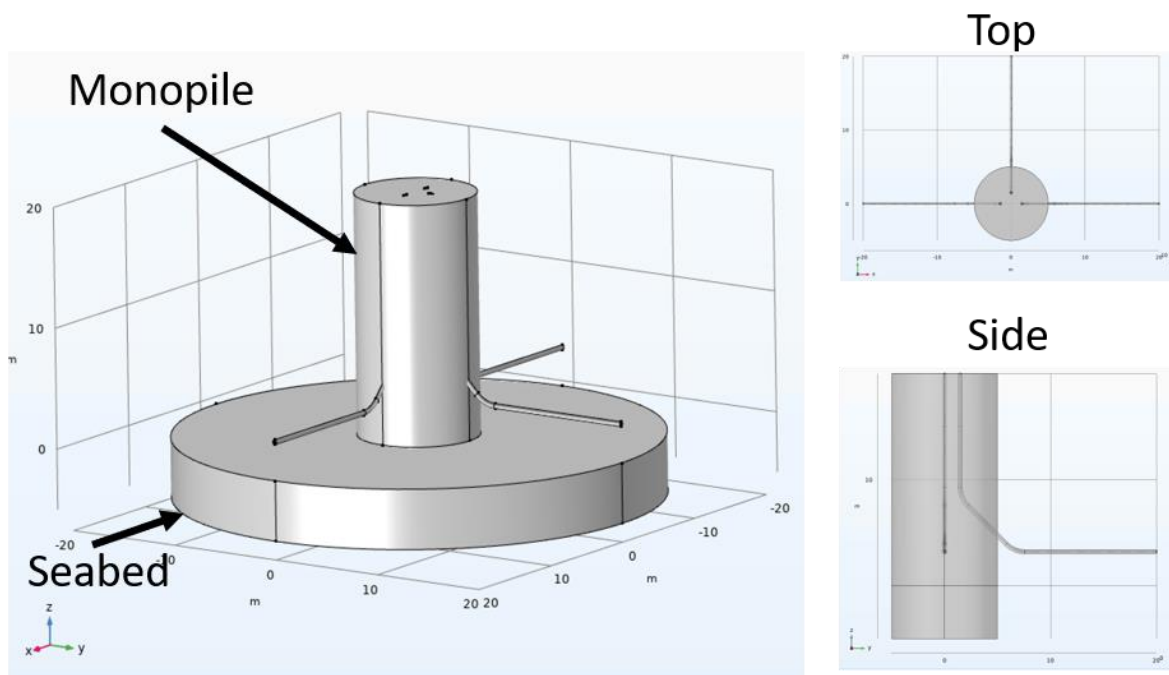
Figure 2.   Modeling geometry of a WTG monopile foundation.

Attachment A provides additional details regarding the design of cables at the monopile foundation for WTG structures, and at both monopile and jacket foundations for OCS–DC structures. Attachment B provides the detailed calculation methodology, and Attachment D includes the results of the calculations.

3.0   Calculated Magnetic and Electric Fields

3.1 DC Cables

Where cables are buried, the interaction of interest will be whether or not EMF can be detected by sensitive species. For this reason, the calculated field levels for buried cables are presented as the maximum above the cables, both at the seabed and at a height of 3.3 ft (1 m) above the seabed as relevant reference locations for most mobile marine species.

The calculated total static magnetic field, the effects of the SRWEC on geomagnetic-based navigation due to compass deflection, and the electric fields induced in marine life due to motion through the total static magnetic field are summarized in Attachment C. Each of these interactions of the SRWEC's static magnetic field with organisms is summarized below.

3.1.1 DC Magnetic Fields

The total static magnetic field, comprised of the field generated by the current flowing within the SRWEC and the earth's geomagnetic field, in the vicinity of the SRWEC is far below the ICNIRP standard for human exposure to static magnetic fields for all configurations considered. Moreover, magnetic fields diminish rapidly with distance, so it is only in the immediate vicinity of the cables that the magnetic-field level will be appreciably different than earth's geomagnetic field. The reduction in the magnetic-field level with distance

from the cables is shown below as a magnetic-field transect across the cable (Figure 3) for east-west oriented cables. Notably, the calculated magnetic fields diminish to within about 10% of earth's ambient geomagnetic field within about 10 ft (3 m) of the cable centerline (0 ft).
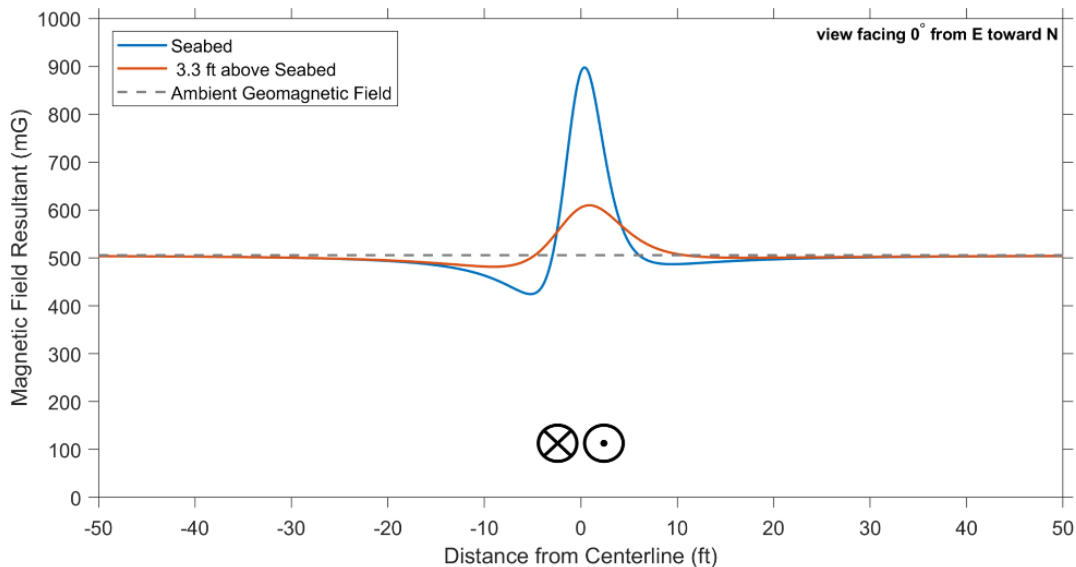
Figure 3.   Total DC magnetic field for the buried (3.3 ft [1 m]) SRWEC at peak loading.

> Calculated magnetic field shown at the seabed (blue line) and 3.3 ft (1 m) above the seabed (orange line). The cables are aligned along the east-west axis, with the current polarity indicated at the bottom center.

Where bundled together along the majority of the SRWEC route, the maximum deviation at peak loading from the earth's geomagnetic field at the seabed surface for a 3.3 ft cable burial depth is 392 mG, decreasing to 104 mG at a height of 3.3 ft (1 m) above the seabed. Over the short segment of the route near landfall where the two cables are installed in separate conduits contained within a single bore hole and installed via HDD, the maximum deviation at peak loading from earth's geomagnetic field at the seabed surface for a 6-ft (1.8-m) burial depth was 253 mG, decreasing by approximately half to 125 mG at a height of 3.3 ft (1 m) above seabed. Calculated magnetic field levels for the SRWEC route are shown as graphical magnetic field transects in Attachment C.

3.1.2 Compass Deflection

Traditional compasses that rely on the earth's geomagnetic field may detect a small effect on compass readings above the cables in shallow water that will diminish quickly with distance. Modern navigational instruments that obtain compass readings and locations from global positioning system receivers would not be affected by the Project cables.

Maximum computed compass deviations at seabed are approximately 155 degrees directly over the buried SRWEC were bundled together along the route from the SRWF to Landfall, but decrease to approximately 29 degrees at a height of 3.3 ft (1 m) above seabed, and rapidly decrease further with increasing horizontal distance, falling to approximately 9 degrees or less within 10 ft (3 m) at either seabed or 3.3 ft (1 m) above seabed. Given the large habitats traversed by migrating fish, and the importance of other senses in marine species, a local deviation of a few degrees for such a short distance would not interfere with the use of the geomagnetic field for navigational purposes by these species. Where the SRWEC is installed via HDD, the

maximum computed compass deviations at seabed for a 6 ft (1.8 m) burial depth are approximately 54 degrees and decrease to approximately 18 degrees at a height of 3.3 ft (1 m) above seabed.

3.1.3 DC Electric Fields

Although the voltage of the conductors of the SRWEC cables does not produce a DC electric field in the marine environment, an electric field can be induced by the movement of electric charges in seawater or fish through the static magnetic field outside the cable. This induced electric field was calculated by applying the Lorentz force equation (discussed in Attachment B). This electric field depends on the speed and direction of charge movement of the water (or organism over the cable). In the analysis presented in Attachment B, the speed of the water or an organism (in meters per second [m/s]) is substituted for the magnitude of the velocity vector **v** in Lorentz's law.

Where the cables are bundled together along the majority of the SRWEC route, at a burial depth of 3.3 ft the maximum calculated induced electric field of ocean current flowing through the total magnetic field in the vicinity of the SRWEC is 0.054 mV/m at the seabed, decreasing to 0.037 mV/m at a height of 3.3 ft (1 m) above the seabed. The maximum calculated induced electric field for dogfish and sturgeon swimming near the SRWEC at the seabed is 0.019 mV/m and 0.027 mV/m, respectively. At a height of 3.3 ft (1 m) above the seabed these values decrease to 0.013 mV/m and 0.018 mV/m, respectively. Over the short segment of the route near landfall where the cables are installed via HDD, for a minimum target burial depth of 6 ft (1.8 m), the maximum calculated induced electric field for dogfish and sturgeon swimming through the total magnetic field at the seabed is 0.016 and 0.023 mV/m, respectively. At a height of 3.3 ft (1 m) above the seabed these values decrease to 0.013 mV/m and 0.019 mV/m, respectively.

3.2 AC Cables

The AC magnetic- and induced electric-field levels were evaluated for the IACs both at a burial depth of 3.3 ft (1 m) and on the surface of the seabed where cables may be covered with protective mattresses. Details for each of the cable configurations are presented in Attachment A. The following sections present a short summary of the results most pertinent for assessing potential effects on marine life; full details of all modeling results are provided in Attachment C.

3.2.1 AC Magnetic Fields

The largest calculated AC magnetic-field level, evaluated at a height of 3.3 ft (1 m) above the seabed, for the 66-kV IACs with a 3.3 ft (1 m) burial depth and peak loading was 4.6 mG. The field levels calculated at seabed were higher (61 mG), but all calculated levels are far below human exposure limits (2,000 mG for ICNIRP or 9,040 mG for ICES). Figure 4 below shows a magnetic-field transect for 3.3 ft buried IACs.
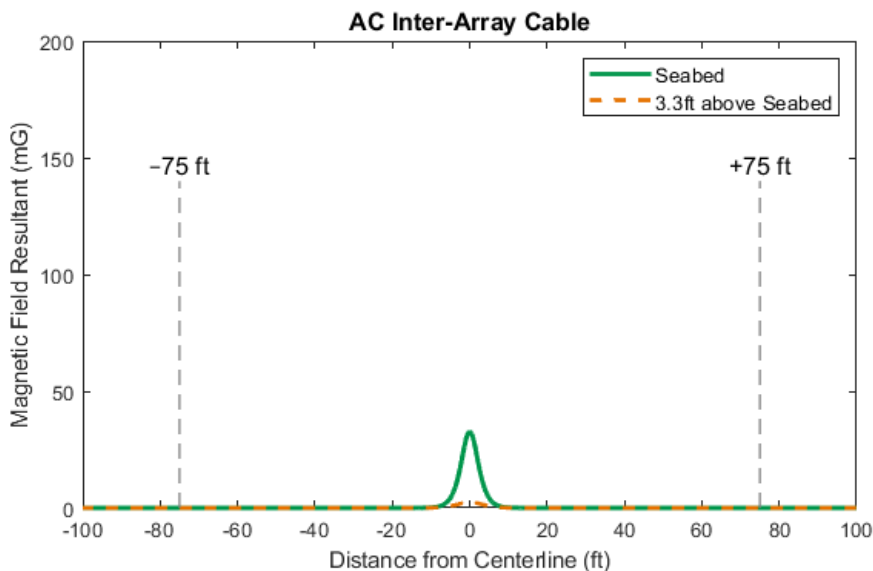
Figure 4.   Calculated AC magnetic-field levels in seawater above the 66-kV IACs for a 3.3-ft (1-m) burial depth and average loading.

As shown in Figure 4, AC magnetic field levels both at the seabed and at 3.3 ft (1 m) above the seabed decrease quickly with distance. Attachment C (Table C-26, Table C-29, and Table C-30, Figure C-16 and Figure C-18), shows that within 10 ft (3 m) of any of the cables, magnetic-field levels are 0.5 mG or lower for either buried or mattress-covered configurations.

3.2.2 AC Electric Fields Induced in Seawater

The maximum AC electric-field level induced in seawater at seabed above the 66-kV IACs buried 3.3 ft (1 m) beneath seabed was 1.0 mV/m, which decreases to <0.1 mV/m at a height of 3.3 ft (1 m) above the seabed. Field levels at the seabed were calculated to be somewhat higher, but all calculated levels are millions of times below human exposure limits (e.g., ICNIRP and ICES). As shown in Attachment C (Table C-27, Table C-31, and Table C-32, Figure C-17 and Figure C-19), field levels both at the seabed and at 3.3 ft (1 m) above the seabed decrease quickly with distance such that within 10 ft (3 m) of any of the cables, electric-field levels are <0.1 mV/m or lower for either buried or mattress-covered configurations.

3.2.3 AC Electric-Field Levels Induced in Marine Organisms

The electric fields induced in two prototypical electrosensitive benthic species, dogfish and sturgeon, were considered. These species were selected for their electrosensitivity, propensity to swim along the sea bottom, and residence within coastal environments. The seabed values were used to calculate induced electric fields to allow for the most conservative estimates of field strengths encountered by these benthic species. The calculated field induced in dogfish at the seabed for a 3.3-ft (1 m) burial depth and peak loading for the 66-kV IACs is 0.39 mV/m and <0.1 mV/m at 3.3 ft (1 m) above seabed. The calculated electric field induced in sturgeon at the seabed for a 3.3-ft (1-m) burial depth and peak loading for the 66-kV IACs is 0.74 mV/m, and <0.1 mV/m at 3.3 ft (1 m) above seabed. The electric field that is calculated to be induced in marine organisms is proportional to the size of the organism and the calculated magnetic field; like the magnetic field, the induced electric field also decreases rapidly with distance from the cables.

3.3 WTG, OCS–DC, and Mattress-Covered Cables

In contrast to the buried cables, the OCS–DC and WTGs are relatively large structures; the portion of these structures above the seabed will introduce a new vertical habitat. Similarly, the mattress-covered portions of cables also will provide hardground habitat for some species. These new habitats will attract certain species regardless of the presence of magnetic and induced electric fields. Detection of fields at these structures, therefore, is less important than potential extended exposure levels since the new habitats may encourage certain fish and shark species to spend a greater amount of time relatively close to these structures, so the evaluation of interest is the volume-average field levels surrounding these structures.

At the WTG and OCS–DC installations, multiple cables converge at portions of these structures and thus the combined effects of multiple cables on field levels were assessed by FEA modeling for both monopile and jacket foundations. The average field strengths were computed within volume averages representative of various marine habitats created by the offshore installations. At the seabed, the maximum exposure scenario due to minimum separation between the cables will occur for the OCS–DC monopile configuration (field levels for the OCS–DC jacket configuration will be lower), while higher in the water column the minimum approach distance between the cables and marine life occurs for the jacket foundation installation. Results, detailed within Attachment D and summarized below, are reported separately for DC and AC fields because the biological responses of marine species to these separate frequencies are not additive.

3.3.1 OCS–DC at Seabed

At the OCS–DC, the SRWEC will produce DC fields and the AC IACs will produce AC fields, and so both DC and AC fields were assessed. At the seabed the largest calculated volume averaged DC magnetic field and electric field (as induced by the movement of seawater through the DC magnetic field) near the OCS–DC monopile structure at peak loading is <3,961 mG and <0.238 mV/m, respectively, as shown in Attachment D. At the seabed the largest calculated volume averaged AC magnetic field and induced electric field near the OCS–DC at peak loading were <253 mG and <2.8 mV/m, respectively.[8,9,10]

3.3.2 OCS–DC in the Water Column

In the water column, the highest field levels for the OCS–DC were calculated for the jacket foundation configuration, and the geometry is conservatively modeled with cables that run vertically down through the water column from the square platform. The cables are equally spaced along the edges of the square with a center-center separation of >6 ft (>1.8 m), and each is contained in an individual J-tube. One side of this arrangement is modeled, with the individual cables of the SRWEC separated and adjacent to each other and next to four IACs, as detailed in Attachment D. The maximum calculated volume averaged DC static magnetic field in the water column near the OCS–DC is <4,333 mG. The induced electric field due to the movement of seawater (2 ft/s [0.6 m/s]) is <0.26 mV/m.[10] In the water column the largest calculated volume averaged AC magnetic field and induced electric field near the OCS–DC at peak loading is ~183 mG and ~2.6 mV/m,

---

[8] Field levels at the seabed for the jacket structure will be less than field levels for the monopile structure due to greater spacing of cables and larger averaging volume.

[9] The maximum calculated AC field level above the IAC cables is within 1 percent of the maximum field calculated for the case of equivalent individual straight cables evaluated at the same distance above these cables (described above in Section 3.2.1).

[10] The PDE for the maximum capacity loading of the SRWEC has decreased by approximately 10% since these calculations were performed. However, since a lower loading will result in overall lower magnetic field levels, the complex models required for the 3D calculations of the DC magnetic field at the OCS–DC were not remodeled. The values in this paragraph therefore represent a conservative upper bound to the fields from the current design. Actual field levels are likely to be approximately 10% lower than these calculated values.

respectively, which is lower than at the seabed because the cables are closer together at seabed.[11] Additional details are provided in Attachment D.

3.3.3 WTG at Seabed

The monopile foundations of the WTG include a central cylindrical pillar, within which the cables traverse vertically through the water column before exiting at an angle of 45 degrees in the vicinity of the seabed. The largest calculated volume averaged magnetic field and induced electric field near the WTG installation at peak loading is 81 mG and 0.9 mV/m, respectively.[11]

3.3.4 Mattress-Covered Cables

The maximum calculated volume-averaged magnetic field and induced electric field above isolated AC submarine cables covered with protective mattresses was 147 mG and 2.0 mV/m, respectively, for the IAC at peak loading.[12] The maximum calculated volume-averaged static magnetic field was 1,322 mG for the SRWEC at peak loading.

3.4 Summary of Marine Exposure Assessment

The maximum magnetic and induced electric-field levels discussed above are relevant only in the immediate vicinity of the IACs and SRWEC since the strength of these fields decreases rapidly with distance. Thus, less than 1 percent of the total marine habitat within the Project Area will have fields above background levels.

The primary sources of magnetic and induced electric fields are the buried SRWEC or the IACs that traverse the site to transfer power among offshore installations and to bring power to onshore facilities. As detailed in Attachment C and summarized in Table 1 the effect of the SRWEC is small, representing a change of less than 10 percent of the ambient geomagnetic field within ±10 ft (±3 m) of the SRWEC. Similarly, AC magnetic- and induced electric-field levels decrease very rapidly from the source (Table 2). Where the cables are laid on the seabed and covered with protective materials, field levels will be higher immediately above the cables, but consistent with the observations of Snyder et al. (2019), within approximately 10 ft (3 m) of the cable, field levels for either buried or mattress-covered installations are similar and low. Where the cables are installed via HDD at a minimum burial depth of 6 ft (1.8 m), field levels will be lower than immediately above either buried or mattress-covered SRWEC configurations and at the typical burial depth of 46 ft (14 m) or more encompassing the majority of the Landfall HDD route field levels will be still lower. Detailed results of the calculated magnetic fields and induced electric fields for the Landfall HDD are included in Attachment C.

---

[11] The PDE for the maximum size and maximum loading of the IAC have both increased incrementally since these calculations were performed. Additional analyses summarized in Section 3.2 show that these design changes to the IAC increase AC magnetic and induced electric field levels by approximately 3%. Since the change in field level resulting from this change is so small, the complex models required for the 3D calculations of the AC magnetic field at the WTG and OCS–DC were not remodeled. The values in this paragraph may therefore be approximately 3% higher than reported above.

[12] The volume over which the calculations were averaged corresponds to a 3.3-ft cube (1-m cube), centered above the cable(s) and extending vertically from the top of the mattress-protection to 3.3 ft (1 m) above the mattress.

Table 1. Calculated DC magnetic-field levels (mG)* and electric-field levels induced by ocean currents (mV/m)** at various horizontal distances at seabed and at 3.3 ft (1m) above the seabed for a 3.3-ft (1 m) burial depth and peak loading

SRWEC Evaluation Height	Magnetic Fields (mG) and Electric Fields (mV/m)					
	Maximum (above cable)		±5 ft (±1.5 m)		±10 ft (±3 m)	
	Magnetic Field	Electric Field	Magnetic Field	Electric Field	Magnetic Field	Electric Field
At seabed	-379 to 392	0.054	-138 to 138	0.039	-42 to 43	0.033
At 3.3 ft (1 m) above seabed	-104 to 104	0.037	-71 to 72	0.035	-34 to 35	0.032

* Results for DC calculations are presented as the maximum *deviation* from earth's static geomagnetic field level of 506 mG. Thus, negative values of the magnetic field represent reductions below a geomagnetic field value of 506 mG.
** Electric-field levels evaluated for the total field (earth + cable) and an ocean current velocity of 2 ft/s (60 cm/s).

Table 2. Calculated AC magnetic-field levels (mG) and induced electric-field levels (mV/m) at various horizontal distances at seabed and at 3.3 ft (1m) above the seabed for a 3.3-ft (1 m) burial depth and peak loading

66-kV IAC Evaluation Height	Magnetic Fields (mG) and Electric Fields (mV/m)					
	Maximum (above cable)		±5 ft (±1.5 m)*		±10 ft (±3 m)*	
	Magnetic Field	Electric Field	Magnetic Field	Electric Field	Magnetic Field	Electric Field
At seabed	61	1.0	7.8	0.2	0.3	<0.1
At 3.3 ft (1 m) above seabed	4.6	<0.1	1.4	<0.1	0.1	<0.1

* Horizontal distance is measured from the center of the IACs.

The following assessment of marine life in Sections 4.0 to 7.0 evaluate the ability of species to detect these fields and potentially alter their behavior as a result. For the SRWEC, calculations were performed to characterize DC magnetic field levels at the OCS–DC and areas of the SRWEC with protective coverings. Additional calculations of induced electric fields in fish and volume-averaged AC magnetic field levels for IACs connecting at WTGs, the OCS-DC, and cables with protective coverings for potential extended durations of exposure. An assessment in Section 8.0 evaluates the likelihood that prolonged exposure to these areas might have any physiological effects on species and evaluations of EMF interactions of marine species at the Landfall HDD.

4.0 Evaluation of EMF Interactions with Large Invertebrates in the SRWF and/or SRWEC

The SRWF and SRWEC are expected to transect habitats utilized by a number of large invertebrate species including epibenthic crustaceans, bivalves, and squid. To determine the potential for effects on regional invertebrate species, the modeled results for the proposed cable configurations are evaluated.

In the vicinity of the SRWF and/or SRWEC, two species of commercially harvested squid are expected to occur—longfin inshore squid (*Doryteuthis pealeii*) and northern shortfin squid (*Illex illecebrosus*) (Table 3). These squid species are known to form large schools over benthic habitats from coastal to deep water areas. Squid also undergo seasonal migrations that could lead to interactions with proposed SRWEC routes. Other migratory invertebrates, like Atlantic rock crab (*Cancer irroratus*), Jonah crab (*Cancer borealis*) and American lobster (*Homarus americanus*), also are commonly found in this region. Because these species are mobile and traverse a range of substrates, it is likely that they will move through the SRWF and the SRWEC route.

In addition to mobile cephalopods and crustaceans, a number of commercially-important bivalve species inhabit the vicinity of the SRWF and/or SRWEC, including the Atlantic sea scallop (*Placopecten magellanicus*), the Atlantic surf clam (*Spisula solidissima*), and the ocean quahog (*Arctica islandica*) (Table 3). Relative to crabs, lobsters, and squid, these bivalve species are relatively sessile and either make infrequent, small-scale movements or are found burrowed in substrates. Given this, populations of harvestable bivalves outside the SRWF and SRWEC are not expected to immigrate into or through the EMF produced by the SRWEC, and the cable route comprises less than 1 percent of the total available habitat for these species.

Table 3.   Important large invertebrate species expected to inhabit the SRWEC and/or SRWF

Species	Preferred Habitat
American Lobster (*Homarus americanus*)	Migratory over rocky and mixed habitat types; occasionally burrows in sand and mud
Atlantic rock crab (*Cancer irroratus*)	Multiple substrate types from the coast to the outer continental shelf
Atlantic sea scallop (*Placopecten magellanicus*)	Found on a variety of substrate, including sand, gravel, and shell bottoms
Atlantic surfclam (*Spisula solidissima*)	Found at depths between 26 to 216 ft (8 to 66 m), burrowing in sand and finer substrates
Jonah crab (*Cancer borealis*)	Multiple substrate types from the coast to the outer continental shelf
Longfin inshore squid (*Doryteuthis pealeii*)	Swims over benthic inshore areas and to the OCS–DC
Northern shortfin squid (*Illex illecebrosus*)	Associated with various bottom substrates from coastal areas throughout the continental shelf
Ocean quahog (*Arctica islandica*)	Inhabits sandy substrates at depths between 82 and 200 ft (25 and 61 m)

4.1 DC Magnetosensitivity of Large Marine Invertebrates

A number of studies have been conducted to examine the impact of static magnetic fields on invertebrate behavior, likely due to the fact that some invertebrate species have demonstrated a geomagnetic sense. Bochert and Zettler (2004) investigated the short-term behavioral effects of static magnetic fields for marine invertebrate species, including common shrimp (*Crangon crangon [C. crangon]*), a marine isopod (*Saduria entomon [S. entomon]*), dwarf crab (*Rhithropanopeus harrisii [R. harrisii]*), common starfish (*Asterias rubens*), and ragworm (*Nereis diversicolor*). The behavior of these organisms exposed to static magnetic fields of 2.7 millitesla (mT) (27,000 mG) were observed in a tank environment. Both *C. crangon* shrimp and dwarf crab distributions within tanks were unaffected by magnetic-field exposure (Bochert and Zettler 2004). Similarly, while *S. entomon* isopods appeared to show some level of avoidance of the static magnetic field, this response was not statistically distinguishable from non-exposed isopods. In addition, observed distributions of exposed echinoderms and polychaetes did not deviate from those observed for controls (Bochert and Zettler 2004). Further, oxygen consumption by two species of shrimp (*Palaemon squilla* and *C. crangon*) was assessed during exposure to static magnetic fields and was found to be statistically indistinguishable from

non-exposed shrimp (Bochert and Zettler 2004). These results led the researchers to conclude that *"static magnetic fields of submarine cables seem thus to have no clear influence on orientation, movement and physiology of the tested benthic animals."* In a different test environment, Woodruff et al. (2012) reported some behavioral effects in Dungeness crab (*Metacarcinus magister*) exposed to 1 mT (10,000 mG) DC magnetic fields. Exposed crabs were observed to be more likely to exhibit changes and variability in behavior, and also spent less time buried in sand. However, American lobsters exposed under similar laboratory conditions exhibited no change in the amount of time spent in shelters, in burrows, or walking, although there were minor effects on distribution (Woodruff et al., 2013).

Movements and distributions of juvenile European lobster (*Homarus gammarus*) were demonstrated to be unaffected by exposure to artificial static magnetic fields up to 230 µT (2,300 mG). Time to enter shelters, time spent inside shelters, mean velocity level, and activity levels were unaffected when lobsters were exposed to DC magnetic fields (Taormina et al., 2020). However, the authors noted that lobsters appeared react to a light gradient within the laboratory, and they could not conclude, in the absence of light, that magnetic cues might have a stronger effect on lobster behavior. Yet, this provides important information that magnetic fields do not act as sole regulators of lobster behavior. There is some evidence from laboratory research that crustaceans may respond to higher intensity static magnetic fields. Scott et al. (2018) examined the effect of 2.8 to 40 mT (28,000 to 400,000 mG) static magnetic fields on the behavior of commercially-important *Cancer pagurus* crabs. Over a 24-hour exposure period, crabs were significantly more likely to inhabit shelter adjacent to the magnetic-field source, and exposure to magnetic fields also reduced time spent foraging by the crabs (Scott et al., 2018). Based on more recent research with *C. pagus* crabs, researchers noted changes in roaming and sheltering behaviors at 5,000 mG and 10,000 mG, but not at 2,500 mG, leading to the conclusion that *"a working limit of a maximum of 250 µT [2,500 mG] could result in minimal physiological and behavioural [sic] changes within this species"* (Scott et. al. 2021).

Invertebrate responses to EMF also were evaluated from field studies, including surveys conducted at submarine cable sites, as well as field cage studies. As part of a large-scale mesocosm study, Hutchison et al. (2018, 2020) assessed the responses of American lobster to a DC cable under field conditions. Field-collected lobsters were held in large cages above the DC cable producing a total magnetic field of 65.3 µT (653 mG); behaviors were contrasted with those of caged lobsters in adjacent areas without a DC cable at levels of approximately 513 mG (characteristic of earth's ambient geomagnetic field). Researchers determined that lobsters in the EMF-exposed cage were more likely to be found in the center of the cage (i.e., adjacent to the cable) versus controls (Hutchison et al., 2018, 2020); however, for both treatment and control cages, lobsters were significantly more likely to spend time at the cage ends. Lobsters in treatment cages were also observed to be closer to the seabed when in the middle of cages as compared to lobsters in control cages (Hutchison et al., 2018, 2020). When the lobster cages were moved between control and DC cable sites, there was a significant increase in the proportion of large turns exhibited by lobsters when in the middle of the cage (Hutchison et al., 2020). As such, researchers concluded that EMF did result in changes in the distribution of lobsters within the cages and the cable was not observed to present a barrier to movement (Hutchison et al., 2018).

In another field study, three years of diver surveys were conducted at sites along the Basslink DC cable in Bass Strait, Australia, to determine the effect of the operating cable on biological communities (Sherwood et al., 2016). Based on these data, it was determined that along the buried portions of the cable there was no adverse effect on benthic invertebrate communities. However, where the cable remained unburied, large abundances of encrusting invertebrates were noted, as the armored cable provided hard substrate for colonization of these species (Sherwood et al., 2016). Thus, this research suggests that the produced EMF from the DC cable did not affect soft sediment communities and did provide enhanced habitat for hardground species where left unburied.

Similarly, six separate ecological surveys were conducted at sites along the combination 10-kV communication/DC Monterey Accelerated Research System (MARS) power cable off the coast of California between 2004 and 2015 to assess whether the installation and operation of the cable affected biological communities (Kuhnz et al., 2015). Comparisons of megafauna and macrofauna communities indicated *"very few potential changes in benthic biological patterns due to the MARS cable"* and researchers concluded that natural variability in abundance superseded any cable effects (Kuhnz et al., 2015).

4.2 AC Magnetosensitivity of Large Marine Invertebrates

Although some marine invertebrates have been documented to be sensitive to the static geomagnetic field (Boles and Lohmann 2003; Cain et al., 2005; Ugolini and Pezzani 1995), these studies cannot be used to predict effects from 60-Hz AC power sources due to the difference in frequencies (0 Hz versus 60 Hz). Unfortunately, laboratory research has not been conducted on the behavioral responses of marine invertebrates to AC magnetic fields; however, a series of field studies conducted at 60-Hz AC power cables can be used to assess the sensitivity of large mobile crustaceans and cephalopods that might move through the EMF produced by AC cables.

Researchers at the Marine Science Institute at the University of California, Santa Barbara, together with the Bureau of Ocean Energy Management (BOEM) conducted field-based studies off the coasts of California and Washington to evaluate if the presence of 60-Hz AC cables impact the behavior and movement of different crab species (Love et al., 2015, 2017a). In addition, multi-year biological studies were carried out to track the presence and abundance of marine organisms, including crustaceans and cephalopods, at similar AC cable sites. The results from these field studies yield important information regarding the potential effects of 60-Hz AC EMF because they are conducted under more realistic conditions than laboratory studies.

Love et al. (2015) introduced the yellow rock crab (*Metacarcinus anthonyi*) and the red rock crab (*Cancer productus*) to large cages alongside unburied 60-Hz AC cables and recorded the distributions of individual crabs around both energized and unenergized cables. Measured magnetic fields along the energized 60-Hz AC cable ranged between 462 and 800 mG but decreased to 9 mG at the distant side of the cages (Love et al., 2015). This design therefore provided crabs with a range of magnetic-field levels to inhabit. Based on four separate observation times, researchers determined that caged crabs were neither more nor less likely to be found either adjacent to the cable or at the distant end of the cages, at either energized or unenergized cables. The authors concluded that the 60-Hz AC magnetic fields did not affect crab behaviors or distributions (Love et al., 2015).

A similar series of field surveys were designed by Love et al. (2017a) to assess the ability of Dungeness crabs in Washington and the red rock crab in California to freely pass across 60-Hz submarine cable routes; this was intended to determine if 60-Hz EMF is likely to disrupt crustacean migratory progress. The cable off the California coast carried a greater electric current than that off Washington, producing magnetic fields up to 1,168 mG versus 428 mG (Love et al., 2017a). Within specialized cages that bridged the cable routes, both species of crabs were observed to move freely throughout the available space, across the energized cable. This led researchers to conclude that energized 60-Hz submarine cables were not barriers to crustacean movements. These caged studies further indicate that energized submarine 60-Hz AC cables do not affect distributions of large crustaceans, like crabs, through a barrier effect.

Love et al. (2017b) also conducted multi-year biological surveys at energized and unenergized AC submarine cable sites to investigate abundances and species composition of marine organisms in these areas, as compared to sedimented sea bottoms. Researchers frequently observed California spot prawn (*Pandalus platyceros*) and the East Pacific red octopus (*Octopus rubescens*) at survey sites (Love et al., 2017b). Based on 2 years of abundance data, both spot prawn and red octopus were observed at energized and unenergized

cables at equivalent rates; however, invertebrate communities at all cable sites (energized and unenergized) were notably different from those observed in natural sedimented areas. This led researchers to conclude that differences resulted from the physical habitat provided by the unburied cable, and not from EMF (Love et al., 2017b). Taken together, these field studies provided evidence that 60-Hz magnetic fields up to 1,100 mG do not appear to affect the behavior of large, mobile marine invertebrates, including crustaceans and cephalopods.

4.3 Interaction of DC and AC Magnetic Fields of Proposed Project Cables with Large Marine Invertebrates

Information from laboratory and field studies regarding the effects of static magnetic fields from a DC source indicates mixed results. For instance, a number of behavioral and physiological endpoints for multiple invertebrate species were reportedly unaffected by exposures to static magnetic fields of 27,000 mG (Bochert and Zettler 2004). However, different laboratory studies have reported behavioral effects in response to 10,000 mG fields, and field studies indicated some measurable behavioral changes in lobsters caged above DC cables with a total field of 653 mG (Hutchison et al., 2018, 2020). Given this, the calculated values have been compared to the lower values that were documented to elicit effects. Modeled total magnetic-field levels for the SRWEC at peak loading is estimated to be 898 mG at the seabed, decreasing to 610 mG at 3.3 ft (1 m) above the seabed (Table 4). These levels are slightly above and approximately equivalent to total field levels associated with small-scale behavioral changes in caged lobsters (Hutchison et al., 2018, 2020). Evaluations of EMF interactions of marine species at the Landfall HDD are discussed in Section 8.

Based on the information summarized above, 60-Hz AC submarine cables producing magnetic fields up to 1,168 mG are unlikely to alter the behaviors and distributions of large marine invertebrates, including crustaceans and cephalopods (Love et al., 2015, 2017b). For the proposed IAC the maximum calculated AC magnetic-field strength at peak loading is 61 mG at the seabed (Table 4). This is below levels associated with no effects on caged crabs and populations of invertebrate species observed in the field. As such, evidence from a series of field surveys demonstrates that the behavior and distributions of large crustacean and cephalopod invertebrates would not be altered by the magnetic-field levels projected for the AC IAC.

Table 4. Calculated maximum magnetic fields at the seabed and 3.3 ft (1 m) above the seabed for 3.3-ft (1 m) burial depth and peak loading

Cable Type	Magnetic Field (mG)	
	Seabed	3.3 ft (1 m) above seabed
SRWEC (Total DC: Cable + Earth)	898	610
IAC (AC)	61	4.6

5.0 Evaluation of EMF Interactions with Finfish at IACs and SRWEC

A number of fish species demonstrate some level of magnetosensitivity, likely as a result of physiological adaptions such as the presence of particles of magnetite in bones and organs (Harrison et al., 2002). Fish including tuna, carp, salmonids, and eels are able to perceive changes in the geomagnetic field and use these to guide migrations (Hanson and Westerberg 1987; Tański et al., 2011; Walker et al., 1998), though this ability is likely used in conjunction with multiple other environmental variables, including photoperiod, changes in

temperature and currents, and olfactory cues(Leggett, 1977). Only a very few fish have demonstrated the capacity to detect low-level electric fields, an ability that is mediated by specialized and sensitive electroreceptors (ampullae of Lorenzini). Electrosensitive fish expected to inhabit the SRWEC and/or SRWF are Atlantic sturgeon (*Acipenser oxyrinchus oxyrinchus*) and shortnose sturgeon (*Acipenser brevirostrum*), which are federally- or state-listed protected species and seasonally reside in estuaries and coastal environments. The electrosensitivity of all species of sturgeon is most likely used to detect prey, which generate low-level, low-frequency electric fields over short distances.

The SRWF and/or SRWEC provides habitat for a number of finfish[13] species, including important commercially-harvested species (Table 5). It should be noted that the behaviors and preferred habitats of regional fish species are expected to influence the likelihood of transitory exposure to cable-associated EMF. Given their close association with the seabed, demersal or bottom-dwelling fish are most likely to be exposed to EMF from the operating cable (Bull and Helix 2011). Conversely, fish species that are pelagic in the upper portions of the water column will be more distant from cables and encounter lower EMF levels along the SRWEC route. As such, fish habitat preferences and vertical distribution in the water column affect the probability that individuals would encounter EMF produced by the submarine cables.

Table 5.   Finfish species expected to inhabit the SRWEC route and SRWF

Species	Demersal, Pelagic, Other (as noted)[1]	Size at first reproduction, (cm)[1]	Common length (cm)[1]
Albacore tuna (*Thunnus alalunga*)	Pelagic	85	100
Alewife (*Alosa pseudoharengus*)	Pelagic	11	30
American Eel (*Anguilla rostrata*)	Pelagic	37	50
American Shad (*Alosa sapidissima*)	Pelagic	49	62
Atlantic Bonito (*Sarda sarda*)	Pelagic	37	50
Atlantic butterfish (*Peprilus triacanthus*)	Pelagic/Benthopelagic	12	20
Atlantic cod (*Gadus morhua*)	Demersal/Benthic	63	NR
Atlantic halibut (Hippoglossus hippoglossus)	Demersal/Benthic	122	NR
Atlantic herring (*Clupea harengus*)	Pelagic	17	30
Atlantic mackerel (*Scomber scombrus*)	Pelagic	29	30
Atlantic Menhaden (*Brevoortia tyrannus*)	Pelagic	18	NR
Atlantic Silverside (*Menidia menidia*)	Pelagic	NR	12
Atlantic Sturgeon (*Acipenser oxyrinchus oxyrinchus*)	Demersal/Benthic	NR	250
Atlantic wolffish (*Anarhichas lupus*)	Demersal/Benthic	60	NR
Bay anchovy (Anchoa mitchilli)	Pelagic	NR	6
Black sea bass (*Centropristis striata*)	Reef-associated	19.1	30
Blueback Herring (Alosa aestivalis)	Pelagic		28

---

[13]   The term finfish is used to distinguish these species from the elasmobranchs, which are discussed in a separate section.

Species	Demersal, Pelagic, Other (as noted)[1]	Size at first reproduction, (cm)[1]	Common length (cm)[1]
Bluefin tuna (*Thunnus thynnus*)	Pelagic	97	200
Bluefish (*Pomatomus saltatrix*)	Pelagic	30	60
Conger Eel (*Conger oceanicus*)	Demersal/Benthic	NR	100
Haddock (*Melanogrammus aeglefinus*)	Demersal/Benthic	35	35
Monkfish (*Lophius americanus*)	Demersal/Benthic	47	90
Northern searobin (Prionotus carolinus)	Demersal/Benthic	NR	30
Ocean pout (*Zoarces americanus*)	Demersal	28.8	110 (max length)
Pollock (*Pollachius virens*)	Demersal/Benthic	39.1	60
Red hake (*Urophycis chuss*)	Demersal/Benthic	26	NR
Sand Lance (Ammodytes americanus)	Demersal/Benthic	NR	24
Scup (*Stenotomus chrysops*)	Demersal/Benthic	16	25
Silver hake (*Merluccius bilinearis*)	Demersal/Benthic	23	37
Skipjack tuna (*Katsuwonus pelamis*)	Pelagic	40	80
Spot (*Leiostomus xanthurus*)	Demersal/Benthic	NR	25
Spotted hake (*Urophycis regia*)	Demersal/Benthic	NR	17
Striped Bass (*Morone saxatilis*)	Demersal/Benthic	NR	120
Striped searobin (*Prionotus evolans*)	Reef-associated	NR	30
Summer flounder (*Paralichthys dentatus*)	Demersal/Benthic	28	NR
Tautog (Tautoga onitis)	Reef-associated	18	NR
Weakfish (*Cynoscion regalis*)	Demersal/Benthic	NR	50
White hake (*Urophycis tenuis*)	Demersal/Benthic	46	70
Windowpane flounder (*Scophthalmus aquosus*)	Demersal/Benthic	22	NR
Winter flounder (*Pseudopleuronectes americanus*)	Demersal/Benthic	27	NR
Witch Flounder (Glyptocephalus cynoglossus)	Demersal/Benthic	30	NR
Yellowfin tuna (*Thunnus albacares*)	Pelagic	103	150
Yellowtail flounder (*Limanda ferruginea*)	Demersal/Benthic	30	NR

[1] Information from fishbase.org; NR = Not reported

5.1 DC Magnetosensitivity of Finfish

A number of laboratory studies have been conducted with multiple fish species to determine both the physiological effects and behavioral effects of short-term exposure to static magnetic fields. These

experiments have been conducted with a number of both marine and freshwater fish species, and when considered in whole, provide a range of magnetosensitivities expected for fish species. Short term (less than 2 hours) exposure to constant static magnetic fields between 5 and 10 mT (50,000 to 100,000 mG) was found to significantly increase the oxygen uptake in rainbow trout (*Oncorhynchus mykiss*) embryos (Formicki and Perkowiski, 1998). Similarly, eggs of various salmonid species, including Atlantic salmon (*Salmo salar*), brown trout or sea trout (*Salmo trutta*), and rainbow trout were exposed to a 2 mT (20,000 mG) DC magnetic field; egg shell-permeability was significantly increased by short-term exposure (Sadowski et al., 2007). This led the authors to conclude that such a finding may have implications for fish hatcheries and their exposure to static magnetic fields; however, it is unclear if this exposure or effects would occur outside of aquaculture settings.

In terms of the ability of fish species to detect a static magnetic field, laboratory behavioral studies provide valuable information. Tanski et al. (2011) exposed sea bream (*Sparus aurata*) and European bass (*Dicentrarchus labrax*) fry to a static 0.2 mT (2,000 mG) magnetic field. While sea bream changed orientation in response to the magnetic field, sea bass showed no indication of being able to detect the field. Authors surmised that this difference in sensitivity may be related to different life histories (i.e., sea bass rely more on physical and chemical cues, given the timing of their migrations) or life stage specific differences in magnetic-field use (Tanski et al., 2011). Bochert and Zettler (2006) exposed young European flounder (*Platichthys flesus*) to 2.7 mT (27,000 mG) magnetic fields produced by a static source to assess possible impacts to behavior and distribution relative to the magnetic-field source. These researchers determined that there was no effect of the static magnetic field on the positioning of flounder within the laboratory tank. Woodruff et al. (2013) reported some minor changes in Atlantic halibut (*Hippoglossus hippoglossus*) distributions in response to a static magnetic field with a maximum value of 1.23 mT (12,300 mG). More recent laboratory studies conducted with Atlantic sturgeon did not detect any *"biologically relevant changes to simple behaviors in sub-adult individuals"* (McIntyre et al., 2016). Juvenile Atlantic sturgeon were exposed to DC fields of 5 µT, 100 µT, and 1 mT (50 mG, 1,000 mG, and 10,000 mG) and they did not demonstrate any clear patterns of behavioral changes in response to different field strengths. The authors concluded that *"results are not consistent with the hypothesis that localized M/EM [magnetic/electromagnetic] fields from anthropogenic sources—specifically benthic HV cables—in coastal ocean habitats may negatively impact behavior of migrating or foraging wild Atlantic sturgeon"* (McIntyre et al. 2016). This suggests that the behaviors of individual sturgeon in the SRWF or SRWEC are unlikely to be altered by the presence of the cable.

Changes to swim behavior have been noted in response to exposure at higher static magnetic-field levels. Zebrafish (*Danio renrio*) exposed to a 11.7 Tesla (T) (1.17×10^8 mG) magnetic field produced by a static source (stronger than fields produced by magnetic resonance imaging devices [1.5 to 3 T] used in medicine) exhibited significant changes in behavior. Swim behavior of fish exposed to the magnetic field was characterized as *"erratic"* with rolling, tight circling, and increased swim speed. Removal from the magnetic field resulted in the restoration of normal swim behaviors (Ward et al., 2014). Similarly, adult Japanese rice fish (*Oryzias latipes*) exposed to a 100 mT (1,000,000 mG) static magnetic field exhibited faster swim velocities than unexposed fish, as well as altered distributions that aligned with proximity to the magnetic-field source (Sun et al., 2019). In a series of laboratory studies conducted with fathead minnow (*Pimephales promelas*), sunfish species, striped bass (*Morone saxatilis*), and channel catfish (I*ctalurus punctatus*), tank distributions and swim behavior were observed in response to a static magnetic field of up to 36.4 mT (364,000 mG) (Cada et al., 2012). Fathead minnow activity was significantly increased by the presence of the magnetic field, but all other tested endpoints—minnow distribution, as well as sunfish, striped bass and catfish activity and distribution—were not significantly altered by the presence of the static magnetic field (Cada et al., 2012). It should be noted that these reported changes to swim behavior were observed only following exposures more than 300 to 100,000 times higher than what is expected to occur along buried DC routes, and that striped bass exposed to these fields showed no change in activity or distribution. Cresci et al (2022) exposed demersal lesser sandeel (*Ammodytes marinus*) larvae to a gradient of static magnetic fields expected to occur at submarine cable sites

(total field levels of 500 to 1500 mG). Exposed larvae exhibited no significant changes in swim speed, swim direction or spatial distribution of larvae. Given this, authors concluded that *"lesser sandeel larvae would not be attracted to or repelled from HVDC subsea cables"* (Cresci et al. 2022).

Both tagging studies and field surveys have been conducted to determine if the presence of DC submarine cables significantly alter fish migration or the distribution of fish populations at submarine sites. Acoustic telemetry tagging and passive acoustic monitoring were employed to investigate the migratory behavior of green sturgeon (*Acipenser medirostris*) and Chinook salmon (*Oncorhynchus tshawytscha*) in relation to the Trans Bay Cable in San Francisco Bay (Kavet et al., 2016). As part of this research, scientists measured the geomagnetic-field distortions along the migratory routes and found that bridges spanning the Bay were associated with larger magnetic-field distortions than the Trans Bay Cable, by an order of magnitude or more. This finding suggests that submarine cables are less likely to be disruptive to magnetosensitive species than large bridges. Results from tagged Chinook salmon indicated that migrating fish were attracted to the cable area following energization, but this did not impede their ability to successfully migrate through the Bay (Kavet et al., 2016). While there also is evidence that green sturgeon could detect the energized cable, the presence of the cable had different effects on outbound and inbound migratory sturgeon: outbound migration times were significantly prolonged, while inbound migration times were shortened by the presence of the energized Trans Bay Cable (Kavet et al., 2016). Additional studies examining the effect of the bridge-associated, magnetic-field distortions in the Bay indicated that these did not constitute a *"strong barrier"* to fish migration (Klimley et al., 2017). Similarly, an acoustic telemetry study monitoring the movements of migratory European eel (*Anguilla Anguilla*) examined the effect of the 450-kV Baltic DC cable on the timing and nature of movements. The authors concluded that the cable (which as a monopole produces a much higher magnetic field than the now common bi-pole cable) did not act as a barrier or obstruction to migration, and that the observed eel movement and alignment were within the expected range of behaviors for tagged eel tracked in areas without DC cables (Westerberg and Begout-Anras 1999).

A series of biological field surveys along the MARS cable off the coast of California tracked the presence of different marine species both before and after cable installation and energization. The cable is a combination submarine communication/DC power cable that is energized to 10 kV.[14] Over 30,000 individuals from 154 taxonomic groups were observed during the course of six separate surveys conducted between 2004 and 2015 (Kuhnz et al., 2015). Based on these data, the authors concluded that *"the MARS cable has had little detectable impact on seabed geomorphology, sediment conditions, or biological assemblages."* Similarly, diver studies conducted at sites along the DC Basslink submarine cable indicated no adverse effects on fish communities, but where burial was impractical and the cable was protected with an iron shell, various fish species were observed to be associated with this vertical structure (Sherwood et al., 2016).

5.2 DC Electrosensitivity of Sturgeon Species

Very few finfish species are known to be electrosensitive, and most of these species are not found in the vicinity of the SRWEC or SRWF. However, the endangered Atlantic sturgeon, which inhabits the US Atlantic coast, is known to be electrosensitive, and may inhabit the SRWF and/or SRWEC. Conversely, shortnose sturgeon are typically distributed in rivers and estuaries, spending limited time in oceanic environments.[15] An investigation of Atlantic sturgeon migrations in the NY area indicated that these were predictable and governed by a series of environmental cues, including photoperiod and water temperature (Ingram et al.,

---

[14]   https://www.mbari.org/at-sea/cabled-observatory/mars-technology/

[15]   https://www.fisheries.noaa.gov/species/shortnose-sturgeon

2019). Atlantic sturgeon were also determined to be strongly correlated with sand and gravel substrates with high densities of prey (Ingram et al., 2019).

Siberian sturgeon (*Acipenser baerri*) exposed to electropositive metal (15 microvolts [μV] to 90 μV) exhibited altered behavior, which largely included sucking at the metal, a behavior pattern associated with feeding or predation. The investigators compared the responses to the electric field to an olfactory feeding stimulus and found the number of feeding strikes to be similar for the two stimuli (Zhang et al., 2012). Shovelnose sturgeon can detect static electric fields as low as 0.1 to 0.2 mV/cm (10 to 20 mV/m) (Teeter et al., 1980). In other studies where species exhibiting both magnetosensitivity and electrosensitivity (like sturgeon) are tested, it is not clear if one or both of these stimuli affected behavior. Because the exquisite sensitivity of such species to electric fields, less attention has been given to the static magnetic-field component of exposure.

5.3 AC Magnetosensitivity of Finfish

The available laboratory studies on the effects of 50- or 60-Hz EMF on fish behavior were reviewed and results demonstrate a lack of evidence for significant effects on fish behavior and distribution. An early study focusing on the effects of 60- to 75-Hz magnetic fields on magnetosensitive Atlantic salmon and American eel (*Anguilla rostrata*) indicated no changes in swimming behaviors occurred in response to a 500-mG magnetic field (Richardson et al., 1976). This led researchers to conclude that AC EMF at these frequencies are either not detectable or do not alter the behavior of these migratory fish (Richardson et al., 1976). More recent studies conducted by the Marine Scotland Science Agency (Armstrong et al., 2015; Orpwood et al., 2015) confirmed these findings. Scottish researchers evaluated the responses of European eel and Atlantic salmon to magnetic fields up to 960 mG, produced by a 50-Hz AC power source. Salmon exposed to 50-Hz magnetic fields up to 950 mG exhibited no significant change in swim behavior (Armstrong et al., 2015). In a separate study, European eels were exposed to a 960 mG 50-Hz magnetic field, which elicited no significant effects on swimming behavior, orientation, or passage through the tank system (Orpwood et al., 2015). The results of multiple laboratory studies of eel and salmon behavior all indicate that magnetic fields from 50- to 75-Hz AC sources are likely not detectable by these migratory fish species (Armstrong et al., 2015; Orpwood et al., 2015; Richardson et al., 1976). These findings indicate that these migratory fish species known to respond to the geomagnetic field do not detect higher frequency AC fields in the same way.

Research conducted at the US Department of Energy's Oak Ridge Laboratory assessed the potential effects of AC magnetic fields on various fish species, including largemouth bass (*Micropterus salmoides*), the redear sunfish (*Lepomis microlophus*), and the magnetosensitive and electrosensitive pallid sturgeon (*Scaphirhynchus albus*). Results for these species support the lack of evidence for behavioral effects resulting from 50-60 Hz AC magnetic fields. For instance, there were no observed changes to largemouth bass behavior or swim metrics when exposed to a 24,500 mG magnetic field from a 60-Hz AC power source (Bevelhimer et al., 2015). When exposed in a mesocosm chamber, swimming behavior and distribution of pallid sturgeon were unaffected by AC EMF between approximately 18,000 and 24,500 mG (Bevelhimer et al., 2015). However, redear sunfish were observed to be significantly more likely to inhabit shelters nearest to a magnetic-field source (1,657,800 mG) but resumed a more random distribution after the field was discontinued (Bevelhimer et al., 2013). Lake sturgeon (*Acipenser fulvescens*) behavior was significantly changed in the presence of an approximately 6,600 μT (66,000 mG) 60-Hz AC magnetic field; notable responses included startle behaviors, fin flares, and slowing or gliding (Cada et al., 2012). However, the authors noted that *"no longer-term changes in behavior or mortalities were observed"* (Cada et al., 2012).

In addition to laboratory studies, field surveys conducted at submarine cable sites can also be used to assess the potential effects of AC EMF on fish populations in the ocean. While these types of studies do not allow for the fine-scale behavioral observations possible in laboratory studies, they incorporate a level of realism and

allow for analysis of regional distributions and populations of key species. Researchers at the Marine Science Institute at the University of California, Santa Barbara, together with BOEM, conducted surveys at energized and unenergized 60-Hz submarine cable sites between 2010 and 2014 to assess whether produced magnetic fields (730 to 1,100 mG) had any effects on the distribution of marine species (Love et al., 2016). Over multiple years of observations, researchers identified more than 40 different fish species at field sites, including California halibut (*Paralichthys californicus*), Pacific sanddab (*Citharichthys sordidus*), and seaperch (*Sebastes* spp), but there were no significant differences in fish communities at the energized and unenergized cable sites. This suggests that the magnetic fields produced by the 60-Hz AC cables had no effect on fish distributions; however, it should be noted that the physical structure of the unburied cables (energized and unenergized) attracted a higher number of fish than did sediment bottoms (Love et al., 2016).

In conclusion, laboratory studies focusing on the effects of AC magnetic fields on fish behavior demonstrate that fish either do not easily detect or do not alter their behavior in response to magnetic fields produced by 50/60-Hz AC cables. Moreover, when the magnetic field is increased high enough to affect fish behavior (i.e., over 1,000,000 mG, which is orders of magnitude higher than levels calculated for the SRWEC), the behavioral effects were observed to be small and reversible, indicating that even these are unlikely to result in population-level effects. Furthermore, field surveys at submarine AC cable sites demonstrated that 60-Hz magnetic fields do not significantly affect fish distributions under field conditions.

5.4 AC Electrosensitivity of Sturgeon Species

Basov (1999) tested the detection abilities and behavioral responses to 50-Hz AC electric fields using two sturgeon species—sterlet (*Acipenser ruthenus*) and Russian sturgeon (*Acipenser gueldenstaedtii*). Exposure to 20 mV/m electric fields resulted in the detection of electric fields by sturgeon. Avoidance behavior was reported only when the electric field exceeded 60 mV/m near the power source (Basov 1999).

5.5 Interactions of DC and AC EMF from Proposed Project Cables with Finfish

The magnetic fields calculated for projected DC cable configurations are presented in Table 6. At peak loading of a cable buried to 3.3 ft (1 m), magnetic-field deviations were calculated to be 392 mG at the seabed (total field of 898 mG), decreasing to 104 mG (total field of 610 mG) at 3.3 ft (1 m) above the seabed. This maximum value is less than half of the 2,000 mG magnetic field that was demonstrated to affect sea bream orientation (Tanski et al., 2011). This calculated level is also far less than the 10,000 mG static magnetic field that had no significant effect on juvenile Atlantic sturgeon swim behavior (McIntyre et al., 2016). Perhaps most important to the use of the geomagnetic field by fish is that to the extent the static magnetic field sensors of fish rely upon the horizontal component of the geomagnetic field, the maximum calculated change to a fish compass within 10 ft (3 m) of the SRWEC centerline, is approximately 9 degrees or less (Attachment C, Table C-22).

In addition to magnetic-field levels, induced electric-field strengths were calculated based on the Atlantic sturgeon model using a swim speed of 1 ft/s (30 cm/s) (Table 6).[16] Atlantic sturgeon was modeled as an ellipsoid 6 ft (1.8 m) in length with a maximum girth of 2.5 ft (0.8 m).[17] The calculated DC induced electric field for the sturgeon model is estimated to be 0.03 mV/m at peak loading of the buried cable. Modeled induced electric fields in seawater at the seabed is predicted to be 0.054 mV/m at peak loading.

---

[16] http://www.fsl.orst.edu/geowater/FX3/help/9_Fish_Performance/Fish_Length_and_Swim_Speeds.htm

[17] Girth was determined using a standard length-girth-weight relationship for the related lake sturgeon (http://files.dnr.state.mn.us/areas/fisheries/baudette/lksweight.pdf).

The magnetic fields calculated based on projected AC cable configurations and burial depths are also presented in Table 6. At peak loading, AC magnetic-field levels were calculated to be 61 mG at the seabed, decreasing to 4.6 mG at 3.3 ft (1 m) above the seabed directly over the cable. This maximum value is approximately 12 percent of the 500 mG magnetic field that was reported to have no behavioral effects on either Atlantic salmon or American eel (Richardson et al., 1976). Field strengths associated with significant changes in fish behavior are multiple orders of magnitude higher (i.e., 1,657,800 mG for redear sunfish) than those expected at the Project cables.

Table 6.　　Calculated maximum magnetic fields and induced electric fields (using sturgeon model) at the seabed and 3.3 ft (1 m) above the seabed for 3.3-ft (1 m) burial depth and peak loading

Cable Type (Field Type)	Magnetic Field (mG)		Induced Electric Field (mV/m) at the Seabed	
	Seabed	3.3 ft (1 m) Above the Seabed	Seawater	Sturgeon Model
SRWEC (Total DC: Cable + Earth)	898	610	0.054	0.03
IAC (AC)	61	4.6	1.0	0.74

In addition to magnetic-field levels, induced electric-field strengths for AC cables were calculated based on an Atlantic sturgeon model (Table 6 above). The calculated value for cables buried to a depth of 3.3 ft (1 m) is estimated to be 0.74 mV/m at peak loading. This maximum calculated induced electric-field strength is significantly lower than the 20 mV/m electric field reported as the detection threshold in Russian sturgeon and sterlet (Basov et al., 1999). Modeled induced electric fields in seawater (1.0 mV/m) are also well below this detection threshold (Table 6).

6.0　Evaluation of EMF Interactions with Elasmobranchs at IACs and SRWEC

Elasmobranchs are cartilaginous fish, and the taxonomic group includes skates, sharks, dogfish, and rays, all of which are common inhabitants of the coastal marine environments where the SRWF and SRWEC are proposed. Elasmobranchs exhibit both magnetosensitivity and electrosensitivity. Like fish and invertebrates, the magnetosensitivity of elasmobranchs allows them to utilize changes in the geomagnetic field to guide migrations. Tagging studies conducted with hammerhead sharks (*Sphyrna lewini*) found that individuals preferentially traveled along areas that coincided with boundaries between different natural geomagnetic gradients, indicating that detection of geomagnetic field variations allows this species to orient during migration and foraging (Klimley 1993). In addition, these species' ability to detect low frequency (approximately 1 to 10-Hz) electric fields is thought to assist in the capture of prey over small distances (Bedore and Kajiura, 2013).

Approximately 14 different shark, skate, and dogfish species are expected to inhabit parts of the proposed SRWF and SRWEC at some point in the year (Table 7). However, some of these, such as the large pelagic sharks, exhibit large ranges across shallow coastal areas and deep oceanic waters; therefore, the SRWF and SRWEC constitutes a minor portion of the total habitat. Conversely, smaller benthic elasmobranch species like skates and dogfish can have small ranges, and due to their position in the water column, these species may be more likely to come into more frequent contact with the cable routes.

Table 7.   Elasmobranch species projected to inhabit the SRWF and/or SRWEC

Species	Demersal, Pelagic, or Other (as noted)[1]	Size at first reproduction, (cm)[1]	Common length (cm)[1]
Barndoor skate (*Dipturus laevis*)	Demersal/ Benthic	NR	NR (163 cm max length)
Basking Shark (*Cetorhinus maximus*)	Pelagic	500	700
Blacktip Shark (*Carcharhinus limbatus*)	Reef-associated	120	150
Blue Shark (*Prionace glauca*)	Pelagic	206	335
Clearnose Skate (*Rostroraja eglanteria*)	Demersal	49	NR (84 cm max length)
Common Thresher Shark (*Alopias vulpinus*)	Pelagic	303	450
Dusky Shark (*Carcharhinus obscurus*)	Pelagic	220	250
Little Skate (*Leucoraja erinacea*)	Demersal/Benthic	32	NR
Porbeagle Shark (*Lamna nasus*)	Pelagic/Oceanic	175	244
Sand Tiger Shark (*Carcharias taurus*)	Pelagic	220	250
Sandbar Shark (*Carcharhinus plumbeus*)	Benthopelagic	126	200
Shortfin Mako Shark (*Isurus oxyrinchus*)	Pelagic	278	270
Smooth Dogfish (*Mustelus canis*)	Demersal/Benthic	102	100
Spiny Dogfish (*Squalus acanthias*)	Demersal/Benthic	81	100
Tiger Shark (*Galeocerdo cuvieri*)	Pelagic/Benthopelagic	210	500
White Shark (*Carcharodon carcharias*)	Pelagic	450	NR
Winter Skate (*Leucoraja ocellata*)	Demersal/ Benthic	73	NR

[1] Information from fishbase.org

6.1 DC Magnetosensitivity of Elasmobranchs

Elasmobranch fishes, which are closely related to sturgeons, are both magnetosensitive and electrosensitive and have been documented to be sensitive to static magnetic fields. For instance, sandbar sharks (*Carcharhinus plumbeus*) have been reported to respond to static magnetic-field deviations at intensities between 25 and 100 μT (250 and 1,000 mG; for an approximate 750 and 1,500 mG total magnetic field) (Nestler et al., 2010). More recently, however, Anderson (2018) found that sandbar sharks were able to detect lower static magnetic-field deviations of 2.8 μT (28 mG, for an approximate 528 mG total magnetic field). Exposed sandbar sharks exhibited a significant increase in the number of swimming passes when first introduced to the magnetic field (Anderson 2018).

In addition to laboratory studies, field studies and surveys can be used to assess the ability of elasmobranchs to detect the magnetic fields produced by DC submarine cables. Hutchison et al. (2018, 2020) examined the effect of DC submarine cables on the behavior of skates that were placed in cages in the field; this approach allows for more realistic conditions than laboratory studies. Skates in both control cages and cages placed above DC cables with a total field of 653 mG spent the majority of the time at the ends of the cage, referred to by authors as the *"end effect"* (Hutchison et al., 2020). This led researchers to remove data related to time spent in the outer edges and focus solely on the time spent in the center area. When in the center of the cage, skates exposed to the DC cable travelled significantly more, exhibited a greater proportion of large turns, and swam significantly closer to the seabed as compared to skates in control cages (Hutchison et al., 2018, 2020).

This suggests that total static magnetic-field levels of 653 mG can elicit measurable behavioral changes in elasmobranchs when adjacent to the source. However, the strength of the end effect may be a factor that complicates the extrapolation of findings from caged studies to field populations.

Six years of biological surveys along the MARS cable off the coast of California revealed only one significant effect of the cable on resident elasmobranch species. In 2008, a notable aggregation of longnose skates (*Raia rhina*) was observed at the cable (Kuhnz et al., 2015). However, this occurred prior to cable energization, so any skate reaction would have been due to the physical presence of the cable and not the EMF generation by power transmission. The operating cable was not observed to have a similar effect on any resident elasmobranch species (Kuhnz et al., 2015).

6.2 DC Electrosensitivity of Elasmobranchs

The majority of studies conducted to determine the potential impacts of EMF on elasmobranch behavior have focused on sensitivity to electric fields. Comparing the general responses of elasmobranchs to AC and DC electric fields, Newton et al. (2019) noted that these species' electroreceptors are capable of detecting DC electric fields, but that the receptor response diminished quickly after the initial stimulus. However, responses to low frequency (less than 15- Hz) AC stimuli are more consistent, which is not surprising given the similarity to natural bioelectric fields produced by prey items (Newton et al., 2019).

Bedore and Kajiura (2013) reported the electric-field sensitivity for several species of elasmobranchs and the maximum distance over which the field is sensed. DC electric-field sensitivities ranged from 5 nanovolts per centimeter (nV/cm)[18] to 48 nV/cm at maximum distances between 22 and 40 cm when produced by a static power source. The authors then assessed the bioelectric signals from potential prey items and determined that this range of detection sensitivities allows for elasmobranch predators to locate nearby prey items (Bedore and Kajiura 2013). The common shovelnose ray (*Glaucostegus typus*) and Eastern shovelnose ray (*Aptychotrema rostrata*) were tested for electrosensitivity in experimental laboratory tanks fitted with electrodes connected to a DC battery source (Wueringer et al., 2012). An analysis of ray behavior in the vicinity of energized electrodes found that the electric field elicited changes in behavior, including attacks at active dipoles. The authors reported that the median DC electric-field strength at the point of response initiation ranged between 5.15 nV/cm and 79.62 nV/cm for the two species of rays tested; detection ability seemed to differ with type of electrode (Wueringer et al., 2012). Bedore et al. (2014) compared the relative electrosensitivity of two ray species with different numbers of electrosensory pores—yellow stingrays (*Urobatis jamaicensis*) and cownose rays (*Rhinoptera bonasus*). Despite having a higher number of these pores, cownose rays were less sensitive than yellow stingrays, with detection sensitivity at 107 nV/cm and 22 nV/cm, respectively. The authors theorized that the schooling cownose rays may benefit from a lesser sensitivity given that they frequently swim surrounded by conspecifics (Bedore et al., 2014).

Neonatal bonnethead sharks (*Sphyrna tiburo*) were determined to be sensitive to electric fields produced by a static source. More than 30 percent of observed orientations occurred at fields of 20 nV/cm or less, and the median stimulus threshold for orientation change was 47 nV/cm (Kajiura 2003). Similar to other studies, the minimum field at which a change in shark detection was observed was 1 nV/cm. In addition, both juvenile scalloped hammerhead *(Sphyrna lewini)* and sandbar sharks were observed to have similar levels of sensitivity to electric fields generated by a static source, as they both altered orientation within their tanks in response to a 20 nV/cm electric field (Kaijura and Holland 2002).

Gill and Taylor (2001) examined the electrosensitivity of field-collected lesser spotted dogfish (*Scyliorhinus canicular)* under laboratory settings. Electric fields of 1000 μV/cm produced by a static power source caused

---

[18]   1 nV/cm = 0.0001 mV/m

avoidance behaviors, although these behaviors were observed to be highly variable among tested individuals. However, lower electric fields that approximate those emitted by dogfish prey (i.e., 0.1 μV/cm within 10 cm [4 inches] of the source) resulted in attraction of individuals (Gill and Taylor 2001). The ability of spiny dogfish (*Squalus acanthias*) and smooth dogfish (*Mustelus canis*) to detect electric fields from a static magnetic-field source were determined to be similar; median response field strengths were 14 nV/cm and 29 nV/cm, respectively (Jordan et al., 2011). However, the authors noted that the types of behavioral responses differ between species and appeared to be dependent on the presence of other sharks.

6.3 AC Magnetosensitivity and Electrosensitivity of Elasmobranches

Laboratory assessments of elasmobranch EMF detection abilities have largely focused on low frequency (~10 Hz or less) sources, most likely because prey items produce bioelectric fields within this range. There is additional evidence that as the frequency of the EMF source approaches 20 Hz, elasmobranch detection ability decreases with increasing frequency. Andrianov et al. (1984) found that an increase in EMF source frequency from 1 Hz to 10 Hz caused a 100-fold decrease in the detection threshold of skates (i.e., a recorded increase of 0.01 mV/m to 1 mV/m). Similarly, shark embryos exhibited the strongest behavioral responses to electric fields produced at frequencies of 0.1 to 2 Hz, with decreasing sensitivity as source frequency was increased to 20 Hz, at which point no responses were observed (Kempster et al., 2013). When higher frequencies were tested, no behavioral responses were observed for catshark (*Cephaloscyllium isabellum)* when exposed to magnetic fields up to 14,300 mG produced by a 50-Hz source (Orr 2016). Catsharks were exposed for 72 hours, during which time the authors noted no significant behavioral changes, and the introduction of an olfactory stimulus still resulted in normal foraging behaviors; this provides evidence that 50-Hz magnetic fields did not interfere with the normal behavioral response to this stimulus (Orr 2016). Thus, laboratory studies demonstrate that elasmobranchs are unlikely to detect EMF produced by 60-Hz AC cables.

Love et al. (2016) focused part of a multi-year survey to specifically address possible effects on elasmobranchs along unburied AC submarine cable sites off the coast of California. It was noted that the selected study area contained a high diversity of elasmobranchs, and thus constituted an appropriate area for addressing these potential changes in elasmobranch distribution. Based on the collected data, researchers determined that there was no evidence *that "energized power cables in this study were either attracting or repelling these fishes [Elasmobranchs]."* Because of this, the researchers concluded that *"energized cables are either unimportant to these organisms [Elasmobranchs] or that at least other environmental factors take precedence"* (Love et al., 2016). In contrast, a mesocosm study conducted off the Scottish coast with three elasmobranch species—thornback ray (*Raja clavata*), spurdog (*Squalus acanthias*), and lesser-spotted dogfish (*Scyliorhinus canicular*)—reported variable results. Mesocosms were constructed over cables supplied with AC 50-Hz power produced by an electric inverter; the resulting magnetic field was estimated to be 80 mG. While some significant responses of benthic elasmobranchs were observed, these were not consistent among trials or individuals. For instance, during one trial, dogfish were significantly more likely to be within 6.6 ft (2 m) of a switched-on cable at night, but not during the day, but these results were not duplicated in the subsequent trial (Gill et al. 2009). This led authors to conclude that although there was some evidence of elasmobranchs responding to the produced EMF, these responses varied both *"within a species and also during times of cable switch on and off, day and night"* and that ultimately elasmobranch responses were *"not predictable and did not always occur"* (Gill et al., 2009). Overall, the bulk of the available evidence suggests that 50/60-Hz EMF are unlikely to be reliably detected by populations of benthic elasmobranchs and therefore will not result in behavioral changes or adverse biological effects. In contrast to finfish, less is known about the potential effects of 50/60-Hz submarine AC power cables on the behavior, distributions, and populations of elasmobranchs.

6.4 Interactions of EMF from DC and AC Proposed Project Cables with Elasmobranchs

Sandbar sharks were observed to react to static magnetic-field deviations of 28 mG when switched on and off in a laboratory setting (Anderson 2018). However, it is unclear whether this type of exposure is an appropriate model of expected field exposures from a submarine cable since the rapid transient change in the magnetic field will induce a far larger transitory peak electric field than from a constant or less rapid field changes from 50/60-Hz AC magnetic fields. Evidence from field studies under more realistic exposure scenarios indicate that exposure to a 520 mG to 653 mG static magnetic field caused measurable changes in elasmobranch activity, swim behavior, and positioning (Hutchison et al., 2020). These values are slightly below the maximum value at the seabed calculated for a buried DC cable at peak loading (898 mG) and approximately equivalent to the value calculated at 3.3 ft (1 m) above the seabed (610 mG), indicating that benthic elasmobranchs that swim directly over the SRWEC route may be able to detect and respond to SRWEC magnetic fields. Evaluations of EMF interactions of marine species at the Landfall HDD are addressed in Section 8.

Table 8.   Calculated maximum DC and AC magnetic fields and induced electric fields (using dogfish model) at the seabed and 3.3 ft (1 m) above the seabed for 3.3 ft (1 m) burial depth and peak loading

	Magnetic Field (mG)		Induced Electric Field (mV/m) at Seabed[*]	
Cable Type (Field Type)	**Seabed**	**3.3 ft (1 m) above seabed**	**Seawater**	**Dogfish Model**
SRWEC (Total DC: Cable + Earth)	898	610	0.054	0.019
IAC (AC)	61	4.6	1.0	0.39

* Assuming an ocean current velocity of 2 ft/s (60 cm/s) and a dogfish swimming velocity of 0.69 ft/s (21 cm/s).

Catsharks exposed to 14,300 mG, 50-Hz magnetic fields under laboratory conditions showed no altered behaviors, suggesting that these levels were not detectable by elasmobranchs (Orr 2016). Evidence from mesocosm studies indicates that some, but not all, exposed elasmobranchs may alter behavior in response to 80 mG, 50-Hz magnetic fields, and that responses are unpredictable and do not consistently occur. The maximum magnetic-field levels calculated at 3.3 ft (1 m) above the seabed for the proposed buried IAC cable is 4.6 mG at peak loading but increases to 61 mG at the seabed (However, field studies suggest that magnetic fields up to 1,100 mG produced by a 60-Hz AC cable had no observable impact on elasmobranchs in an ocean environment (Love et al., 2016). Considered in concert, these results suggest that the AC magnetic fields associated with the buried Project cables likely would not be consistently detectable by resident elasmobranch populations, though there is a chance that some individuals of some species might respond under the most conservative scenario (at the seabed immediately over the cable during peak loading).

6.4.1 DC Electric Fields Induced by Movement in Static Magnetic Fields

A dogfish was used as a representative model to estimate the DC electric fields induced as a result of movement through DC magnetic fields, wherein the dogfish is approximated as an ellipsoid with a length of 3.3 ft (1 m) and a maximum girth of 1.25 ft (0.4 m) (see Table 8). Swim speed was estimated to be 0.7 ft/s (21 cm/s), based on data presented by Fish and Shannahan (2000). Induced DC electric fields in a fish model were estimated to be 0.021 mV/m for dogfish swimming at the seabed and 0.059 mV/m in seawater caused by a bottom 2 ft/s (60 cm/s) (Oliver et al., 2012) current moving across the cable route. In contrast, behavioral responses of elasmobranchs are generally observed to be in the range of 20 nV/cm (0.002 mV/m) (Kaijura and Holland 2002; Kaijura 2003). Based on these comparisons, a model dogfish would be able to detect electric fields from ocean currents or by swimming through the geomagnetic field alone or with changes in the

static magnetic field produced by the Project cables. The mere detection of the electric field, however, as indicated by measurable and statistically significant responses of skates (Hutchison et al., 2018, 2020) did not result in the skates being more likely to spend time in areas adjacent to the cable.

6.4.2 Induced AC Electric Fields In Dogfish Model

Induced AC electric fields were again estimated using a dogfish model generated as an ellipsoid with a length of 3.3 ft (1 m) and a maximum girth of 1.25 ft (0.4 m). The scientific literature indicates that elasmobranchs are capable of detecting a 1 mV/m electric field produced by a 10-Hz power source (Andrianov et al., 1984), but detection abilities of elasmobranchs also rapidly decline as the frequency of the source increases above 20 Hz (Kempster et al., 2013). Given this diminishment of detection ability with frequency, it is not expected that resident elasmobranchs in the SRWF and/or IAC would be capable of detecting the induced electric fields from the 60-Hz IAC calculated for seawater or a model dogfish.

7.0 EMF Sensitivity of Sea Turtles and Marine Mammals

Marine mammals and sea turtles are federally- and state-protected groups of aquatic species and are widely distributed along the Atlantic coast. Marine mammals include dolphins, whales, and seals and are all protected under the Marine Mammal Protection Act. Sea turtles that may inhabit the SRWF and/or SRWEC are listed under the Endangered Species Act. All of these species surface to breathe air and many exhibit large migratory ranges.

There is evidence that sea turtles can detect changes in the geomagnetic field to assist in long-term migrations. For instance, researchers noted that variability in the geomagnetic field has been demonstrated to predict genetic differences between loggerhead sea turtles (*Caretta caretta*) at different nesting beaches (Brothers et al., 2018). Similarly, Nyqvist et al. (2020) reviewed the evidence for magnetosensitivity in multiple types of marine organisms including marine mammals and sea turtles. Homing paths of green sea turtles (*Chelonia mydas*) with manipulated magnetic-field sensing abilities were observed to be significantly longer, indicating that homing behaviors are at least partially governed by magnetic sense (Luschi et al., 2007, as cited in Nyqvist et al., 2020). Juvenile loggerhead sea turtles also have been observed to use geomagnetic cues while undergoing migration (Goff et al., 1998, as cited in Nyqvist et al., 2020). These findings suggest that geomagnetic cues allow migrating sea turtles to successfully travel to nesting and foraging areas, though this research provides limited insight concerning the significance of localized anthropogenic magnetic fields. Recent research has suggested that magnetic sense does not guide fine-scale movements for turtles but is instead used on a *"coarse scale,"* with frequent and large deviations (Hays et al., 2020). This would suggest that localized artificial magnetic fields would not be disruptive to these migrations.

The evidence that marine mammals detect the geomagnetic field is much weaker. Observations of migrating fin whales (*Belaenoptera physalus*) off the US Atlantic coast coincided with an area of low geomagnetic signals, suggesting that individuals use signals from the earth's geomagnetic field to guide migration paths (Walker et al., 1992, as cited in Nyqvist et al., 2020). This raised the hypothesis that, like sea turtles, some migrating marine mammals might use the geomagnetic field during long-distance movements. Moreover, it has been hypothesized that geomagnetic storms may be correlated to marine mammal stranding events (Ferrari 2016). Although laboratory studies with marine mammals are difficult to conduct due to size and protected status, captive bottlenose dolphins (*Tursiops truncates*) were exposed to a 0.051 T to 0.24 T (510,000 mG to 2,400,000 mG) static magnetic field to determine if these species were magnetosensitive.

While responses were somewhat individualized, overall, there was no significant effect on time spent in proximity to the magnetic-field source, number of contacts, or duration of contacts; however, the time to approach the magnetic-field source was significantly shorter versus the control device, indicating some sensitivity to magnetic fields (Kremers et al., 2014). These authors concluded that it was unclear if, or to what degree, dolphins could detect lower intensity anthropogenic magnetic fields (Kremers et al., 2014).

Marine mammals and sea turtles are unlikely to have high or prolonged exposure to EMF produced by submarine cables. First, they are unlikely to encounter or spend prolonged time at the SRWF or along the SRWEC route given their wide distribution and large migratory ranges. Second, since these animals breathe air, they will periodically surface, so even individuals foraging on the seabed will frequently move into the pelagic environment to access air.

8.0 Evaluation of EMF Interactions with Hardground-Associated Species and at Landfall

The installation of vertical and hardground structures at an offshore wind farm can create new habitat for some marine species. Artificial structures, including offshore platforms, footings, and concrete mattresses or rock berms, can be utilized as important habitat for reef and hardground-associated species (Petersen and Malm 2006; Quigel and Thornton 1989), especially when installed in areas dominated by soft sediment bottoms and with limited hardground areas. It is important to note that this attraction occurs independently of cable-associated EMF, and thus the exposure of reef-associated species to EMF produced near vertical and hardground structures is expected to be different than that of species migrating across the transmission cable route. In this Project, the vertical and hard ground structures include the OCS–DC, WTGs, and mattress-covered cables. To evaluate the potential effects of the longer time that hardground species may spend around these structures, the scientific literature on extended DC and AC EMF exposure to invertebrates and fish was reviewed.

8.1 Studies of extended DC magnetic-field exposures on invertebrates

Limited research is available concerning the physiological effects associated with extended exposures of invertebrates to artificial static magnetic fields. However, the available research indicates effects are unlikely below 30 mT (300,000 mG). Bochert and Zettler (2004) exposed several marine invertebrate species to a static magnetic field of 3.7 mT (37,000 mG) for multiple weeks—including blue mussel (*Mytilus edulis*), North sea prawn (*C. crangon*), glacial relict isopod (*S. entomon*), round crab (*R. harrisii*), and *Sphaeroma hookeri* isopods—and determined that there was no effect on survival. Even a 3-month exposure did not alter reproductive measures and endpoints in blue mussel. Conversely, exposure to a higher static magnetic field (30 mT; 300,000 mG) did alter the development of the purple sea urchin (*Strongylocentrotus purpuratus*) and painted sea urchin (*Lytechinus pictus*) embryos (Levin and Ernst 1997). A 26-hour exposure reduced the hatching rate of fertilized embryos, and an increased rate of deformations were observed in the painted sea urchin embryos exposed for 2 to 3 days. More recently, egg-bearing female lobsters (*H. gammarus*) and crabs (*C. pagurus*) were exposed to a 2.8 mT (28,000 mG) static magnetic field throughout the egg developmental period; both larval and egg metrics were recorded. Both lobster and crab egg volumes exhibited different volumes versus non-exposed eggs during the development: lobster eggs exposed to the magnetic field were

initially larger than control eggs, but then found to be smaller, while exposed eggs were consistently smaller until the final stage, at which point they significantly exceeded the size of control eggs (Harsanyi et al. 2022). In addition, lobster and crab larvae hatched from magnetic field -exposed eggs exhibited physiological changes including reduced length and eye diameters.

Field-collected blue mussels (*M. edulis*) were exposed to a 3000 mG static magnetic field to assess potential impacts of feeding rate. Researchers determined that the exposure did not alter filtration rates or the valve angle or activity, leading them to conclude that there were no effects of EMF exposure on mussel feeding (Albert et al 2022). Similarly, cockles (*Cerastoderma glaucum*) were exposed to 64,000 mG and observed for effects on food consumption, growth, respiration, and excretion. Food consumption was reduced during the exposure, which affected the organisms' energy budget, but other endpoints were unaltered (Jakubowska-Lehrmann et al. 2022).

8.2 Studies of extended DC magnetic-field exposure on finfish

A number of laboratory studies examined the possible deleterious effects of extended static magnetic-field exposure on various life stages and species of fish. Many of these have focused on early life stages and embryos, as these are generally considered the most sensitive life stages; as such, these would provide a conservative estimate of potential effects. Rainbow trout embryos were exposed to 3 mT (30,000 mG) static magnetic fields for 17 days, over which time the researchers observed and measured development (Woodruff et al., 2012). Although fertilization rates and days until hatch were unaffected by magnetic-field exposure, increased rates of developmental abnormalities were observed during later stages of embryonic development. However, the authors reported that this difference, although significant, was *"extremely small"* leading to the conclusion that exposure to lower levels of magnetic fields would be unlikely to result in any developmental effects (Woodruff et al., 2012). A similar extended 7- to 27-day exposure of Atlantic halibut larvae produced no statistically significant difference in developmental score or standard length. While the mortality trends over time did differ for Atlantic halibut larvae exposed to magnetic fields, the higher degree of mortality is not outside the generally-accepted range for flatfish larvae (Woodruff et al., 2012). Furthermore, studies with larval California halibut found no effects of a 12-day exposure to 3 mT (30,000 mG) magnetic fields on developmental parameters (Woodruff et al., 2012).

Loghmannia et al. (2015) exposed Caspian kutum (*Rutilus frisii kutum*) fry to static magnetic fields (2.5 mT to 7.5 mT; 25,000 mG to 75,000 mG) over 1- and 3-week periods and examined the effects on enzymes concentrations. Enzymes indicative of organ lesions were increased following the 1-week exposure, while immune function indicators were decreased at exposures to 5.0 mT and 7.5 mT (50,000 mG and 75,000 mG). Three-week exposure indicated more mixed effects on lesion indicators, but a similar response for the immune function indicators (Loghmannia et al., 2015). Similarly, Japanese rice fish embryos were exposed to a 100 mT (1,000,000 mG) static magnetic field during development to ascertain possible effects on early life stages, as determined by rates of deformities and characteristics of the growth cycle. However, following a 15-day exposure to the magnetic field, no statistically significant effects on embryonic development were observed (Sun et al., 2019). Brown trout and rainbow trout embryos exposed to static magnetic fields (2.5 mT to 13 mT; 25,000 mG to 130,000 mG) for up to 15 days exhibited longer embryonic development periods that resulted in larger larvae (Formicki and Winnicki 1998). In addition, heart rhythms of magnetic-field exposed embryos and larvae were significantly increased compared to non-exposed fish; however, in larvae this was preceded by a period of slowed heartbeat. Putman et al. (2014) cultivated juvenile steelhead (rainbow) trout in a distorted magnetic field under laboratory conditions for almost 1 month to determine whether this had long-term impacts on migratory and homing ability. The distorted magnetic-field intensity was similar to that of controls (between 40 µT and 55 µT [400 mG to 550 mG]), but juveniles reared under a distorted field were found to demonstrate an inability to orient to natural magnetic fields in the same way as the control fish.

However, while this may have implications for the location of fish hatcheries, it is unlikely that magnetic fields at mattressed submarine cable sites would present this type of prolonged exposure to large field populations of developing fish embryos, and juveniles, including those species near the OCS–DC and mattressed portions of the SRWEC, such as winter flounder and Atlantic herring that may deposit eggs on bottom substrates.

Finally, Fey et al. (2019) investigated the possible effects of static magnetic-field exposure on the embryonic development of northern pikeminnow (*Esox lucius*). The embryos and developing larvae of this species are found adhered to submerged substrates and are thus relevant to extended exposures at the OCS–DC and mattressed portions of the SRWEC. Exposure to a 10 mT (100,000 mG) static magnetic field during the first 6 days post hatching had no significant effects on hatching success, larval mortality, size at hatch, and growth rate. Conversely, exposed embryos hatched earlier and exhibited a faster absorption of yolk sacs; however, the authors reported that these effects seemed to have negligible effects for larval mortality risk or fitness (Fey et al., 2019).

The potential effects of an extended exposure to static magnetic fields on juvenile and adult fish physiology, behavior, and reproductive capacity has been studied in the laboratory. Preliminary studies on the effects of magnetic fields on salmonid melatonin and cortisol levels demonstrated variable effects of exposure to static magnetic fields on these physiological endpoints. The cortisol levels of juvenile coho salmon (*Oncorhynchus kisutch*) were unaffected by exposures to static magnetic fields between 0.1 mT and 3 mT (1,000 mG and 30,000 mG); however, melatonin levels were affected by these static magnetic-field exposures. Eighty-hour exposures to these field strengths significantly reduced nighttime melatonin levels in fish (Woodruff et al., 2012). Concentrations of cortisol, glucose, estradiol, and progesterone in zebrafish were observed to be significantly altered following 1- to 3-week exposures to static magnetic fields of 2.5 mT to 7.5 mT (25,000 mG to 75,000 mG (Sedigh et al., 2019). This led the authors to hypothesize that exposed fish exhibited a stress-response, given the increase in observed cortisol and glucose and concurrent decreases in sex hormones. They concluded that at higher intensities and longer exposures, there could be a disruption in the reproductive physiology of the fish (Sedigh et al., 2019).

In addition, a series of laboratory studies were conducted with juvenile coho salmon to determine if exposure to static magnetic fields disrupted the species' behavioral response to an alarm substance. Fish were exposed to 3 mT (30,000 mG) magnetic fields for periods ranging between 1 and 14 days, but no change in the rate of alarm response behavior was observed in response to magnetic-field exposure (Woodruff et al., 2012). Similar studies conducted with smaller juvenile coho salmon resulted in the same determination of no magnetic-field effect on alarm response behaviors. Finally, Brewer (1979) exposed several generations of guppy (*Lebistes reticulatus*) to a 500-Gauss (500,000 mG) magnetic field produced by a static source. By the third generation of exposed fish, no fertilization or spawning took place; however, when these fish were removed from the magnetic field, they produced a small fourth generation cohort (Brewer 1979). Despite the observed sterility of fish in the third generation of exposure, fish were significantly larger than control third generation fish, and exhibited increased lifespans.

8.3 Studies of extended AC magnetic-field exposure on invertebrates

A series of studies were conducted to describe the effects of AC-generated EMF on the embryonic development of purple sea urchins. Levin and Ernst (1995) examined the timing of embryonic cell division during exposure to AC magnetic fields. A field strength of 3.4 mT (34,000 mG) changed the timing of cell division in developing embryos over the approximate 36-hour embryonic development time, but when the field strength was reduced by 50 percent, embryonic cell division rates were unchanged versus unexposed controls (Levin and Ernst 1995). More important, neither exposure caused an increase in embryonic mortality; however, minor developmental effects were observed in the purple sea urchin embryos when exposed to 500

mG and 1,000 mG 60-Hz magnetic fields during embryonic development up to 48 hours (Cameron et al., 1993; Zimmerman et al., 1990).

Though these studies suggest some physiological effects in developing invertebrate embryos exposed to AC magnetic fields, these are not expected to occur under field conditions indicated in the SRWF. Invertebrate embryos are passively dispersed and experience naturally high mortality rates, meaning that the minor developmental delays observed during certain exposures to AC EMF under laboratory conditions would have no population-level impacts in the field. That mortality rates were unaffected by EMF and normal development was re-established following removal from EMF underscores the lack of significant physiological effects on invertebrate embryos. Even when embryos are not passively distributed, such as squid eggs deposited on the seabed, the field strengths reported to produce physiological effects are much higher than calculated cable-related EMF in this Project and the proportion of eggs likely to be exposed on the sedimented cable route will be miniscule. Moreover, recent research focused on potential effects of AC EMF on the behavior and physiology of small sediment-dwelling worms, but overall, these researchers concluded that these organisms are not affected by such exposures (Jakubowska et al., 2019; Stankevičiūtė et al., 2019).

8.4 Studies of extended AC magnetic-field exposure on fish

Evidence from laboratory studies largely suggests that exposure to AC EMF does not affect developmental endpoints of fish. Early life stage studies can be considered a conservative assessment of the effects of Project-associated EMF on fish development and growth, given that these life stages tend to be more sensitive to stressors. Moreover, because most fish eggs and larvae exhibit high natural mortality and passively float throughout the water column, extended exposure of these life stages to EMF is unlikely. However, information from laboratory studies of fish embryos and larvae exposed to AC magnetic fields provides some insight as to potential magnitude of effects from extended exposure. For instance, a 48-hour exposure to a 60-Hz, 1,000 mG magnetic field was found to prolong the embryonic development of Japanese rice fish, but had no observed significant effects on hatching rate, physical abnormalities, or survival (Cameron et al., 1985). The observed delay in embryonic development was approximately 18 hours, and therefore was not considered likely to cause long-term, population-level effects. Likewise, zebrafish embryos exposed to a 50-Hz, 10,000 mG magnetic field during the embryonic developmental stage (up to 48 hours) also exhibited similar developmental delays (Skauli et al., 2000). Recently, Fey et al. (2019) found that a 36-day exposure to 50-Hz magnetic fields at a level of 1 mT (10,000 mG) did not significantly increase larval mortality rates or alter hatching time and larval growth; however, the rate of yolk sac absorption was increased. In terms of electric-field exposure, rainbow trout embryos, larvae, and fry exposed to electric fields between 5 mV/m and 5,000 mV/m were found to exhibit no significant developmental effects or reduction in survival, even after a 2-month exposure to these electric fields (Brouard et al., 1996). However, evidence of cytotoxic and genotoxic responses was observed in early life stage rainbow trout exposed to a 1 mT (10,000 mG) magnetic field from a 50-Hz source for 40 days, although survival rates were not affected by exposure (Stankevičiūtė et al., 2019).

In addition to studying developmental effects, a number of laboratory studies examined potential effects of extended exposure to AC magnetic fields on juvenile and adult fish; these largely demonstrate that effects are minor or only occur at levels not projected to occur under field conditions. Effects on brain histopathology were studied in young common carp (*Cyprinus carpio*) exposed to 50-Hz magnetic fields between 1,000 mG and 70,000 mG for 1 hour (Samiee and Samiee 2017); however, only exposures greater than 30,000 mG were observed to result in a significant increase in brain lesions and other histopathological changes. Conversely, Nofuzi et al. (2015) utilized a 60-day periodic exposure to examine the effects of 15-Hz magnetic fields between 1 mG and 500 mG on rainbow trout; this intermittent exposure may mirror expected exposures where fish may move in and out of a produced magnetic field under field conditions. Daily 1-hour exposure for 3 months resulted in increased growth and improved immune system activity in fish (Nofouzi et al., 2015).

Increased immune function was also reported by Cuppen et al. (2007), who exposed goldfish (*Carassius auratus*) to 200-Hz to 5,000-Hz magnetic fields between 1.5 mG and 500 mG for up to 27 days, resulting in decreased mortality of disease-challenged fish. Conversely, juvenile tilapia (*Oreochromis niloticus*) exposed for 1 month to magnetic fields between 300 mG and 2,000 mG produced by a 50-Hz source demonstrated reduced growth and lowered digestive enzyme activity. There was no notable trend of increased effects on growth, however, with increased magnetic-field strength, and the authors reported that recovery of digestive function improved following removal of fish from magnetic fields (Li et al., 2015).

8.5 Interactions of Finfish with Magnetic Fields at Proposed Project Structures

Hardground structures expected to be installed as part of the Project include concrete mattresses or rock berms along portions of the transmission cable route and structure foundations. Depending on the selected cable configurations, areas with concrete mattresses may be characterized by magnetic-field levels from either DC or AC sources that are higher than magnetic-field levels over more deeply buried cables. At the vertical and hard ground structures the magnetic fields also are calculated to be higher than fully buried cables and certain finfish species may spend more time at these structures. Calculations of expected magnetic-field levels for different areas and geometries are presented in Attachment D.

For SRWEC cables, the maximum volume averaged magnetic field was calculated to be 4,413 mG at the OCS–DC in the water column. In the scientific literature, effects to juvenile or adult fish are reported to occur at magnetic-field levels of approximately 25,000 mG and higher, and these include a series of generalized stress responses. Melatonin levels were slightly depressed by static magnetic-field exposures of 1,000 mG, but it is unclear if this constitutes an adverse effect.

For the IACs, the maximum volume-averaged magnetic-field level at the concrete mattresses at peak loading was calculated to be 147 mG. The maximum volume-averaged magnetic-field levels at the WTG, as well as magnetic-field levels at the OCS–DC for the monopile and jacket foundation types are summarized in Table 9, with additional details in Attachment C. The maximum volume averaged calculated AC magnetic field was <253 mG at the OCS–DC monopile. Given the information summarized above, juvenile and adult fish appear to be unaffected by magnetic fields of these intensities; adverse effects occurred after extended exposure to field levels more than 100 times greater than this maximum calculated volume averaged magnetic-field level. Moreover, while lower 50-Hz magnetic-field levels between 300 mG and 2,000 mG were associated with reduced growth in juvenile tilapia (Li et al., 2015), this occurred following a 1-month constant exposure.

Table 9.   Calculated maximum volume-averaged, magnetic-field levels (mG) for peak loading at different structure foundation types and mattress-covered cables*

Structure	AC Magnetic Field (mG)[†]	DC Magnetic Field (mG)[‡]
WTG Monopile	~81	N/A
OCS–DC at Seabed[§]	<253	<3,961
OCS–DC in Water Column	~183	<4,333
Cables with Protective Covering	147	<1,322

*   Volume averages are described in Attachment D.
‡   Actual DC field levels may be approximately 10% lower than these calculated values. See footnote 10.
†   Calculated AC values in this table may be approximately 3% higher than reported above. See footnote 11.
§   A OCS–DC monopile is not part of the current design, however, this configuration was used as a model for a conservative exposure scenario, which will produce higher volume-averaged field levels than the jacket foundation at seabed.

8.6 Evaluations of EMF Interactions at Landfall

For a short segment (up to approximately 3,200 ft [975 m]) of the cable route at landfall, the two DC cables will be separated into horizontally adjacent conduits and placed together in a single 55-inch bore hole installed via HDD. Although the lateral separation between the adjacent cables will be slightly greater where installed via HDD, and thus there will be a corresponding slight diminishment of the cancelling of fields that occurs when cables are installed together, this effect will largely be offset by the greater minimum burial depth.

Table 10 shows the calculated maximum total magnetic field (cable + earth) at the Landfall HDD for both peak and average loading and 6 ft and 46 ft (1.8 m and 14 m) burial depths (to the center of the HDD conduit)[19]. For a very small portion (less than 5%) of the HDD installation, the cables will be at a burial depth of approximately 6 ft (1.8 m), where the maximum total magnetic field at peak loading at the seabed surface was calculated to be 759 mG, decreasing to 631 mG at a height of 3.3 ft (1 m) above seabed. These levels are slightly above and approximately equivalent to total field levels associated with small-scale behavioral changes in caged lobsters (Hutchison et al., 2018, 2020). However, for the majority of the Landfall HDD installation the cables will be at a burial depth of 46 ft (14 m) or greater, where the total magnetic field level at both seabed and 3.3 ft above seabed was calculated to be 512 mG, which is only a 6 mG deviation from Earth's local geomagnetic field of 506 mG.

Table 10.   Calculated maximum total magnetic fields and induced electric fields for sturgeon at seabed for Landfall HDD Installation at peak and average loading and at 6 ft burial depth

EMF Levels at Landfall		Peak Loading		Average Loading	
		6 ft (1.8 m) burial depth	46 ft (14 m) burial depth	6 ft (1.8 m) burial depth	46 ft (14 m) burial depth
At seabed	Total Magnetic Field	759 mG	512 mG	641 mG	509 mG
	Induced Electric Field*	0.023 mV/m	0.015 mV/m	0.019 mV/m	0.015 mV/m
3.3 ft (1 m) above seabed)	Total Magnetic Field	631 mG	512 mG	573 mG	509 mG
	Induced Electric Field*	0.019 mV/m	0.015 mV/m	0.017 mV/m	0.015 mV/m

* Assuming a sturgeon swimming velocity of 0.98 ft/s (30 cm/s).

---

[19]   The cable configuration depicts the scenario where the southern cable is carrying current toward shore and the northern cable is carrying current away from shore.

Induced electric fields were calculated based on the Atlantic sturgeon swim speed of 1 ft/s (30 cm/s), and determined to be 0.023 mV/m or less at a 6 ft (1.8 m) burial depth and 0.015 mV/m or less at a 46 ft (14 m) burial depth. At average loading, these fields are expected to be 0.019 and 0.015 mV/m or less, respectively. These are below the reported sturgeon response range of 10 mV/m and 20 mV/m (Teeter et al. 1980). While some elasmobranchs can detect static electric fields as low as 0.002 mV/m (Kaijura and Holland 2002; Kajiura 2003), it should be reiterated that these have not been documented to cause long-term and/or detrimental attraction to or repulsion from the field source.

9.0 Evaluation of Biological Survey Data from Wind Farm Sites

Years of biological surveys have been conducted at existing offshore wind farm sites and data from these can be used to define overall effects on fish and invertebrate distribution and abundance. Artificial structures in coastal waters have been observed to act as fish aggregating devices, which results in an enhanced fish and invertebrate community in the vicinity of the structure. Niquil et al. (2018) describes two possible ecological benefits from these artificial structures: a reef effect, in which additional hard substrate provides habitat for hard-ground species, and a reserve effect[20] where the presence of windfarm structures creates a zone of reduced or limited boat traffic, resulting in a quieter area for fish to rest and congregate. Results from studies at operational wind farms strongly indicate that turbines and associated transmission cables have not reduced populations of fish and invertebrates, and in some cases demonstrated improvement in populations of certain hard-ground species.

In the United Kingdom spot measurements of EMF around 36-kV 50-Hz submarine cables from the Burbo Bank and North Hoyle wind farms were presented in an unpublished report (Gill et al., 2009) but no surveys of fish or other organisms around these windfarms were made.

Based on nearly a decade of pre- and post-operational data from the Horns Rev Offshore Wind Farm site near Denmark, researchers determined that there were *"no general significant changes in the abundance or distribution patterns of pelagic and demersal fish"* (Leonhard et al., 2011), including species similar to those expected to inhabit the SRWEC and/or SRWF, such as various flatfish species. Researchers did note an increase in fish species associated with hard-ground and vertical features, especially around WTG footings (Leonhard et al., 2011). Similarly, submarine transmission cables were determined to have *"little to no effect … on local fish communities"* based on a series of surveys conducted at the Wolfe Island Wind Farm site in Lake Ontario (Dunlop et al., 2016). Some short-term changes in fish and invertebrate abundance were noted at the Thorntonbank Wind Farm in Belgium; however, these were temporary and theorized to be the result of construction phase effects and not related to EMF produced by the operating cables (Vandendriessche et al., 2015). At the Nysted Wind Farm in Denmark, researchers noted some *"asymmetries in the catches"* but these effects were minor and not well correlated to cable energy loading (Vattenfall and Skov-og 2006).

A review of reef effects associated with offshore renewable energy projects documented the development of enhanced biological communities in these areas (Kramer et al., 2015). During the first few years of operation, these sites were found to function as artificial reefs, attracting fish like cod, eel, gobies, and other demersal species. Structures also supported a large number of benthic invertebrate prey items, like amphipods and crab, and so reserve effects have been hypothesized to improve adult fish survival in these areas (Kramer et

---

[20] The presence of windfarm structures allows for a zone of reduced or limited boat traffic, which creates a quieter area for fish to rest and congregate.

al., 2015). Similarly, a survey of established offshore wind farms in the Baltic Sea indicated that these structures had a positive effect on fish populations, likely resulting from the presence of encrusting sessile invertebrate on and around the structures (Andersson and Ohman 2010). Authors also noted a likely succession of different sessile and algal communities based on the age of the structure, indicating that communities are likely to mature and possibly increase in complexity. A lesser effect was reported in 7 years of surveys (4 baseline years and 3 operation years) of fish communities at the Lillgrund Wind Farm off the coast of Sweden found no overall impact on biodiversity or total fish abundance; however, the abundance of certain species, including sculpin and eel, were enhanced by the presence of the wind farm (Bergstrom et al., 2013).

A meta-analysis of 13 different studies of fish communities at offshore wind farm sites determined that finfish were consistently more abundant inside wind farm areas versus reference areas (Methratta and Dardick 2019). More specifically, fish species that benefited from the presence of wind farms included soft-bottom and complex-bottom fish; however, pelagic fish were not significantly enhanced by the addition of wind farms. Siting depth and age of the wind farm also impacted the fish communities present at wind farm sites. Most important, no negative population-level effects were identified through this meta-analysis (Methratta and Dardick 2019). Finally, acoustic monitoring of harbor porpoises at the Dutch Egmon aan Zee wind farm demonstrated that densities of porpoises were significantly higher within the operational wind farm site than in nearby reference areas (Scheidat et al., 2011). The authors hypothesized that an increased abundance of prey due to the reef effect of the WTG footings may have attracted the porpoises, or that exclusion of vessels may have created a safe zone preferentially inhabited by porpoises.

Installations of wind farms near Norway were associated with increased biodiversity, in general, and the proliferation of harvestable oysters (Didderen et al., 2019). Sampling for hard substratum species was conducted at monopiles in the Princess Amalia Wind Farm off the Dutch coast. Between 84 and 88 different species were collected during sampling in 2011 and 2013, 4 and 6 years following the construction of the wind farm, respectively; these included crustaceans, polychaetes (worms), bryozoans, and cnidarians. Not only were the numbers of species enhanced with the age of the installed monopiles, but densities of encrusting invertebrates had increased by factors of 3 to 10, and biomass had approximately doubled over this time (Vanagt and Faasse 2014). Researchers estimated that the future addition of 5,000 WTGs in the German Bight could provide enough hard ground habitat to result in an estimated 320 percent increase of brown crabs (*Cancer pagurus*) and 50 percent increase in Goldsinny wrasse (*Ctenolabrus rupestris*) (Krone et al., 2017). The invertebrate community was surveyed at the scour protection area at three different wind farms in the North Sea, as well as at nearby gas platforms. Mean invertebrate biomass observed at wind farm-associated scour protection ranged from 1.4 kilograms per square meter (kg/m^2) at the Princess Amalia Wind Farm to 13.1 kg/m^2 at the Horns Rev Wind Farm (Coolen et al., 2019). Gas platforms supported lower densities of less than 1 kg/m^2. In addition, a number of fish species were observed to be positively associated with scour protection, including dragonet, wrasse, and butterfish (Coolen et al., 2019). Because of findings like this, Linley et al. (2008) proposed that the addition of artificial substrate in coastal areas of wind farm footings and scour protection increases or enhances local biodiversity to the degree that it could potentially mitigate any observed negative impacts associated with construction.

Prospective predictions of ecosystem-level effects of wind farms in French waters were developed using established tropic web models. The potential reef effect of wind farm installation was modelled using biological data generated from a series of zooplankton, benthic macroinvertebrates, and demersal fish surveys conducted at the proposed Dieppe-Le Tréport and Courseulles-sur-Mer Wind Farm sites (Pezy et al., 2019). Results indicated that ecosystem activity, omnivorous feeders, and nutrient cycling would all be improved by the presence of the wind farm, and it was predicted that these increased resources may benefit *"important higher trophic levels such as exploited piscivorous fish species, endangered marine mammals and seabirds"*

(Pezy et al., 2019). Similar results were found with ecological structure and energy flow modeling for the Rudong Wind Farms near China. Models based on biological data collected before and after the construction of the wind farms demonstrated significant ecological benefits associated with the offshore structures (Wang et al., 2019). Phytoplankton, zooplankton, and abundances of certain fish species (including benthic fish and anchovies) were enhanced, and the proportion of energy flow from detrital feeding increased. Although the authors noted that the overall ecosystem function at the offshore wind farm *was "immature"* they proposed that structure-associated communities are likely to mature into more complex ecosystem with time (Wang et al., 2019).

10.0   Conclusions

The calculated magnetic-field levels generated by the Project's cables alone and at marine structures are well below limits established by ICES and ICNIRP to protect the health and safety of the general public. Moreover, these calculated magnetic-field and induced electric-field levels are not expected to affect populations of marine organisms residing in the SRWF and/or SRWEC.

Many marine species, including certain fish, invertebrates, and elasmobranchs, can detect and respond to the static geomagnetic field and in a few cases, low-frequency electric fields (~0 to 10 Hz). However, magnetic and electric fields generated by 50/60-Hz AC cables, are not as easily detected as those produced by DC cables. As such, evidence from laboratory and field studies addressing both static and 50/60 Hz fields were evaluated independently to assess the likelihood of detection and elicitation of biological effects in marine species.

Exponent calculated the magnetic-field levels and induced electric-field levels associated with the proposed Project's cable configurations. These maximum calculated field levels were then compared to magnetic- and electric-field levels reported in the scientific literature as causing behavioral or other responses in marine species expected to inhabit the SRWF and/or SRWEC, including fish, elasmobranchs, and marine invertebrates. This conservative evaluation resulted in the following conclusions, which are consistent with those of a 2019 BOEM report (Snyder et al., 2019).

SRWEC (DC Fields):

o   The magnetic-field levels at the seabed immediately above the buried SRWEC calculated at peak loading are slightly higher than DC magnetic fields that caused minor changes in lobster behavior and distribution, indicating that large crustaceans will be able to detect the elevated magnetic field, but only when in close proximity to the cable during peak loading.

o   Magnetic-field levels calculated for the SRWEC configuration buried under the seabed are below thresholds at which laboratory and field studies reported behavioral changes in magnetosensitive fish species. Striped bass did not respond to DC fields over 300 times higher than those expected to occur at the site.

o   Magnetic-field values calculated for the SRWEC at peak loading at the seabed immediately above the buried cables are slightly higher than fields associated with small scale changes in skate movement.

o   Induced electric-field levels associated with the SRWEC are expected to be within the range of detection of benthic elasmobranchs. However, based on evidence from field studies of DC cables (Hutchison 2018, 2020; Kavet et al., 2016) detection is not expected to have adverse population-level effects.

- o Based on field studies of sturgeon behavior in relation to a DC cable, potential detection of EMF produced by the SRWEC would not result in adverse individual effects for those sturgeon that are in the Project Area.

- o For those areas expected to attract certain marine species (e.g., OCS–DC structures, and mattress-covered SRWEC areas), calculated magnetic-field levels (for the SRWEC) are below levels reported to cause physiological effects following extended exposures.

- o Magnetic and electric fields at the Landfall HDD are similar to those calculated for the buried SRWEC cables. While modeled levels are expected to be detectable by some species, these levels are constrained to a localized segment and any responses expected to be minor and transitory.

IACs (AC Fields):

- o Biological survey data demonstrate that magnetic fields produced by 60-Hz AC submarine cables do not affect behaviors and distributions of large crustaceans or cephalopods.

- o Magnetic-field levels calculated for the 60-Hz IAC configurations buried 3.3 ft (1 m) under seabed are below thresholds at which laboratory and field studies reported behavioral changes in magnetosensitive fish species.

- o Elasmobranchs are not expected to detect the magnetic fields generated by the 60-Hz IAC.

- o Calculated electric-field levels associated with 60-Hz AC cables are lower than the published detection thresholds of electrosensitive fish such as sturgeon and elasmobranchs.

- o For those areas expected to attract certain marine species (WTG, and OCS–DC structures, and mattress-covered cables), calculated magnetic-field levels in water volumes close to IACs were below levels reported to cause physiological effects in species that might be expected to congregate at hardground structures for extended periods.

Moreover, biological field surveys conducted at existing wind farm sites report no adverse effects of fish populations due to the presence of operating wind turbines and cables; conversely, beneficial effects for fish and invertebrate populations have been reported frequently, since the installed structures can support a higher diversity and density of marine organisms.

In conclusion, conservative calculations of magnetic-field and induced electric-field levels based on the Project's cable specifications and peak loading indicate that EMF produced by the proposed AC cables will be below the detection thresholds for magnetosensitive and electrosensitive marine organisms. Similarly, magnetic-field levels calculated for peak loading of proposed DC cables are below the levels associated with behavioral changes in finfish species. Although the DC magnetic fields and resultant electric fields may be detectable by crustaceans and elasmobranchs that pass directly above the cable route at peak loading, the resulting behavioral responses would be minor. Moreover, it has been reported that if species respond to elevated DC fields, the response quickly diminishes after the initial stimulus. Minor and transient behavioral response are highly unlikely to result in adverse effects on individual fitness or impacts to the overall populations.

Years of biological surveys conducted at existing wind farm sites suggest no long-term or large-scale changes to populations of marine organisms residing at these sites. These findings also are corroborated by a review of the ecological effects of Marine Renewable Energy (MRE) projects; the authors reported that *"the ecological impacts of EMFs … are likely to be limited, and marine animals living in the vicinity of MRE [Marine Renewable Energy] devices and export cables are not likely to be harmed by emitted EMFs"* (Copping et al., 2020). As such, the conclusions of this evaluation for the Project cables agree with the general scientific and regulatory understanding of EMF and responses of marine species.

11.0   References

Albert, L., Maire, O., Olivier, F., Lambert, C., Romero-Ramirez, A., Jolivet, A., Chauvaud, L. and Chauvaud, S., 2022. Can artificial magnetic fields alter the functional role of the blue mussel, *Mytilus edulis*?. Marine Biology, 169(6), pp.1-14.

Andrianov, Y., G.R. Broun, O.B. Il'inskii, and V.M. Muraveiko. 1994. Frequency characteristics of skate electroreceptive central neurons responding to electrical and magnetic stimulation. Neurophysiology 16.4: 364-369, 1984.

Armstrong, J.D., D.C. Hunter, R.J. Fryer, P. Rycroft, and J.E. Orpwood. 2015. Behavioural responses of Atlantic Salmon to mains frequency magnetic fields. Scottish Marine and Freshwater Science. 6:9.

ASM Handbook Committee. Metals Handbook— Volume 1 Properties and Selection: Irons and Steels. 9th Ed., p. 150. Metals Park, OH: American Society for Metals, 1978

Anderson, J.M. 2018. Perception & Use of Magnetic Field Information in Navigation Behaviors in Elasmobranch Fishes (Doctoral dissertation, University of Hawaiʻi at Mānoa).

Andersson, M.H. and M.C. Öhman. 2010. Fish and sessile assemblages associated with wind-turbine constructions in the Baltic Sea. Marine and Freshwater Research. 61(6):642-650.

Andrianov, Y., G.R. Broun, O.B. Il'inskii, and V.M Muraveiko. 1984. Frequency characteristics of skate electroreceptive central neurons responding to electrical and magnetic stimulation. Neurophysiology. 16.4:364-369.

Basov, B.M. 1999. Behavior of sterlet Acipenser ruthenus and Russian sturgeon A. gueldenstaedtii in low-frequency electric fields. J Ichthyol. 39:782-787.

Bedore, C.N. and S.M. Kajiura. 2013. Bioelectric fields of marine organisms: voltage and frequency contributions to detectability by electroreceptive predators. Physiol Biochem Zool. 86: 298-311.

Bedore, C.N., L.L. Harris, and S.M. Kajiura. 2014. Behavioral responses of batoid elasmobranchs to prey-simulating electric fields are correlated to peripheral sensory morphology and ecology. Zoology. 117(2):95-103.

Bergström, L., F. Sundqvist, and U. Bergström. 2013. Effects of an offshore wind farm on temporal and spatial patterns in the demersal fish community. Marine Ecology Progress Series. 485:199-210.

Bevelhimer M.S., G.F. Cada, A.M. Fortner, P.E. Schweizer, and K. Riemer. 2013. Behavioral responses of representative freshwater fish species to electromagnetic fields. Trans Am Fish Soc. 142: 802-813.

Bevelhimer M.S., G.F. Cada, and C. Scherelis. 2015. Effects of electromagnetic fields on behavior of largemouth bass and pallid sturgeon in an experimental pond setting. Oak Ridge National Laboratory, Oak Ridge, TN.

Bochert, R. and M.L. Zettler. 2004. Long-term exposure of several marine benthic animals to static magnetic fields. Bioelectromagnetics. 25(7):498-502.

Bochert, R. and M.L. Zettler, M.L. 2006. Effect of electromagnetic fields on marine organisms. In: Koller J., J. Koppel, W. Peters (eds.). Offshore Wind Energy. Research on Environmental Impacts. Springer-Verlag, Berlin. pp. 223-234.

Boles, L.C. and K.J. Lohmann. 2003. True navigation and magnetic maps in spiny lobsters. Nature. 421: 60-63.

Brewer, H.B. 1979. Some preliminary studies of the effects of a static magnetic field on the life cycle of the Lebistes reticulatus (Guppy). Biophysical Journal. 28(2):305-314.

Brothers, J.R. and K.J. Lohmann. 2018. Evidence that magnetic navigation and geomagnetic imprinting shape spatial genetic variation in sea turtles. Current Biology. 28(8):1325-1329.

Brouard D., C. Harvey, D. Goulet, T. Nguyen, R. Champagne, and P. Dubs. 1996. Technical Notes: Evaluation of potential effects of stray voltage generated by alternating current on hatchery-raised rainbow trout. The Progressive Fish-culturist. 58:47-51.

Bull A.S. and M.E. Helix. 2011. Highlights of renewable energy studies and research in the bureau of ocean energy management, regulation and enforcement. OCEANS'11 MTS/IEEE KONA, Waikoloa, HI. pp. 1-5.

Cada, G.F., M.S. Bevelhimer, A.M. Fortner, K.P. Riemer, and P.E. Schweizer. 2012. Laboratory Studies of the Effects of Static and Variable Magnetic Fields on Freshwater Fish. ORNL/TM-2012/119. Oak Ridge National Laboratory, Tennessee.

Cain, S.D., L.C. Boles, J.H. Wang, and K.J. Lohmann. 2005. Magnetic orientation and navigation in marine turtles, lobsters, and molluscs: concepts and conundrums. Integrat Compar Biol. 45:539-546.

Cameron, I.L., K.E. Hunter, and W.D. Winters. 1985. Retardation of embryogenesis by extremely low frequency 60 Hz electromagnetic fields. Physiol Chem Phys Med NMR. 17:135-138.

Cameron, I.L., W.E. Hardman, W.D. Winters, S. Zimmerman, and A.M. Zimmerman. 1993. Environmental magnetic fields: influences on early embryogenesis. Journal of Cellular Biochemistry. 51(4):417-425.

Cihlar J. and F.T. Ulaby. 1974. Dielectric Properties of Soils as a Function of Moisture Content. The University of Kansas Center for Research, Inc., Lawrence, KS.

Chave A.D., A.H. Flosadóttir, and C.S. Cox. 1990. Some comments on seabed propagation of ULF/ELF electromagnetic fields. Radio Sci. 25.5:825-836.

Coolen, J.W., W. Lengkeek, T. van der Have, and O. Bittner. 2019. Upscaling positive effects of scour protection in offshore wind farms: Quick scan of the potential to upscale positive effects of scour protection on benthic macrofauna and associated fish species (No. C008/19). Wageningen Marine Research.

Copping, A. and L. Hemery, editors. 2020. OES-Environmental 2020 State of the Science Report: Environmental effects of Marine Renewable Energy development around the world. Report for Ocean Energy Systems (OES).

Copping, A., N. Sather, L. Hanna, J. Whiting, G. Zydlewski, G. Staines, A. Gill, I. Hutchison, A. O'Hagan, T. Simas, J. Bald, C. Sparling, J. Wood, and E. Masden. 2016. Annex IV 2016 State of the Science Report: Environmental effects of Marine Renewable Energy development around the world.

Cresci, A., Perrichon, P., Durif, C.M., Sørhus, E., Johnsen, E., Bjelland, R., Larsen, T., Skiftesvik, A.B. and Browman, H.I., 2022. Magnetic fields generated by the DC cables of offshore wind farms have no effect on spatial distribution or swimming behavior of lesser sandeel larvae (Ammodytes marinus). Marine Environmental Research, 176, p.105609.

Cuppen, J.J.M., G.F. Wiegertjes, H.W.J. Lobee, H.F.J. Savelkoul, M.A. Elmusharaf, A.C. Beynen, H.N.A. Grooten, and W. Smink. 2007. Immune stimulation in fish and chicken through weak low frequency electromagnetic fields. The Environmentalist. 27:577-583.

Didderen, K., J.H. Bergsma, and P. Kamermans. 2019. Offshore flat oyster pilot Luchterduinen wind farm. Results Campaign. 2:19-184.

Dunlop, E.S., S.M. Reid, and M. Murrant. 2016. Limited influence of a wind power project submarine cable on a Laurentian Great Lakes fish community. J Appl Ichthyol. 32:18-31.

European Committee for Electrotechnical Standardization (CENELEC). Procedure for the Assessment of the Exposure to Electromagnetic Fields of Workers Bearing Active Implantable Medical Devices – Part 1 – General. EN 50527-1. Brussels: Cenelec, 2010.

Exponent, Inc. (Exponent). 2022. Onshore DC and AC Magnetic-Field Assessment. Prepared for Sunrise Wind LLC. Exponent, Bowie, MD.

Ferrari, T.E. 2016. Cetacean beachings correlate with geomagnetic disturbances in Earth's magnetosphere: an example of how astronomical changes impact the future of life. International Journal of Astrobiology. 16(2):163-175.

Fey, D.P., Greszkiewicz, M., Otremba, Z., Andrulewicz, E., 2019b. Effect of static magnetic field on the hatching success, growth, mortality, and yolk-sac absorption of larval Northern pike *Esox lucius*. Sci. Total Environ. 647, 1239–1244.

Fish, F.E., and L.D. Shannahan. 2000. The role of the pectoral fins in body trim of sharks. J Fish Biol. 56:1062-1073.

Formicki, K. and A. Winnicki. 1998. Reactions of fish embryos and larvae to constant magnetic fields. Italian Journal of Zoology. 65(S1):479-482.

Formicki, K. and T. Perkowski. 1998. The effect of a magnetic field on the gas exchange in rainbow trout Oncorhynchus mykiss embryos (Salmonidae). Italian Journal of Zoology. 65(S1):475-477.

Gill, A.B. and H. Taylor. 2001. The potential effects of electromagnetic fields generated by cabling between offshore wind turbines upon elasmobranch fishes. Countryside Council for Wales.

Gill, A.B., Y. Huang, I. Gloyne-Philips, J. Metcalfe, V. Quayle, J. Spencer, and V. Wearmouth. 2009. COWRIE 2.0 Electromagnetic Fields (EMF) Phase 2: EMF-sensitive fish response to EM emissions from sub-sea electricity cables of the type used by the offshore renewable energy industry. Commissioned by COWRIE Ltd. (project reference COWRIE-EMF-1-06).

Goff M., M. Salmon, and K.J. Olhmann. 1998. Hatchling sea turtle use surface waves to establish a magnetic compass direction. Anim Behav. 55:59-77.

Haber, F., 1974. The Magnetic Field in the Vicinity of Parallel and Twisted Three-Wire Cable Carrying Balanced Three-Phased Current. IEEE Transactions on Electromagnetic Compatibility EMC-16, 76–82. https://doi.org/10.1109/TEMC.1974.303335

Hanson M. and H. Westerberg. 1987. Occurrence of magnetic material in teleosts. Compar Biochem Physiol Part A: Physiol. 86:169-172.

Harrison R.J., R.E. Dunin-Borkowski, and A. Putnis. 2002. Direct imaging of nanoscale magnetic interactions in minerals. Proceed Nat Acad Sci. 99:16556–16561.

Harsanyi, P., Scott, K., Easton, B.A., de la Cruz Ortiz, G., Chapman, E.C., Piper, A.J., Rochas, C.M. and Lyndon, A.R., 2022. The effects of anthropogenic Electromagnetic Fields (EMF) on the early development of two commercially important crustaceans, European lobster, *Homarus gammarus* (L.) and edible crab, *Cancer pagurus* (L.). Journal of Marine Science and Engineering, 10(5), p.564.

Hays, G.C., G. Cerritelli, N. Esteban, A. Rattray, and P. Luschi. 2020. Open Ocean Reorientation and Challenges of Island Finding by Sea Turtles during Long-Distance Migration. Current Biology. In Press. https://doi.org/10.1016/j.cub.2020.05.086

Hellinger J. and K.P. Hoffman. 2012. Magnetic field perception in the rainbow trout, Oncorhynchus mykiss: magnetite mediated, light dependent or both? J Comp Physiol A 198:593-605.

Hulbert M.H., R.H. Bennett, and D.N. Lambert. 1982. Seabed geotechnical parameters from electrical conductivity measurements. Geo-Marine Lett. 2(3-4):219-222.

Hutchison Z., P. Sigray, H. He, A. Gill, J. King, and C. Gibson. 2018. Electromagnetic Field (EMF) Impacts on Elasmobranch (shark, rays, and skates) and American Lobster Movement and Migration from Direct Current Cables. Report by University of Rhode Island, Cranfield University, and FOI (Swedish Defence Research Agency).

Hutchison, Z.L., A.B. Gill, P. Sigray, H. He, and J.W. King. 2020. Anthropogenic electromagnetic fields (EMF) influence the behaviour of bottom-dwelling marine species. Scientific Reports. 10(1):1-15.

Ingram, E.C., R.M. Cerrato, K.J. Dunton, and M.G. Frisk, 2019. Endangered Atlantic Sturgeon in the New York Wind Energy Area: implications of future development in an offshore wind energy site. Scientific Reports. 9(1):1-13.

Institute of Electrical and Electronics Engineers (IEEE). 2021. IEEE Recommended Practice for Measurements and Computations of Electric, Magnetic, and Electromagnetic fields with respect to Human Exposure to Such Fields, 0 Hz to 300 GHz (IEEE Std. C95.3-2021). IEEE, New York.

Institute of Electrical and Electronics Engineers (IEEE). 2019. Approved Draft Standard Procedures for Measurement of Power Frequency Electric and Magnetic Fields from AC Power Lines (ANSI/IEEE Std. 644-2019). IEEE, New York.

International Commission on Non-Ionizing Radiation Protection (ICNIRP). Guidelines on limits of exposure to static magnetic fields. Health Phys. 96:504-14, 2009.

International Commission on Non-ionizing Radiation Protection (ICNIRP). Guidelines for limiting exposure to time-varying electric and magnetic fields (1 Hz to 100 kHz). Health Phys 99:818-836, 2010.

International Committee on Electromagnetic Safety (ICES). IEEE Standard for Safety Levels with Respect to Human Exposure to Electromagnetic Fields 0 to 300 GHz. IEEE Std C95.1-2019 (Revision of IEEE Std C95.1-2005/ Incorporates IEEE Std C95.1-2019/Cor 1-2019). New York, NY: IEEE, 2019.

ISO 2019 - ISO/ANSI/AAMI Active implantable medical devices — Electromagnetic compatibility — EMC test protocols for implantable cardiac pacemakers, implantable cardioverter defibrillators and cardiac resynchronization devices.

International Geomagnetic Reference Field Model 1945 – 2025 (IGRF-13) and Related Parameters. https://ccmc.gsfc.nasa.gov/modelweb/models/igrf_vitmo.php

Jakubowska, M., B. Urban-Malinga, Z. Otremba, and E. Andrulewicz. 2019. Effect of low frequency electromagnetic field on the behavior and bioenergetics of the polychaete Hediste diversicolor. Marine Environmental Research. 150:104766.

Jakubowska-Lehrmann, M., Białowąs, M., Otremba, Z., Hallmann, A., Śliwińska-Wilczewska, S. and Urban-Malinga, B., 2022. Do magnetic fields related to submarine power cables affect the functioning of a common bivalve?. Marine Environmental Research, p.105700.

Jordan, L.K., J.W. Mandelman, and S.M. Kajiura. 2011. Behavioral responses to weak electric fields and a lanthanide metal in two shark species. Journal of Experimental Marine Biology and Ecology. 409(1-2):345-350.

Kempster, R.M., N.S. Hart, and S.P. Collin. 2013. Survival of the stillest: predator avoidance in shark embryos. Plos One, 8:e52551.

Kajiura, S.M. and K.N. Holland. 2002. Electroreception in juvenile scalloped hammerhead and sandbar sharks. Journal of Experimental Biology. 205(23):3609-3621.

Kajiura, S.M. 2003. Electroreception in neonatal bonnethead sharks, Sphyrna tiburo. Marine Biology. 143(3):603-611.

Kavet, R., M.T. Wyman, A.P. Klimley, and X. Vergara. 2016. Assessment of potential impact of electromagnetic fields from undersea cable on migratory fish behavior. Electric Power Research Institute (EPRI) for the US Department of Energy and US Department of the Interior, Bureau of Ocean Energy Management.

Kempster, R.M., N.S. Hart, and S.P. Collin. 2013. Survival of the stillest: predator avoidance in shark embryos. PLoS One. 8:e52551.

Klimley, A.P. 1993. Highly directional swimming by scalloped hammerhead sharks, Sphyrna Lewini, and subsurface irradiance, temperature, bathymetry, and geomagnetic field. Marine Biol. 117:22.

Klimley, A.P., M.T. Wyman, and R. Kavet. 2017. Chinook salmon and green sturgeon migrate through San Francisco Estuary despite large distortions in the local magnetic field produced by bridges. PLoS One. 12(6):30169031.

Kramer, S.H., C.D. Hamilton, G.C. Spencer, and H.D. Ogston. 2015. Evaluating the potential for Marine and Hydrokinetic Devices to act as artificial reefs or fish aggregating devices, based on analysis of surrogates in tropical, subtropical, and temperate U.S. West Coast and Hawaiian Coastal Waters. OCS Study BOEM 2015-021. US Department of Energy, Energy Efficiency and Renewable Energy, Golden, CO.

Kremers, D., J.L. Marulanda, M. Hausberger, and A. Lemasson. 2014. Behavioural evidence of magnetoreception in dolphins: detection of experimental magnetic fields. Naturwissenschaften. 101(11):907-911.

Krone, R., G. Dederer, P. Kanstinger, P. Krämer, C. Schneider, and I. Schmalenbach. 2017. Mobile demersal megafauna at common offshore wind turbine foundations in the German Bight (North Sea) two years after deployment-increased production rate of Cancer pagurus. Marine Environmental Research. 123:53-61.

Kuhnz, L.A., J.P. Barry, K. Buck, C. Lovera, and P.J. Whaling. 2015. Potential impacts of the Monterey Accelerated Research System (MARS) cable on the seabed and benthic faunal assemblages. MARS Biological Survey Report, Monterey Bay Aquarium Research Institute.

Leggett, W.C., The ecology of fish migrations. Annu Rev Ecol Syst 8:.285-308, 1977.

Leonhard, S.B., C. Stenberg, J.G. Støttrup (eds.). 2011. Effect of the Horns Rev 1 Offshore Wind Farm on Fish Communities: Follow-up Seven Years after Construction. Danish Energy Authority.

Levin, M. and S.G. Ernst. 1995. Applied AC and DC magnetic fields cause alterations in the mitotic cycle of early sea urchin embryos. Bioelectromagnetics. 16:231-240.

Levin, M. and S.G. Ernst. 1997. Applied DC magnetic fields cause alterations in the time of cell divisions and developmental abnormalities in early sea urchin embryos. Bioelectromagnetics. 18(3):255-263.

Li, Y., B. Ru , X. Liu, W. Miao, K. Zhang, L. Han, H. Ni, H. Wu. 2015. Effects of extremely low frequency alternating-current magnetic fields on the growth performance and digestive enzyme activity of tilapia Oreochromis niloticus. Environ Biol Fishes. 98:337-343.

Linley, E.A.S., T.A. Wilding, K. Black, A.J.S. Hawkins, and S. Mangi. 2007. Review of the reef effects of offshore wind farm structures and their potential for enhancement and mitigation. Report to the Department for Business, Enterprise and Regulatory Reform. RFCA, 5.

Loghmannia, J., B. Heidari, S.A, Rozati, and S. Kazemi. 2015. The physiological responses of the Caspian kutum (Rutilus frisii kutum) fry to the static magnetic fields with different intensities during acute and subacute exposures. Ecotoxicology and Environmental Safety. 111:215-219.

Lohmann, K.J., N.D. Pentcheff, G.A. Nevitt, G.D. Stetten, R.K. Zimmerfaust, H.E. Jarrard, and L.C. Boles. 1995. Magnetic orientation of spiny lobsters in the ocean – experiments with undersea coil systems. J Exper Biol. 198:2041-2048.

Love, M.S., M.M. Nishimoto, S. Clark, and A.S. Bull. 2015. Identical response of caged rock crabs (Genera Metacarcinus and Cancer) to energized and unenergized undersea power cables in Southern California, USA. Bull S Calif Acad Sci. 114:33-41.

Love, M.S., M.A. Nishimoto, S. Clark, and A.S. Bull. 2016. Renewable Energy in situ Power Cable Observation. OCS Study 2016-008. U.S. Department of the Interior, Bureau of Ocean Energy Management, Pacific OCS Region, Camarillo, CA.

Love, M.S., M.M. Nishimoto, S. Clark, M. McCrea, and A.S. Bull. 2017a. Assessing potential impacts of energized submarine power cables on crab harvests. Continental Shelf Research. 1(151):23-29.

Love, M.S., M.M. Nishimoto, S. Clark, M. McCrea, and A.S. Bull. 2017b. The organisms living around energized submarine power cables, pipe, and natural Sea floor in the inshore waters of Southern California. Bulletin, Southern California Academy of Sciences. 116(2):61-88.

Luschi P., S. Benhamou, C. Girard, S. Cicione, D. Roos, J. Sudre, and S. Benvenuti. 2007. Marine turtles use geomagnetic cues during open-sea homing. Current Biology. 17(2):126-133.

McIntyre III, A. 2016. Behavioral responses of sub-adult Atlantic Sturgeon (Acipenser oxyrinchus oxyrinchus) to electromagnetic and magnetic fields under laboratory conditions.

Methratta, E.T., and W.R. Dardick. 2019. Meta-analysis of finfish abundance at offshore wind farms. Reviews in Fisheries Science & Aquaculture. 27(2):242-260.

Nestler, E., A. Pembroke, and W. Bailey. 2010. Effects of EMFs from undersea power lines on marine species. Energy. Ocean International, Ft. Lauderdale, FL.

Newton, K.C., A.B. Gill, and S.M. Kajiura. 2019. Electroreception in marine fishes: chondrichthyans. Journal of Fish Biology. 95(1):135-154.

Niquil, N., A. Raoux, M. Haraldsson, E. Araignous, G. Halouani, B. Leroy, G. Safi, Q. Noguès, K. Grangeré, J.C. Dauvin, and F. Riera. 2020. Toward an ecosystem approach of Marine Renewable

Energy: The case of the offshore wind farm of Courseulles-sur-Mer in the Bay of Seine. In Estuaries and Coastal Zones in Times of Global Change (pp. 137-148). Springer, Singapore.

Nofouzi, K., N. Sheikhzadeh, D. Mohamad-Zadeh Jassur, and J. Ashra-Helan. 2015. Influence of extremely low frequency electromagnetic elds on growth performance, innate immune response, biochemical parameters and disease resistance in rainbow trout, Oncorhynchus mykiss. Fish Physiol Biochem. 41:721731.

Normandeau, Exponent, T. Tricas, and A. Gill. 2011. Effects of EMFs from Undersea Power Cables on Elasmobranchs and Other Marine Species. OCS Study BOEM RE 2011-09. US Dept. of the Interior, Bureau of Ocean Energy Management, Regulation, and Enforcement, Pacific OCS Region, Camarillo, CA.

Nyqvist, D., C. Durif, M.G., Johnsen, K. De Jong, T.N. Forland, and L.D. Sivle. 2020. Electric and magnetic senses in marine animals, and potential behavioral effects of electromagnetic surveys. Marine Environmental Research. 155:104888.

Oliver E.C.J., J. Sheng, K.R. Thompson, and J.R. Urrego Blanco. 2012. Extreme surface and near-bottom currents in the northwest Atlantic. Nat Hazards. 64:1425-1446.

Orpwood, J.E., R.J. Fryer, P. Rycroft, and J.D. Armstrong. 2015. Effects of AC Magnetic Fields (MFs) on Swimming Activity in European Eels Anguilla. Scottish Marine and Freshwater Sci. 6:8.

Orr, M. The potential impacts of submarine power cables on benthic elasmobranchs. Doctoral Dissertation, The University of Auckland, 2016.
https://researchspace.auckland.ac.nz/bitstream/handle/2292/30773/whole.pdf?sequence=2

Petersen, J.K. and T. Malm. 2006. Offshore windmill farms: threats to or possibilities for the marine environment. AMBIO: A Journal of the Human Environment. 35(2):75-80.

Pettersson, P. and N. Schönborg. 1997. Reduction of power system magnetic fields by configuration twist, IEEE Trans Power Del. 12:1678-1683.

Pezy, J.P., A. Raoux, N. Niquil, and J.C. Dauvin. 2019. Towards an ecosystem approach to assess the impacts of marine renewable energy. In: Bispo R., J. Bernardino, H. Coelho, and J.L. Costa (eds). Wind Energy and Wildlife Impacts. Springer, Cham. pp. 153-164.

Putman, N.F., A.M. Meinke, and D.L. Noakes. 2014. Rearing in a distorted magnetic field disrupts the 'map sense' of juvenile steelhead trout. Biology Letters. 10(6):20140169.

Quigel, J.C. and W.L. Thornton. 1989. Rigs to reefs—a case history. Bulletin of Marine Science. 44:799-806.

Richardson, NE, J.D. McCleave, and E.H. Albert. 1976. Effect of extremely low frequency electric and magnetic fields on locomotor activity rhythms of Atlantic salmon (Salmo salar) and American eels (Anguilla rostrata). Environmental Pollution. 10:65-76.

Sadowski, M., A. Winnicki, K. Formicki, A. Sobocinski, and A. Tanski A. 2007. The effect of magnetic field on permeability of egg shells of salmonid fishes. Acta Ichthyologica et Piscatoria. 2(37):129-135.

Samiee, F. and K. Samiee. 2017. Effect of extremely low frequency electromagnetic field on brain histopathology of Caspian Sea Cyprinus carpio. Electromag Biol Med. 36:31-38.

Scheidat, M., J. Tougaard, S. Brasseur, J. Carstensen, T. van Polanen Petel, J. Teilmann, and P. Reijnders. 2011. Harbour porpoises (Phocoena phocoena) and wind farms: a case study in the Dutch North Sea. Environmental Research Letters. 6(2):025102.

Scott, K., P. Harsanyi, and A.R. Lyndon. 2018. Understanding the effects of electromagnetic field emissions from Marine Renewable Energy Devices (MREDs) on the commercially important edible crab, Cancer pagurus (L.). Marine Pollution Bulletin. 131:580-588.

Scott, K., P. Harsanyi, B.A Easton, A.J. Piper, C. Rochas, and A.R. Lyndon. 2021. Exposure to Electromagnetic Fields (EMF) from submarine power cables can trigger strength-dependent behavioural and physiological responses in edible crab, *Cancer pagurus* (L.). Journal of Marine Science and Engineering. 9(7):776.

Sedigh, E., B. Heidari, A. Roozati, and A. Valipour. 2019. The Effect of Different Intensities of Static Magnetic Field on Stress and Selected Reproductive Indices of the Zebrafish (Danio rerio) During Acute and Subacute Exposure. Bulletin of Environmental Contamination and Toxicology. 102(2):204-209.

Sherwood, J., S. Chidgey, P. Crockett, D. Gwyther, P. Ho, S. Stewart, D. Strong, B. Whitely, and A. Williams. 2016. Installation and operational effects of a HVDC submarine cable in a continental shelf setting: Bass Strait, Australia. Journal of Ocean Engineering and Science. 1(4):337-353.

Silva, J.M. 2006. EMF Study: Long Island Power Authority (LIPA), Offshore Wind Project.

Skauli, K.S., J.B. Reitan, and B.T. Walther. 2000. Hatching in zebrafish (Danio rerio) embryos exposed to a 50 Hz magnetic field. Bioelectromagnetics. 21:407-410.

Snyder, D.B., W.H. Bailey, K. Palmquist, B.R.T. Cotts, K.R. Olsen. 2019. Evaluation of Potential EMF Effects on Fish Species of Commercial or Recreational Fishing Importance in Southern New England. OCS Study BOEM 2019-049. US Dept. of the Interior, Bureau of Ocean Energy Management, Headquarters, Sterling, VA.

Somaraju, R. and J. Trumpf. 2006. Frequency, temperature and salinity variation of the permittivity of seawater. IEEE Trans Antenn Propag. 54:11:3441-3448.

Stankevičiūtė, M., M. Jakubowska, J. Pažusienė, T. Makaras, Z, Otremba, B. Urban-Malinga, D.P. Fey, M. Greszkiewicz, G. Sauliutė, J. Baršienė, and E. Andrulewicz. 2019. Genotoxic and cytotoxic effects of 50 Hz 1 mT electromagnetic field on larval rainbow trout (Oncorhynchus mykiss), Baltic clam (Limecola balthica) and common ragworm (Hediste diversicolor). Aquat Toxicol. 208:109-117.

Sun, W., Y. He, S.W. Leung, and Y.C. Kong. 2019. In Vivo Analysis of Embryo Development and Behavioral Response of Medaka Fish under Static Magnetic Field Exposures. International Journal of Environmental Research and Public Health. 16(5):844.

Tański, A., A. Korzelecka-Orkisz, L. Grubišić, V. Tičina, J. Szulc, and K. Formicki. 2011. Directional responses of sea bass (Dicentrarchus labrax) and sea bream (Sparus aurata) fry under static magnetic field. Electronic J Polish Agricult Universities, Series Fisheries, 14:1-11.

Taormina, B., C. Di Poi, A.L. Agnalt, A. Carlier, N. Desroy, R.H. Escobar-Lux, J.F. D'eu, F. Freytet, and C.M. Durif. 2020. Impact of magnetic fields generated by AC/DC submarine power cables on the behavior of juvenile European lobster (Homarus gammarus). Aquatic Toxicology. 220:105401.

Taylor, P.B. 1986. Experimental-evidence for geomagnetic orientation in juvenile salmon Oncorhynchus tschawytscha Walbaum. Journal of Fish Biology. 28:607-662.

Teeter, J.H., R.B. Szamier, and M.L.V. Bennett. 1980. Ampullary electroreceptors in the Sturgeon Scaphirhynchus platorynchus (Rafinesque). J Comp Physiol. 138:213-223.

Ueno S., P. Lövsund, and P.A. Öberg. 1986. Effect of time-varying magnetic fields on the action potential in lobster giant axon. Med Biol Eng Comput. 24:21-526.

Ugolini, A. and A. Pezzani. 1995. Magnetic compass and learning of the y-axis (sea-land) direction in the marine isopod Idotea baltica basteri. Animal Behav. 50:295-300.

Vanagt, T. and M. Faasse M. 2014. Development of hard substratum fauna in the Princess Amalia Wind Farm. Monitoring six years after construction. eCOAST report 2013009.

Vandendriessche, S., J. Derweduwen, and K. Hostens. 2015. Equivocal effects of offshore wind farms in Belgium on soft substrate epibenthos and fish assemblages. Hydrobiologia. 756:19-35.

Vattenfall, A. and N. Skov-og. 2006. Danish Offshore Wind: Key Environmental Issues (No. NEI-DK--4787). DONG Energy.

Walker, M.M., T.P. Quinn, J.L. Kirschvink, and C. Groot. 1988. Production of single-domain magnetite throughout life by sockeye salmon, Oncorhynchus nerka. J Exper Biol. 140:51-63.

Walker M.M., J.L. Kirschvink, G. Ahemd, and A.E. Dizon. 1998. Evidence that fin whales respond to the geomagnetic field during migration. J Exp Biol. 171:67-78.

Wang J., X. Zou, W. Yu, D. Zhang, and T. Wang. 2019. Effects of established offshore wind farms on energy flow of coastal ecosystems: A case study of the Rudong offshore wind farms in China. Ocean and Coastal Management. 171:111-118.

Ward, B.K., G.X. Tan, D.C. Roberts, C.C. Della Santina, D.S. Zee, and J.P. Carey. 2014. Strong static magnetic fields elicit swimming behaviors consistent with direct vestibular stimulation in adult zebrafish. PloS One. 9(3):e92109.

Westerberg, H. and M.L. Begout Anras. 1999. Orientation of silver eel (Aguilla anguilla) in a disturbed geomagnetic field. Advances in fish telemetry. In Proceedings of the Third Conference on Fish Telemetry in Europe, Norwich, England.

Wilson, J.G. 1986. Electrical Properties of Concrete. Doctoral Thesis, The University of Edinburgh.

Woodruff, D.L., I.R. Schultz, K.E. Marshall, J.A. Ward, and V.I. Cullinan. 2012. Effects of Electromagnetic Fields on Fish and Invertebrates: Task 2.1. 3: Effects on Aquatic Organisms-Fiscal Year 2011 Progress Report-Environmental Effects of Marine and Hydrokinetic Energy (No. PNNL-20813 Final). Pacific Northwest National Laboratory (PNNL), Richland, WA.

Woodruff, D.L., V.I. Cullinan, A.E. Copping, K.E. Marshall. 2013. Effects of Electromagnetic Fields on Fish and Invertebrates: Task 2.1. 3: Effects on Aquatic Organisms-Fiscal Year 2012 Progress Report-Environmental Effects of Marine and Hydrokinetic Energy (No. PNNL-22154). Pacific Northwest National Laboratory (PNNL), Richland, WA.

Wueringer, B.E., L. Squire Jr., S.M. Kajiura, I.R. Tibbetts, N.S. Hart, and S.P. Collin. 2012. Electric field detection in sawfish and shovelnose rays. PLoS One. 7(7):340605.

Zhang, X., J. Song, C. Fan, H. Guo, X. Wang, and H. Bleckmann, H. 2012. Use of electrosense in the feeding behavior of sturgeons. Integrative Zoology. 7(1):74-82.

Zimmerman, S., A.M. Zimmerman, W.D. Winters WD, and I.L. Cameron. 1990. Influence of 60-Hz magnetic fields on sea urchin development. Bioelectromagnetics. 11:37-45.

Attachment A

## Cable Configurations and Burial Depths

DC Cable Configurations and Burial Depths

Since the vector sum (which depends on both magnitude and direction) of the earth's geomagnetic field and the static field from the SRWEC comprise the effective static field experienced by marine wildlife, both the orientation of the SRWEC relative to the earth's geomagnetic field, and the direction of current flow in each individual conductor will determine the calculated total static magnetic-field level.

DC magnetic-field levels for the Project were calculated for three representative cable directions associated with the cable route (30, 161, and 356 degrees north of east), as shown in Figure A-1. Additionally, calculations were performed for a cable orientation along the north-south axis and along the east-west axis. The two cables of the SRWEC, a cross section of which is illustrated in Figure A-2, will be strapped together, and during installation the cables may be oriented either side by side, or one on top of the other (i.e., two installation configurations). Since the polarity of the cables (i.e., which will carry current towards land and which will carry current away from land) cannot be specified at this time, both options were modeled (the interaction of the DC magnetic-field vectors from the cable with the earth's geomagnetic field vectors will yield different results for each of these configurations).

At landfall, the SRWEC will be installed via HDD (i.e., Landfall HDD installation). The burial depth over most of this portion of the route is expected to be significantly greater than in other portions of the route, with the minimum burial depth of 6 ft (1.8 m) and most of the HDD at least 46 ft (14 m).
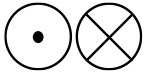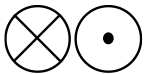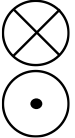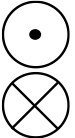
Figure A-1.   Geographic orientation of the SRWEC route. The interaction of the DC magnetic-field vectors from the cable with the earth's geomagnetic field vectors will yield different results for each segment of the route.
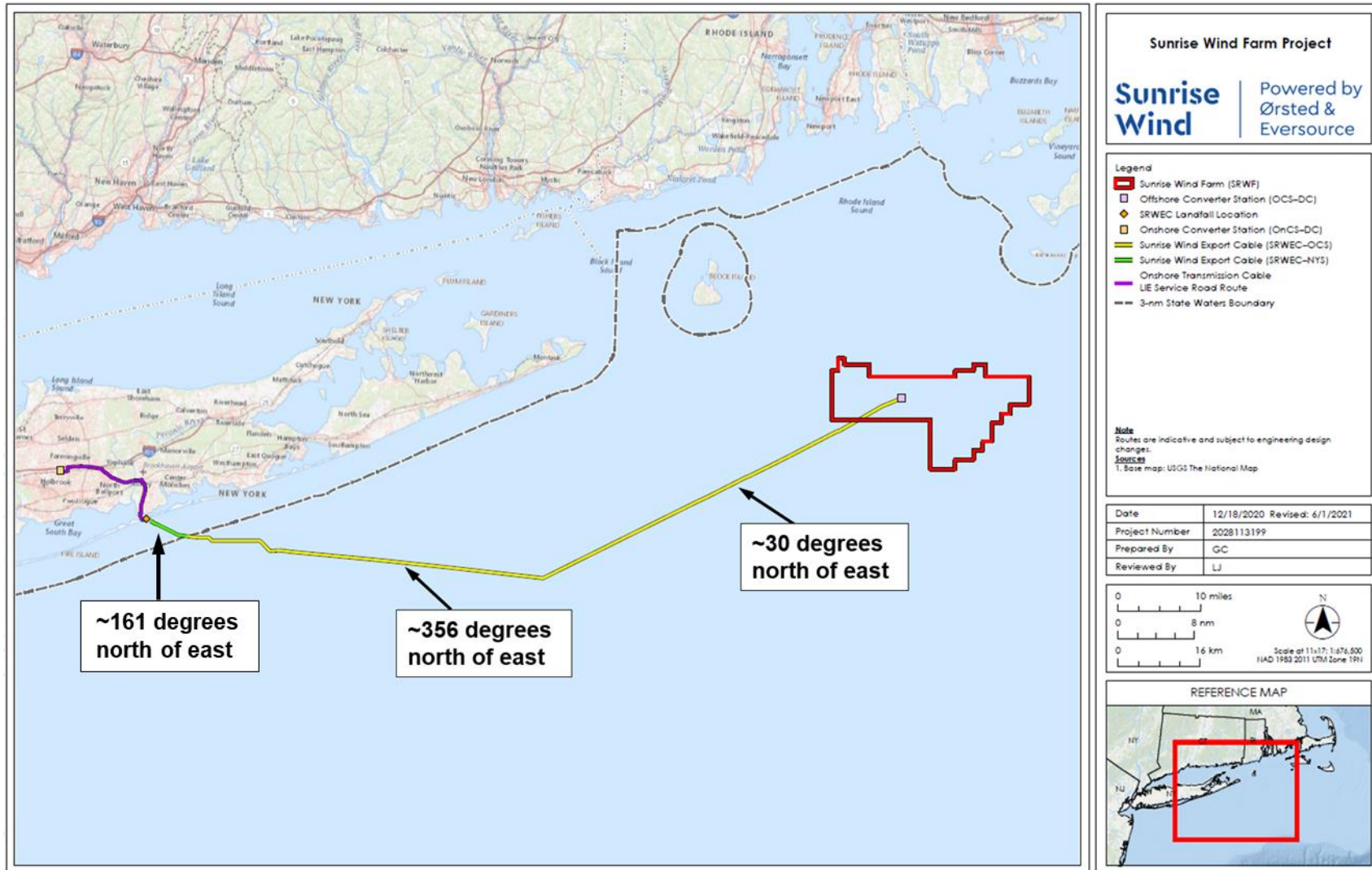
The modeling cases for offshore SRWEC are summarized in Table A-1. Modeling was performed for each of four cable and current flow configurations at two loading levels (average loading and peak loading), four different burial depths, and four geographic directions.

Table A-1.   Summary of offshore modeling of ±320 kV DC configurations

DC Modeling Cases	Cable Diameter (mm)*	Current Flow Direction†	Burial Depths (To the Top of the Cable)	Loading Levels	Geographic Directions‡ (Degrees North of East)
Side-by-Side Installation	134	⊙ ⊗	3.3 ft (1 m) and 1 ft (30 cm) (mattress-covered)	Average, Peak	Cable Route: 30°, 161°, and 356° (north-south & east-west)
	134	⊗ ⊙	3.3 ft (1 m) and 1 ft (30 cm) (mattress-covered)	Average, Peak	Cable Route: 30°, 161°, and 356° (north-south & east-west)
Cables Stacked Installation	134	⊗ ⊙	3.3 ft (1 m) and 1 ft (30 cm) (mattress-covered)	Average, Peak	Cable Route: 30°, 161°, and 356° (north-south & east-west)
	134	⊙ ⊗	3.3 ft (1 m) and 1 ft (30 cm) (mattress-covered)	Average, Peak	Cable Route: 30°, 161°, and 356° (north-south & east-west)

* Since cables are strapped together the distance between cables a larger cable diameter will result in higher field levels than a smaller cable. Modeling was performed for a 150-mm cable diameter, larger than the proposed ±320 kV cable to conservatively overestimate field values

† The current flow options are shown as vectors into and out of the page with reversed configurations each representing a separate modeling case.

‡ North-south (90º) and east-west (0º) also are included to provide an estimate of values for other similar directions. All configurations are assessed to determine the highest expected field level for each geographic direction.
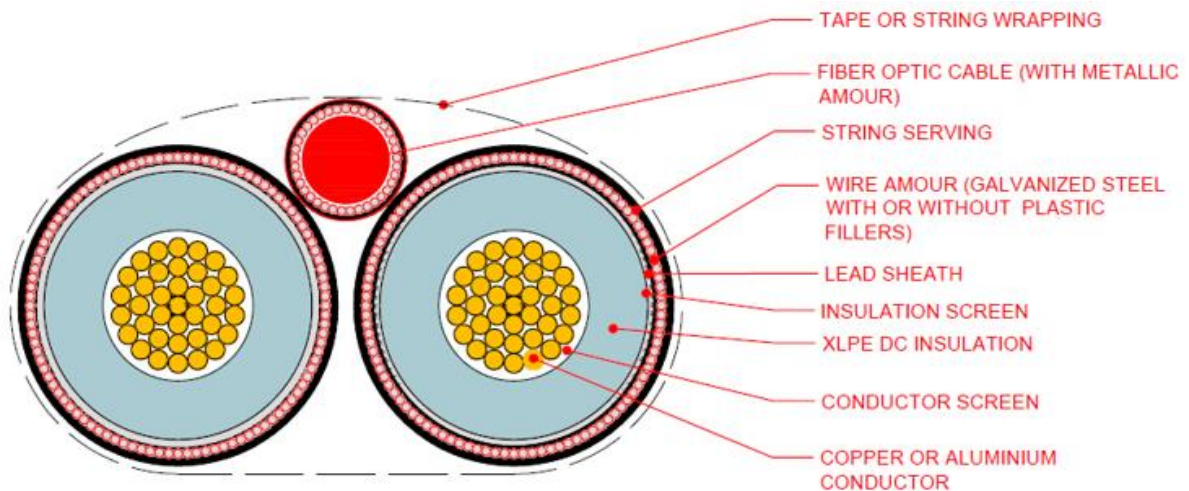

Figure A-2.   Illustrative cross-section of a bundled pair of single core DC submarine cables.

Previous measurements of a DC cable showed the presence of low-strength AC fields emanating from the cable (Hutchison et al., 2018, 2020). The applicability of those measurements to the present case, however, is unclear because the likely source and magnitude of these currents in the Hutchison et al. studies was not well understood by the authors and they are likely to be quite site-specific. Nevertheless, these measurements provide some context regarding the relative magnitude of DC and AC magnetic fields measured in these previous studies.[21]

Landfall HDD

The portion of the route over which the HDD will be used for installation covers approximately 3,200 ft, including approximately 2,000 ft offshore (i.e., the HDD exit pit to the mean high-water level [MHWL]) and approximately 1,200 ft from the MHWL to the HDD entry. This portion of the route is called the Landfall–HDD. An illustrative profile of the Landfall HDD target burial depth (see Figure A-3) shows that over the majority of the Landfall HDD installation offshore, the burial depth will be approximately 46 ft, but in other locations will be buried much deeper, up to a 79 ft. Figure A-3 also shows that over the very small distances at the beginning and end of the Landfall HDD, the minimum target burial depth will be 6 ft (1.8 m).
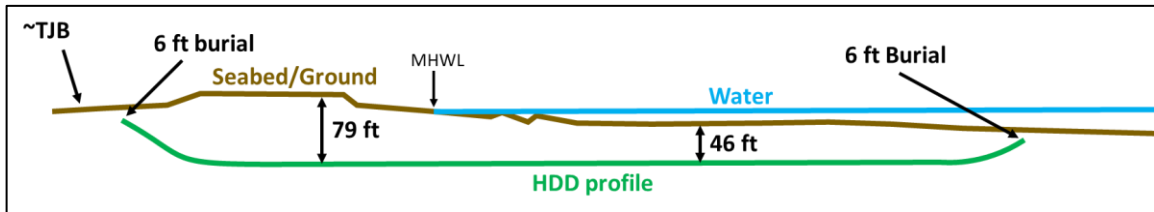

Figure A-3.   Illustrative profile of HDD burial depth (not to scale).

At the Landfall HDD, the SRWEC will be placed inside a 55-inch conduit as shown in Figure A-4. The outer bore hole is proposed to be approximately 55 inches and will contain two conduits (approximately 16 inches in diameter). One DC cable will be installed in each of the interior 16-inch conduits. A third smaller conduit will contain the fiber optic cable for communications. In contrast to the trench configuration where the orientation of the conductors of the SRWEC (i.e., side-by-side or stacked) cannot be controlled, the orientation of the HDD (i.e., 16-inch conduits side-by-side) will be maintained throughout the installation. The modeling cases for the SRWEC in the Landfall HDD configuration was performed for two current flow configurations at WNC rating for two burial depths and one geographic direction.

---

[21]   The median AC magnetic and electric fields measured near the DC cables were about 1.7 mG and 0.84 mV/m, respectively or less (Hutchison et al., 2018, Table 3.1).
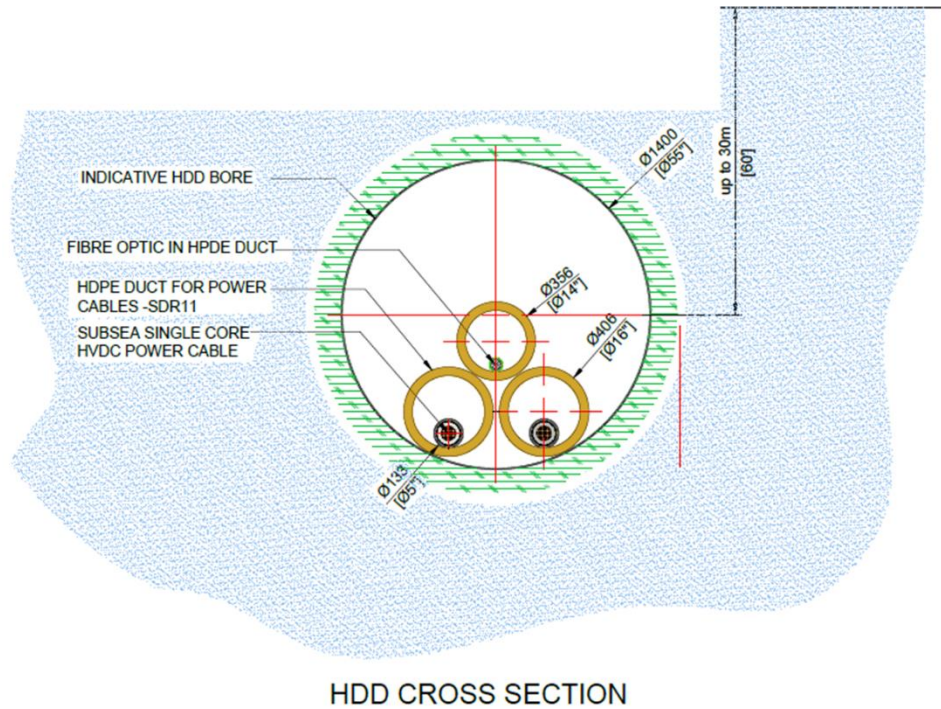
HDD CROSS SECTION

Figure A-4.   Conceptual drawing of HDD bore hole.

AC Cable Configurations and Burial Depths

AC electricity is proposed to flow along the IACs as part of the Project. IACs (66 to 161 kV) are proposed to be installed between the WTGs and between WTGs and the OCS–DC. The 66-kV cables will result in higher magnetic- and induced electric-field levels than the 161-kV cables, so IACs were modeled at 66 kV;

AC magnetic-field and induced electric-field levels for the Project were calculated for the IACs, modeled at two burial depths, as summarized in Table A-2. The IACs are constructed with a three-core configuration, with all three phase conductors contained within a single larger cable. A cross-sectional drawing indicating the various components and dimensions of the IAC is shown in Figure A-5.

The target burial depth of all cables is 3 to 7 ft (1 to 2 m) beneath the seabed and was modeled at the 3.3-ft (1-m) burial depth.[22] Where burial cannot occur, sufficient burial depth cannot be achieved, or protection is required due to cables crossing other existing cables, the cables will be covered with protective concrete mattresses or rock berms. For the purposes of this study, the protective coverings for these areas will be at least 1-ft (0.3-m) thick. The PDE is currently considering both concrete mattresses and rock berms. Modeling was performed for a minimum concrete mattress thickness of 1 ft (0.3 m), which conservatively estimated EMF over coverings by either mattresses or rock berms The potential ability of these mattresses or other covering to attenuate magnetic-field levels was not considered; their primary effect to calculations was in effectively changing the cable burial depth to 1 ft (0.3 m).

---

[22]   The specified minimum burial depth of 3.3 ft (1 m) was used in modeling. Elsewhere in the COP references to 1 to 2 m burial depths are rounded to 3 to 7 feet.

Table A-2.   Summary of offshore modeling AC configurations

Configuration	1a	1b
Description	IAC	
Voltage	66 kV*	
Average Loading	377 A	
Peak Loading	Confidential	
Ampacity Rating		
Cable Cross Section	800 square millimeters [mm^2]	
Cable Type, Nominal Outer Diameter (OD)	3-core XLPE, 7.1-inch OD (179.4 millimeter [mm])	
Distance Between Conductor Centers within Cable	2.8-inches (70.2 mm)	
Cable Pitch**	9.8 ft (3 m)	
Installation Type	Buried	Surface-Laid‡
Minimum Target Burial Depth to Top of Cable	3.3 ft (1 m)	1 ft (0.3 m)
Evaluation Heights	At seabed and 3.3 ft (1 m) above seabed§	

*   For the same total power, cable current-levels would be expected to be lower for higher voltage cables (e.g., 161 kV IAC). Magnetic- and induced electric-field levels would also be expected to be lower.
**   Cable pitch is the distance over which the helically-twisting conductors of the IAC make one complete revolution. Cables are conservatively modeled with a cable pitch of 10 ft (3 m). Magnetic- and induced electric-field levels would also be expected to be lower for shorter cable pitch (e.g., 8.2 ft [2.5 m]).
‡   Surface-laid cables will be covered with a rock berm or a concrete mattress that is 1-ft (0.3-m) thick.
§   Where covered by a rock berm or concrete mattress, the evaluation heights are at the top of the protective cover and at a height of 3.3 ft (1 m) above the protective cover.

a)   b)
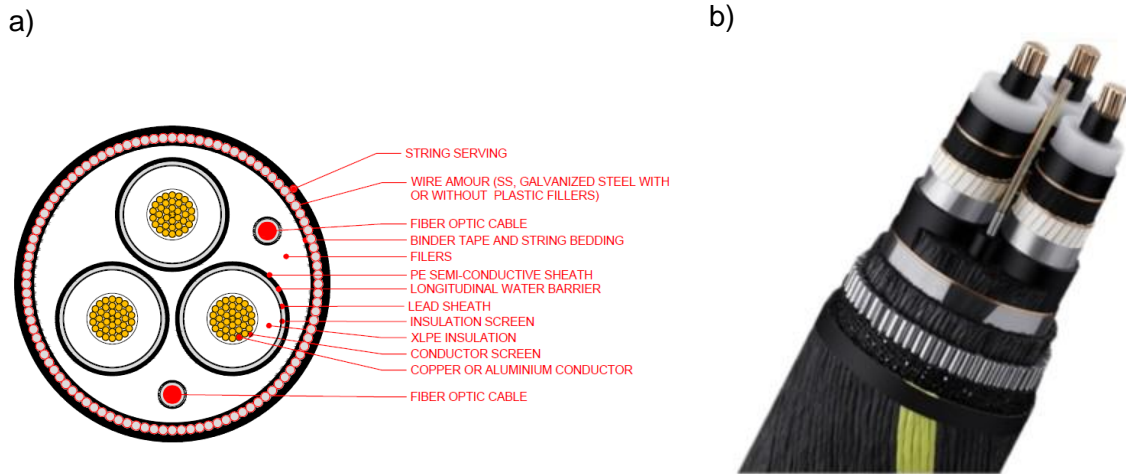

Figure A-5.   a) Illustrative cross-section of an example three-core AC submarine cable, b) photograph showing the various layers of a submarine cable.

OCS–DC Modeling Scenarios

Separate models of the OCS–DC were evaluated for the seabed (based on the 5.6-ft [1.7-m] minimum spacing of cables at a monopile at a 16-ft [5-m] radius) and for higher in the water column (based on the minimum spacing of 5.9-ft [1.8-m]) of J-tubes at a jacket foundation. Although only the jacket lattice structure is now being considered for the OCS–DC structures, the monopile configuration provides a more conservative scenario for assessment of the field levels at seabed because cables will be closer together.[23]

OCS–DC at Seabed

At the seabed, field levels were calculated for a monopile with an outer radius of 16 ft (5 m) running vertically through the water column, with SRWEC and IACs traversing down through the interior of the monopile. This is the smallest monopile anticipated for use, which results in the closest spacing of cables and hence the highest average EMF levels. The SRWEC exit the monopile at a height of 23 ft (7 m) above the seabed, and the IACs exit the monopile at a height of 16 ft (5 m) above the seabed. All cables leave the monopile inside a cable protection system (CPS) of approximately a 16-inch (400-mm) OD and travel from the edge of the monopile at an angle of 45° from vertical to the scour protection below. A 6.6-ft (2 m) thick layer of scour protection material is around the base of the monopile, upon which the cables lie as they travel radially away from the monopile. Exponent modeled the OCS–DC monopile configuration with eight IACs and two SRWEC, spanning 180 degrees, as shown below in Figure A-6, wherein each J-tube contains a single three-core IAC cable or a single (positive or negative) DC cable.

---

[23]   In the most recent design of the OCS–DC jacket structure, the minimum spacing between J-tubes in the water column increased to approximately 6.6 ft (2 m). The calculated volume-average field levels (AC and DC) will decrease slightly as a result of this design change.
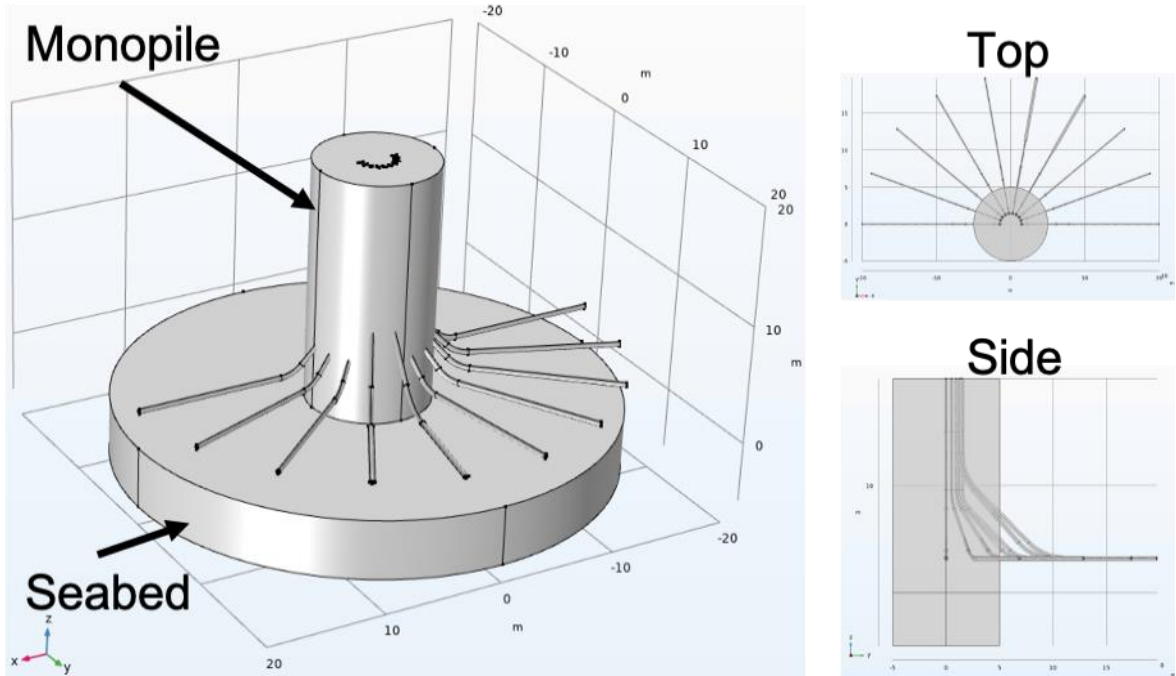
Figure A-6.   OCS–DC modeled at the seabed for a monopile foundation.

OCS–DC in the Water Column

In the water column, the IACs and SRWEC travel vertically inside J-tubes composed of high permeability metal. The cables are conservatively assumed to be arranged around the sides of a square platform, with 5.9-ft (1.8-m) spacing between cables. Exponent modeled cables along one side of the platform, consisting of four J-tubes containing IACs and two J-tubes each containing one cable of the SRWEC, as shown below in Figure A-7. Details are reported in Attachment D.[23]
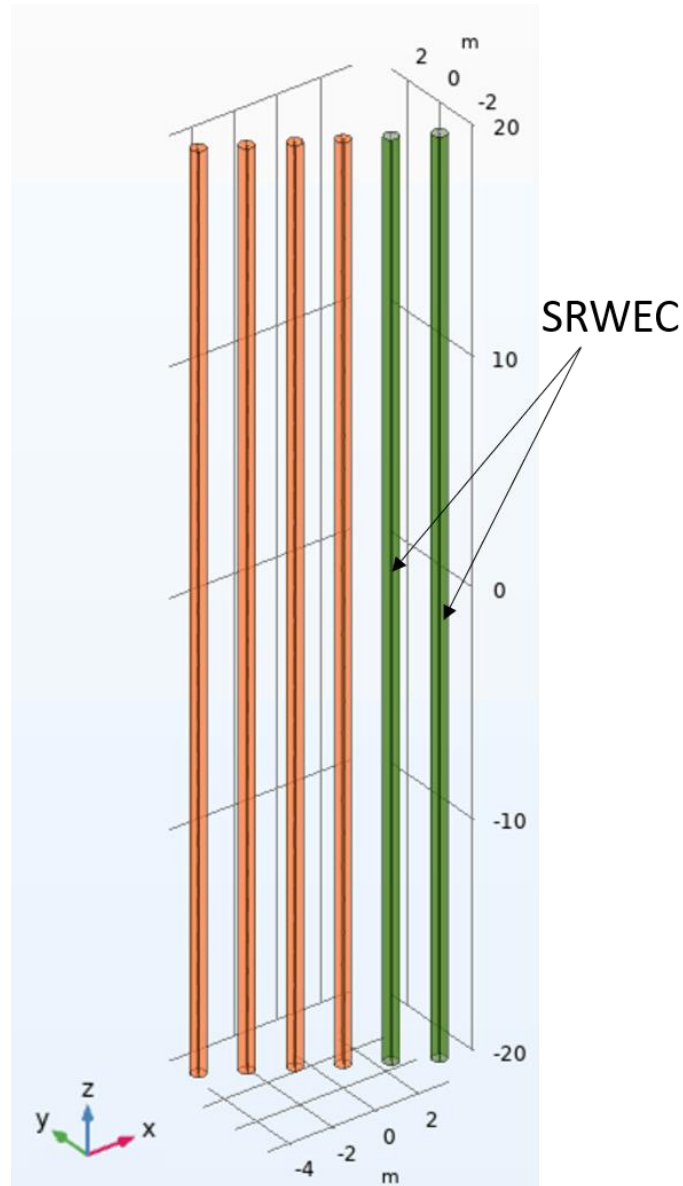

Figure A-7. OCS–DC modeled in the water column for a jacket foundation. Green cables are SRWEC and orange cables are IAC.

WTG Configuration

The WTG configuration is based on a 16-ft (5-m) radius monopile, inside which IACs travel down through the water column. Each WTG is expected to connect to a maximum of three IACs. The IACs exit the monopile in CPS at height of 16 ft (5 m) above the seabed and travel at a 45° angle until they reach a layer of scour protection material located around the base of the monopile. This configuration is shown below in Figure A-8.
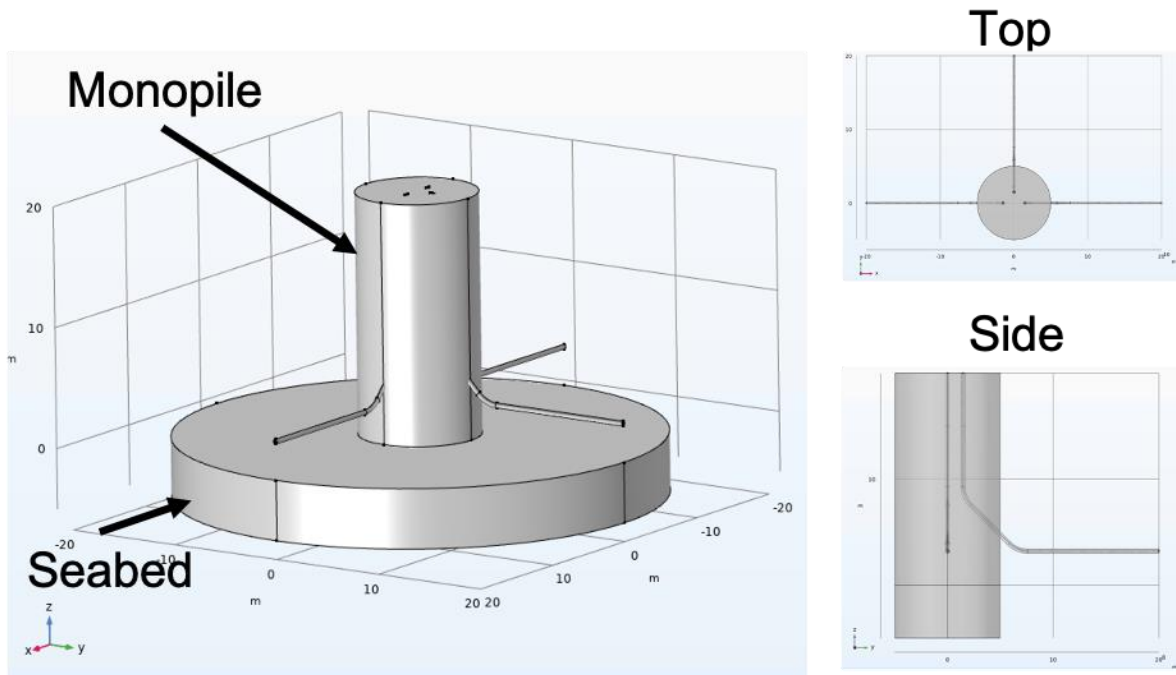

Figure A-8.   Monopile foundation modeling configuration of the WTG.

Attachment B

EMF Calculation Methods and Assumptions

Sunrise Wind provided data to Exponent regarding the preliminary cable design, as well as the loading for each proposed cable configuration. These input data were discussed in Attachment A, wherein Table A-1 and related text address inputs for DC cables, and Table A-2 and related text address inputs for AC cables. From these data, Exponent developed models of the offshore DC and AC cable configurations, for computation of the magnetic and induced electric fields. Where Landfall HDD design or cable loading specifications have changed, they have been addressed.

DC Magnetic Fields and Induced Electric Fields

Earth's Geomagnetic Field

The total DC magnetic field near the SRWEC depends on the magnitude and direction of the cables and the strength and direction of earth's ambient geomagnetic field. The geomagnetic field at 40.83°N, 71.53°W (approximately at the center of SRWEC cable route) is used in all calculations, corresponding to the geomagnetic components shown in Table B-1. At this location, the geomagnetic field has a -14-degree declination (westward of geographic north) and a 65.8-degree inclination (downward). Along the SRWEC route, the ambient geomagnetic field does not vary by more than approximately 1 percent.

Table B-1.   Geomagnetic magnetic field at coordinates 40.83°N, 71.53°W

Component	Geomagnetic field (in nanotesla [nT] and mG)		
Northern component	20,510.9 nT	=	205 mG
Eastern component	–5,036.1 nT	=	–5.0 mG
Downward component	45,945.6 nT	=	459 mG
Total geomagnetic field*	50,567.36 nT		506 mG

* Total geomagnetic field is calculated as the square root of the sum of the components squared

Magnetic Field Strength

DC current flowing through a conductor results in a DC (i.e., static) magnetic field. The static magnetic field from the DC current is calculated by the application of the Biot-Savart Law, which is derived from fundamental laws of physics. Application of the Biot-Savart Law is particularly appropriate for long straight conductors such as the SRWEC for which analytical solutions are relatively straightforward.[24] In order to calculate the total magnetic field, the calculated magnetic-field vector from the SRWEC is added to earth's geomagnetic-field vector.

Compass Deflection

The strength of the total DC magnetic field due to the combined field from the SRWEC and the earth's geomagnetic field is one way to describe the effect of the DC cable on the local environment, another is evaluating how much the horizontal component of the local static magnetic field (i.e., the portion used for compass navigation) changes direction as a result of the SRWEC. A number of species use the earth's geomagnetic field as an environmental cue; and changes in direction of the horizontal component of the magnetic field are therefore an important way to describe the local effect of the cable (Hanson and Westerberg 1987; Tański et al., 2011; Walker et al., 1998). For example, a compass needle typically points along the direction of the earth's geomagnetic field, but a new DC magnetic-field source may cause a local deviation to a new apparent direction of magnetic north around the cable. Here, this deviation is calculated as the compass deflection, which is the difference in angular direction in degrees between the horizontal component of the

---

[24] $|B| = \mu_0|H| = \mu_0\ I/2\pi r$, where B is the magnetic flux density, μ_0 is the magnetic permeability of a vacuum, I = current, and r = the distance from each cable conductor.

ambient geomagnetic field and the horizontal component direction of the combined DC field from the earth and from the SRWEC.

Induced Electric Field

The designed dielectric insulation and the grounded metallic sheath of the SRWEC will effectively block the electric field from the voltage applied to the conductors from reaching the marine environment (e.g., Snyder, et al., 2019). However, the changes to the geomagnetic field around a DC cable can affect the electric field produced by the movement of electric charges through the static magnetic field. The induced electric field is calculated by applying the Lorentz force equation, shown below, which can be used to calculate the induced electric field in fish and in sea water by the movement of electric charges in the total magnetic field. The DC electric fields were calculated by applying the Lorentz force equation, in which the electric field magnitude *E* is expressed as:

$$E = \frac{F}{q}$$

and

$$F = qvB \sin \theta$$

where

F = magnitude of the force vector **F**,

q = the electric charge,

v = magnitude of the velocity vector **v**,

B = magnitude of the magnetic flux density vector **B**, and

$\sin \theta$ = sine of the angle θ between the directions of the vectors **v** and **B**.

The resulting induced DC electric fields were calculated by applying the Lorentz force equation for a representative perpendicular water flow velocity of 2 ft/s (60 cm/s) (Oliver et al., 2012) as well as movement of electrosensitive species (1 ft/s [30 cm/s] for sturgeon [Fish and Shannahan 2000] and 0.7 ft/s [21 cm/s] for dogfish[25]).

AC Magnetic Fields and Induced Electric Fields

Electric Fields Induced In Seawater

Magnetic-field calculations were performed using data including current, burial depth, and conductor configurations. As noted in the body of this report, the electric field associated with voltage applied to the conductors within the cables are entirely shielded by cable insulation, grounded metallic sheaths and steel armoring around each cable. Magnetic fields, however, will induce a small electric field in the seawater, which may be detectable by certain electrosensitive marine organisms.

Exponent modeled the AC magnetic- and induced electric-field levels for IACs using 3D FEA in COMSOL Multiphysics (version 5.5) that included helically-twisting, three-phase conductors within each of the AC cables. The simulation used the magnetic-field physics interface of COMSOL to solve the time-harmonic Maxwell-Ampere's law for the magnetic fields generated by the IACs. The FEA model was validated against

---

[25]   http://www.fsl.orst.edu/geowater/FX3/help/9_Fish_Performance/Fish_Length_and_Swim_Speeds.htm

two published references (Haber, 1974; Pettersson and Schönborg, 1997) for the case of a straight section of helically-twisting, three-phase conductors. Both references implemented different analytical solutions and Pettersson and Schönborg (1997) also included a comparison to empirical measurements. DC magnetic fields from the SRWEC in the vicinity of the OCS–DC structures also were calculated using FEA modeling, using a similar approach as above but solving for static fields.

The inputs to the simulations were the conductor geometry (i.e., cable diameter, conductor spacing, and pitch of the helical twisting), burial depth of the cable, cable loading, and material properties of seawater.[26] The proposed separation of the IACs will be greater in regions away from WTGs and OCS–DC, and thus were modeled in isolation from one another

The magnetic-field levels offshore were calculated at the seabed surface, as well as at a height of 3.3 ft (1 m) above the seabed, in accordance with IEEE Standard 644-2019 and IEEE Standard C95.3-2021 (IEEE 2019, 2021). Results are reported in units of mG as the maximum root-mean-square flux density value. Where applicable, the effects of the metallic J-tubes that enclose some stretches of cables were qualitatively evaluated. In particular, the degree to which AC fields may be shielded by the J-tubes was considered, and the DC magnetization of the J-tubes enclosing the SRWEC at the OCS–DC was evaluated. The material properties used in simulations included conductivity, relative permittivity, and relative permeability, as noted in Table B-2. The inclusion of the steel J-tubes (see Table B-2) would result in a decrease in the reported field levels in all calculated values in the water column at the OCS–DC.

Table B-2. Material properties used for calculating 60-Hz field levels in seawater

Material	Conductivity (S/m)	Relative Permittivity	Relative Permeability	Reference
Seawater	5	72	1	Chave et al., 1990; Somaraju and Trumpf 2006
Seabed	1.1	30	1	Cihlar and Ulaby 1974; Chave et al., 1990; Hulbert et al., 1992;
Concrete	0.04	200	1	Wilson 1986
J-tube	1.46×10^6	1	1 - 4000	Values representative of likely range for AISI-SAE grade 1008 steel

Electric Fields Induced in Marine Organisms

The oscillating magnetic fields from the submarine cables in the seawater above the cables will induce a weak electric field within the body of marine organisms, which may be detectable by certain electrosensitive marine organisms. As such, the magnitude of the electric field induced in marine organisms swimming over the offshore cable segments was calculated by modeling representative species as homogeneous ellipsoids. In general, while a larger electric field will be induced in a larger animal, the specific detection thresholds for electrosensitive species are also important in determining the likelihood that a specific species will be capable of detecting and responding to the 60-Hz cable.

---

[26] Calculated magnetic-field levels in other common sediment types or in freshwater would not be substantially different from those calculated here for seawater.

Other Modeling Considerations

Cable Composition

The modeling approach is designed to produce conservative estimates of the maximum expected magnetic-field and induced electric-field levels. The models do not account for the attenuation of magnetic fields from conductor sheaths and outer steel armoring of the cables, nor do they include the significant shielding of AC magnetic fields likely to occur due to the high permeability metal J-tubes at the OCS–DC jacket foundation.

A previous study shows that flux shunting accounted for an almost two-fold reduction in the AC magnetic field, with a much smaller reduction attributable to eddy currents (Silva et al., 2006). In addition, Hutchison et al., (2018) reported post-construction measurements over similar AC three-core XLPE submarine cables. One finding from that report was that *"[t]he magnetic field produced by the [AC cable] was ~10 times lower than modeled values commissioned by the grid operator…"*[27] The modeling method applied in this assessment for the AC cables is more sophisticated than those cited in Hutchison et al., 2018), because it accounts for the helical twisting of the conductors, which results in lower calculated magnetic-field levels.

In addition, the effects of magnetization in the metallic J-tubes due to exposure to DC magnetic fields from the SRWEC in the OCS–DC configurations was assessed to have minimal effect on the volume average DC magnetic-field levels. The magnetization of the high permeability metal J-tubes does not substantially affect calculated results because the magnetic-field level decreases rapidly with distance from the J-tube. Throughout a region that extends 5 ft (1.5 m) away from the J-tubes, the magnetization of the J-tube increases the average magnetic-field strength by approximately 0.6 percent.

Unbalanced Currents and Ground Currents

Another factor not accounted for in these models is the magnetic field resulting from unbalanced currents flowing along the sheaths or armoring of the cables. These unequal currents on the three phases of an AC transmission line or between two DC cables) can be controlled to some extent by system design and operation, but also may be completely unrelated to the generation or transmission of electricity by the Project and therefore are more difficult to control or predict. The combination of unbalanced phase currents and grounding-related currents can be thought of as a single-phase, effective net current flowing straight along the cable. Hutchison et al. (2018) reported measurement data for an AC submarine cable that indicate the highest measured AC field (near to the cable itself) is produced by the phase currents, but at some distance away, unbalanced AC currents on the cable can have a much weaker, but noticeable, contribution to the AC magnetic field.

AC Currents on DC Cables

In addition, previous measurements (Hutchison et al., 2018, 2020) showed the presence of low-strength AC fields emanating from a DC cable. The applicability of those measurements to the present case is unclear because the source and magnitude of these currents was not well understood and they are likely to be quite site-specific. Nevertheless, these measurements provide some context regarding the relative magnitudes of DC magnetic fields and AC magnetic fields from past measurements. The reported AC magnetic- and induced electric-field levels from the DC cable reported by Hutchison et al. (2018, 2020) were approximately 1.7 mG and 0.84 mV/m or less. These levels are far below those of other AC installations (Love, 2016).

---

[27] Note that while the Hutchison et al. (2018) report focused on DC submarine transmission lines, a portion of the report also reported measurements around an AC transmission cable, which is referenced here.

Attachment C

Calculated EMF Levels for Cables

DC Cables

DC Magnetic Fields

The DC current load within the SRWEC generates a static magnetic field around these cables. This section presents the total static magnetic field due to the earth's geomagnetic field and static magnetic field from the SRWEC. The total magnetic field (geomagnetic field + SRWEC) in the vicinity of the SRWEC is far below the ICNIRP standard for human exposure to static magnetic fields for all configurations considered. Moreover, magnetic fields diminish rapidly with distance, so it is only in the immediate vicinity of the cables that the magnetic-field level will be appreciably different than earth's geomagnetic field. The opportunity for human exposure to magnetic-field levels above that of the ambient geomagnetic field in the Project Area would be extremely limited and short term.

The magnetic field was calculated for three cable directions plus north-south and east-west. The cable directions 30° north of east, 161° north of east, and 356° north of east correspond to the Project cable route. For each of the cable orientations, the magnetic field was calculated for each of the four cable configurations, using peak loading levels.

Figure C-1 shows that the configuration of the cables (i.e., side by side or stacked on top of one another) and current direction both have significant effects on the total calculated field level. Each of the sub-plots below shows three curves. The dashed gray line is value of earth's ambient geomagnetic field at the location of the cable. The solid blue line is the total magnetic-field level (SRWEC + earth's geomagnetic field) calculated at the seabed, while the solid orange line is the total magnetic field level calculated at 3.3 ft (1 m) above the seabed.

For cables laid side by side (top two plots of Figure C-1), if the cable on the left carries current toward the OCS–DC, the net effect near the cables is to substantially decrease the total magnetic-field level near the cables (top-left figure). If the current direction reverses so that the cable on the right carries current toward the OCS–DC, the net effect near the cables is to substantially *increase* the total magnetic-field level near the cables. Similarly, if the cables lay beneath the seabed stacked on top of one another (bottom two figures in Figure C-1), then the total magnetic-field level will be increased on one side of the cable and decreased on the other (depending on the direction of current flow).

While Figure C-1 shows the total magnetic-field level ($B_{total} = B_{cable} + B_{earth}$), Table C-1 shows the *difference* (or deviation) between the ($B_{Deviation} = |B_{total}| - |B_{earth}|$), which provides a summary of the *deviation* of the total magnetic-field level from the ambient geomagnetic field *evaluated at a height of 3.3 ft (1 m) above the seabed.*[28] The first four rows of Table C-1 show the maximum positive deviation '(+) Max', maximum negative deviation '(–) Max' and the deviation at ±10 ft (±3 m) from the SRWEC centerline. For example, the first row of Table C-1 corresponds to the solid orange line (the top-left plot) in Figure C-1. The maximum negative deviation from earth's geomagnetic field is larger (–103 mG) than the maximum positive deviation (+26 mG). At a distance of -10 ft (-3 m) from the SRWEC centerline, the deviation is +25mG, while at +10 ft (+3 m) from the SRWEC centerline, the deviation is -0.1 mG.

Table C-1 shows similar comparisons for the remaining configurations. The last row of Table C-1 shows a summary of the variation in the magnetic-field deviation from ambient for any of the four configurations evaluated. For example, the maximum positive deviation (i.e., increase in field level) ranges from +26 mG (top-left plot of Figure C-1) to +104 mG (top-right plot of Figure C-1). Table C-2 shows similar results for the other

---

[28] Tabular results are shown as the deviation from the ambient geomagnetic field because in tabular form, even very far from the cables, the reported total field values will be ~506 mG (the remaining ambient geomagnetic field), which in tabular format can make it difficult to see the distance at which the effect of the cable on the local magnetic field decreases to near background levels.

geographic orientation of the cable route (161° and 356° north of east) as well as for the east-west and north-south orientations, and shows that within ±10 ft (±3 m) from the SRWEC center line, the effect of the SRWEC is quite small—a change of less than 10 percent relative to the ambient geomagnetic field. Detailed results corresponding to every geographic orientation evaluated at seabed and 3.3 ft (1 m) above seabed for both buried and mattress-covered cables are presented below in Table C-3 to Table C-10 and graphical results of buried cables are shown in Figure C-2 to Figure C-6. A tabular summary of magnetic field levels for the Landfall HDD is shown in Table C-11 and Table C-12 with corresponding graphical results shown in Figure C-7.
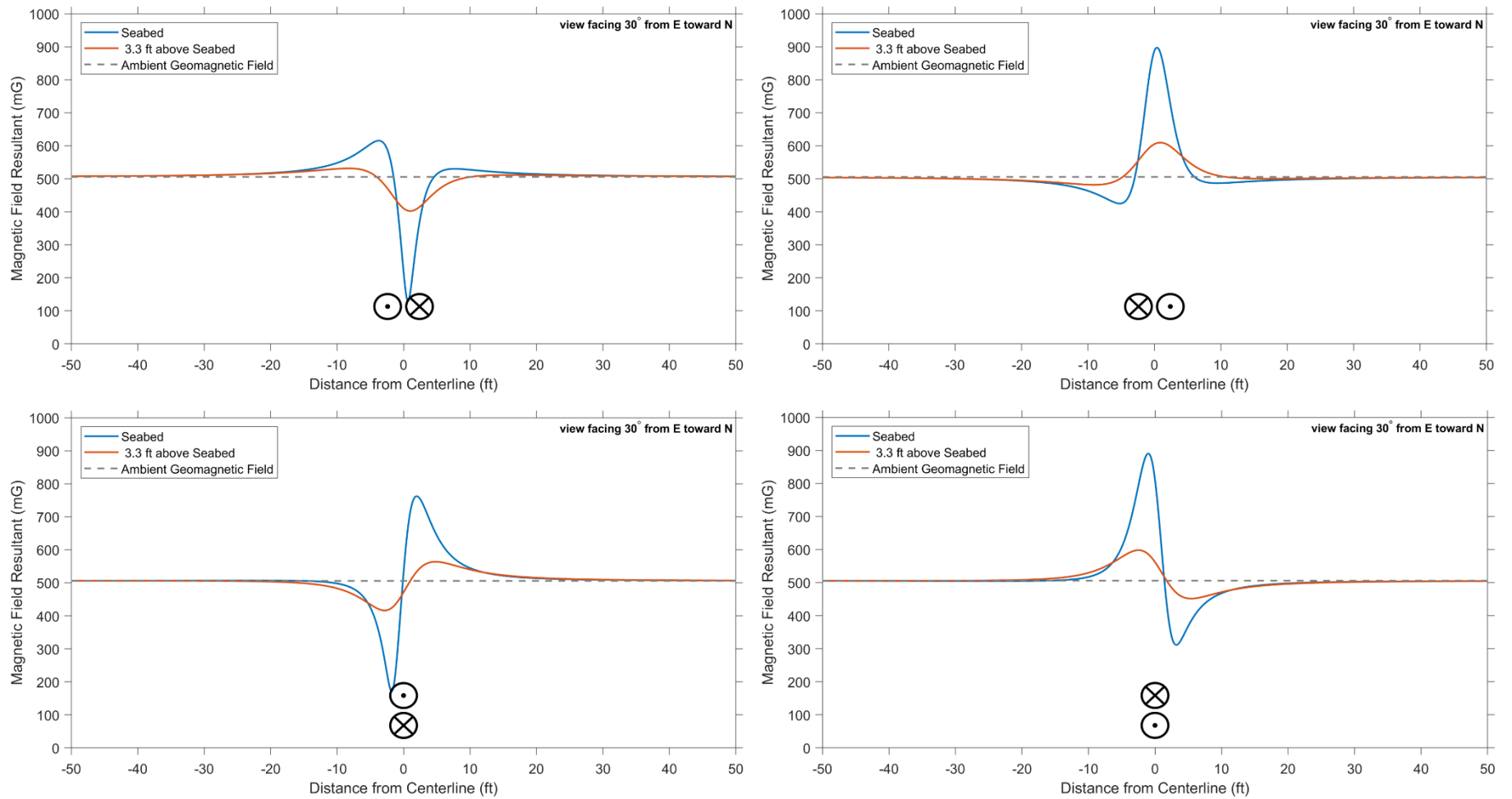
Figure C-1.   Total DC magnetic field at peak loading on the seabed (blue line) and 3.3 ft (1 m) above the seabed (orange line) for four different installation scenarios, indicated by the figure at the bottom center of each plot. In all four plots the cable is oriented 30° north of east.

Table C-1. DC magnetic-field deviation (mG) for a 30° north of east cable orientation at various horizontal distances 3.3 ft (1 m) above the seabed at peak loading

Installation Type	Configuration	DC Magnetic Field Deviation (mG)			
		−10 ft (−3 m)	(+) Max	(−) Max	+10 ft (+3 m)
Buried (3.3 ft)	⊙ ⊗ (horizontal)	25	26	-103	-0.1
	⊗ ⊙ (horizontal)	-23	104	-24	2.4
	⊙ over ⊗ (vertical)	24	93	-54	-34
	⊗ over ⊙ (vertical)	-23	58	-90	34
	30° north of east Summary	-23 to 25	26 to 104	-103 to -24	-34 to 34

Table C-2. DC magnetic-field deviation (mG) summary of cable configurations for four cable orientations at various horizontal distances 3.3 ft (1 m) above the seabed at peak loading

Installation Type	Cable Route	DC Magnetic Field Deviation (mG)			
		−10 ft (−3 m)	(+) Max	(−) Max	+10 ft (+3 m)
Buried (3.3 ft)	30° north of east	-23 to 25	26 to 104	-103 to -24	-34 to 34
	161° north of east	-34 to 34	24 to 103	-102 to -22	-23 to 25
	356° north of east	-23 to 25	26 to 104	-103 to -24	-34 to 34
	east-west	-24 to 25	26 to 104	-104 to -24	-34 to 35
	north-south	-27 to 28	16 to 100	-96 to -14	-30 to 31

DC Magnetic Field Results

Calculated DC magnetic-field levels in seawater are provided in Table C-3 to Table C-7 below, each summarizing the maximum range of the variation in the magnetic-field deviation from ambient for any of the four DC cable-pair configurations evaluated for four orientations at peak loading with both buried and mattress-covered cables, as summarized in Attachment A, Figure A-1. Table C-9 and Table C-10 provide summaries of calculated magnetic-field levels at peak loading for buried (Table C-9) and mattress-covered (Table C-10) for all cable configurations and orientations.

The plots in Figure C-2 to Figure C-6 below show the deviation of the magnetic field in the vicinity of the cables from that of the earth's geomagnetic field for buried cables at peak loading with each of the four DC cable-pair configurations.

Table C-3.   DC Magnetic-field deviation (mG) at various horizontal distances above buried and mattress-covered cables for a 30° north of east cable orientation at peak loading

Installation Type	Location	DC Magnetic Field Deviation (mG)		
		(+) Max	(–) Max	±10 ft (±3 m)
Buried (3.3 ft [1 m])	Seabed	110 to 392	-376 to -81	-42 to 43
	3.3 ft (1 m) above seabed	26 to 104	-103 to -24	-34 to 34
Mattress-Covered (1 ft [0.3 m])	Top of protective cover	2291 to 4948	-331 to 0.1	-48 to 48
	3.3 ft (1 m) above protective cover	62 to 237	-233 to -52	-39 to 39

Table C-4.   DC Magnetic-field deviation (mG) at various horizontal distances above buried and mattress-covered cables for a 161° north of east cable orientation at peak loading

Installation Type	Location	DC Magnetic Field Deviation (mG)		
		(+) Max	(–) Max	±10 ft (±3 m)
Buried (3.3 ft [1 m])	Seabed	102 to 390	-352 to -74	-41 to 41
	3.3 ft (1 m) above seabed	24 to 103	-102 to -22	-34 to 34
Mattress-Covered (1 ft [0.3 m])	Top of protective cover	2286 to 4925	-295 to 0.1	-47 to 47
	3.3 ft (1 m) above protective cover	58 to 235	-226 to -47	-37 to 38

Table C-5.   DC Magnetic-field deviation (mG) at various horizontal distances above buried and mattress-covered cables for a 356° north of east cable orientation at peak loading

Installation Type	Location	DC Magnetic Field Deviation (mG)		
		(+) Max	(–) Max	±10 ft (±3 m)
Buried (3.3 ft [1 m])	Seabed	109 to 392	-374 to -80	-42 to 42
	3.3 ft (1 m) above seabed	26 to 104	-103 to -24	-34 to 34
Mattress-Covered (1 ft [0.3 m])	Top of protective cover	2291 to 4947	-328 to 0.1	-48 to 48
	3.3 ft (1 m) above protective cover	62 to 237	-232 to -51	-39 to 39

Table C-6.   DC Magnetic-field deviation (mG) at various horizontal distances above buried and mattress-covered cables for east-west cable orientation at peak loading
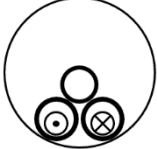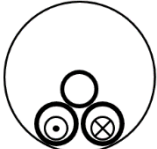
Installation Type	Location	DC Magnetic Field Deviation (mG)		
		(+) Max	(–) Max	±10 ft (±3 m)
Buried (3.3 ft [1 m])	Seabed	111 to 392	-379 to -81	-42 to 43
	3.3 ft (1 m) above seabed	26 to 104	-104 to -24	-34 to 35
Mattress-Covered (1 ft [0.3 m])	Top of protective cover	2291 to 4951	-334 to 0.1	-48 to 48
	3.3 ft (1 m) above protective cover	63 to 237	-233 to -52	-39 to 39

Table C-7.   DC Magnetic-field deviation (mG) at various horizontal distances above buried and mattress-covered cables for north-south cable orientation at peak loading

Installation Type	Location	DC Magnetic Field Deviation (mG)		
		(+) Max	(–) Max	±10 ft (±3 m)
Buried (3.3 ft [1 m])	Seabed	67 to 383	-292 to -47	-33 to 35
	3.3 ft (1 m) above seabed	16 to 100	-96 to -14	-30 to 31
Mattress-Covered (1 ft [0.3 m])	Top of protective cover	2267 to 4806	-187 to 0.1	-44 to 45
	3.3 ft (1 m) above protective cover	38 to 229	-206 to -30	-30 to 31

Table C-8.   Magnetic-field deviation (mG) from the 506 mG geomagnetic field at peak loading, evaluated at a height of 3.3 ft (1 m) above seabed and offset from the centerline of the Landfall HDD along a geographic direction of 161° north of east.

Configuration	Cable Orientation	DC Magnetic-Field Deviation (mG)			
		-10 ft (-3 m)	(+) Max	(-) Max	+10 ft (+3 m)
Landfall HDD (6-ft [1.8-m] burial depth)		-27	29	-123	23
		36	125	-27	-14
	161° north of east Summary	-27 to 36	29 to 125	-123 to -27	-14 to 23
Landfall HDD (46 ft [14-m] burial depth)		-5.8	1.3	-5.8	-4.2
		5.8	5.8	-1.3	4.2
	161° north of east Summary	-5.8 to 5.8	1.3 to 5.8	-5.8 to -1.3	-4.2 to 4.2

Table C-9. Summary of DC magnetic-field deviation (mG) from background* at various horizontal distances 3.3 ft (1 m) above cables buried 3.3 ft (1 m) beneath seabed for all cable configurations and orientations at peak loading

Evaluation Height	DC Magnetic Field Deviation (mG)											
	−75 ft (−23 m)	−50ft (−15 m)	−25 ft (−18 m)	−10ft (−3 m)	−5 ft (−1.5 m)	(+) Max	(−) Max	+5 ft (+1.5 m)	+10 ft (+3 m)	+25 ft (+18 m)	+50 ft (+15 m)	+75 ft (+23 m)
At seabed	-0.8 to 0.8	-1.9 to 1.9	-7.7 to 7.7	-42 to 43	-133 to 136	67 to 392	-379 to -47	-138 to 138	-41 to 41	-7.5 to 7.5	-1.9 to 1.9	-0.8 to 0.8
At 3.3 ft (1 m) above seabed	-0.8 to 0.8	-1.9 to 1.9	-7.3 to 7.3	-34 to 34	-71 to 72	16 to 104	-104 to -14	-70 to 71	-34 to 35	-7.1 to 7.1	-1.9 to 1.9	-0.8 to 0.8

* Geomagnetic field at coordinates: 40.83°N, 71.53°W is approximately 506 mG

Table C-10. Summary of DC magnetic-field deviation (mG) from background* at various horizontal distances 3.3 ft (1 m) above mattress-covered (1-ft [0.3-m]) cables for all cable configurations and orientations at peak loading

Evaluation Height	DC Magnetic Field Deviation (mG)											
	−75 ft (−23 m)	−50ft (−15 m)	−25 ft (−18 m)	−10ft (−3 m)	−5 ft (−1.5 m)	(+) Max	(−) Max	+5 ft (+1.5 m)	+10 ft (+3 m)	+25 ft (+18 m)	+50 ft (+15 m)	+75 ft (+23 m)
At seabed	-0.8 to 0.8	-1.8 to 1.8	-7.5 to 7.5	-48 to 48	-185 to 186	2267 to 4951	-334 to 0.1	-178 to 183	-47 to 47	-7.4 to 7.4	-1.8 to 1.8	-0.8 to 0.8
At 3.3 ft (1 m) above seabed	-0.8 to 0.8	-1.9 to 1.9	-7.6 to 7.6	-37 to 38	-107 to 110	38 to 237	-233 to -30	-109 to 111	-39 to 39	-7.5 to 7.5	-1.9 to 1.9	-0.8 to 0.8

* Geomagnetic field at coordinates: 40.83°N, 71.53°W is approximately 506 m

Table C-11.   Summary of DC magnetic-field deviation (mG) from background* from Landfall HDD at 6 ft (1.8 m) burial depth and at peak loading.

Evaluation Height	DC Magnetic-Field Deviation (mG)											
	−75 ft (−23 m)	−50ft (−15 m)	−25 ft (−18 m)	−10ft (−3 m)	−5 ft (−1.5 m)	(+) Max	(−) Max	+5 ft (+1.5 m)	+10 ft (+3 m)	+25 ft (+18 m)	+50 ft (+15 m)	+75 ft (+23 m)
At seabed	-2.3 to 2.3	-4.7 to 4.8	-12 to 13	-2.0 to 21	-108 to 145	63 to 253	-243 to -51	22 to 44	-49 to 62	-22 to 22	-6.1 to 6.1	-2.7 to 2.7
At 3.3 ft (1 m) above seabed	-2.1 to 2.1	-4.1 to 4.1	-7.1 to 7.9	-27 to 36	-90 to 96	29 to 125	-123 to -27	-26 to 46	-14 to 23	-19 to 19	-5.9 to 5.9	-2.7 to 2.7

* Geomagnetic field at coordinates: 40.83°N, 71.53°W is approximately 506 m

Table C-12.   Summary of DC magnetic-field deviation (mG) from background* from Landfall HDD at 46 ft (14 m) burial depth and at peak loading.

Evaluation Height	DC Magnetic-Field Deviation (mG)											
	−75 ft (−23 m)	−50ft (−15 m)	−25 ft (−18 m)	−10ft (−3 m)	−5 ft (−1.5 m)	(+) Max	(−) Max	+5 ft (+1.5 m)	+10 ft (+3 m)	+25 ft (+18 m)	+50 ft (+15 m)	+75 ft (+23 m)
At seabed	-0.1 to 0.1	-1.0 to 1.0	-4.4 to 4.4	-6.5 to 6.5	-6.7 to 6.7	1.5 to 6.7	-6.7 to -1.5	-5.6 to 5.7	-4.6 to 4.7	-1.2 to 1.3	-1.3 to 1.3	-1.4 to 1.4
At 3.3 ft (1 m) above seabed	<0.1	-1.2 to 1.2	-4.1 to 4.1	-5.8 to 5.8	-5.8 to 5.8	1.3 to 5.8	-5.8 to -1.3	-5.0 to 5.0	-4.2 to 4.2	-1.4 to 1.4	-1.0 to 1.0	-1.3 to 1.3

* Geomagnetic field at coordinates: 40.83°N, 71.53°W is approximately 506 m
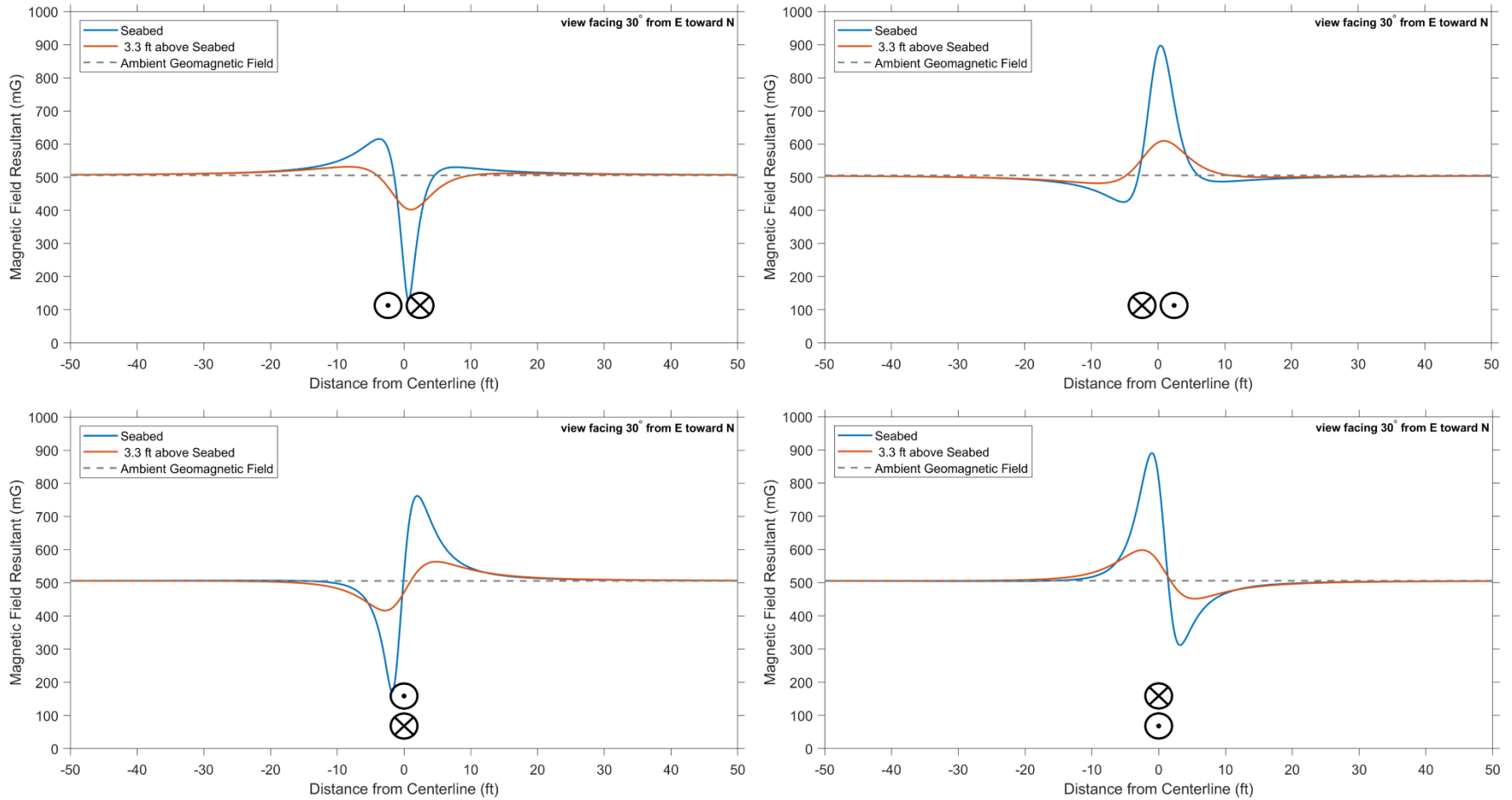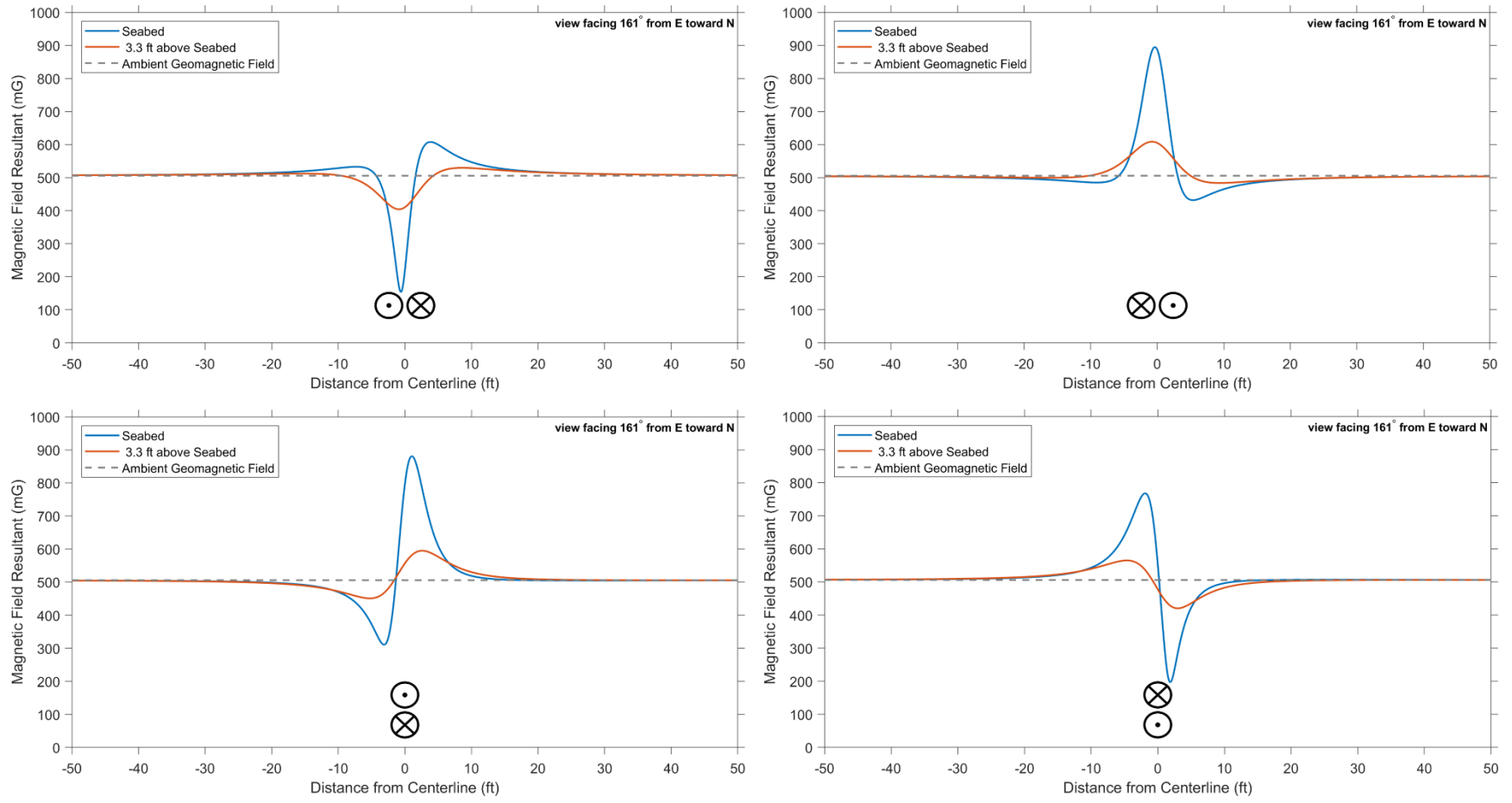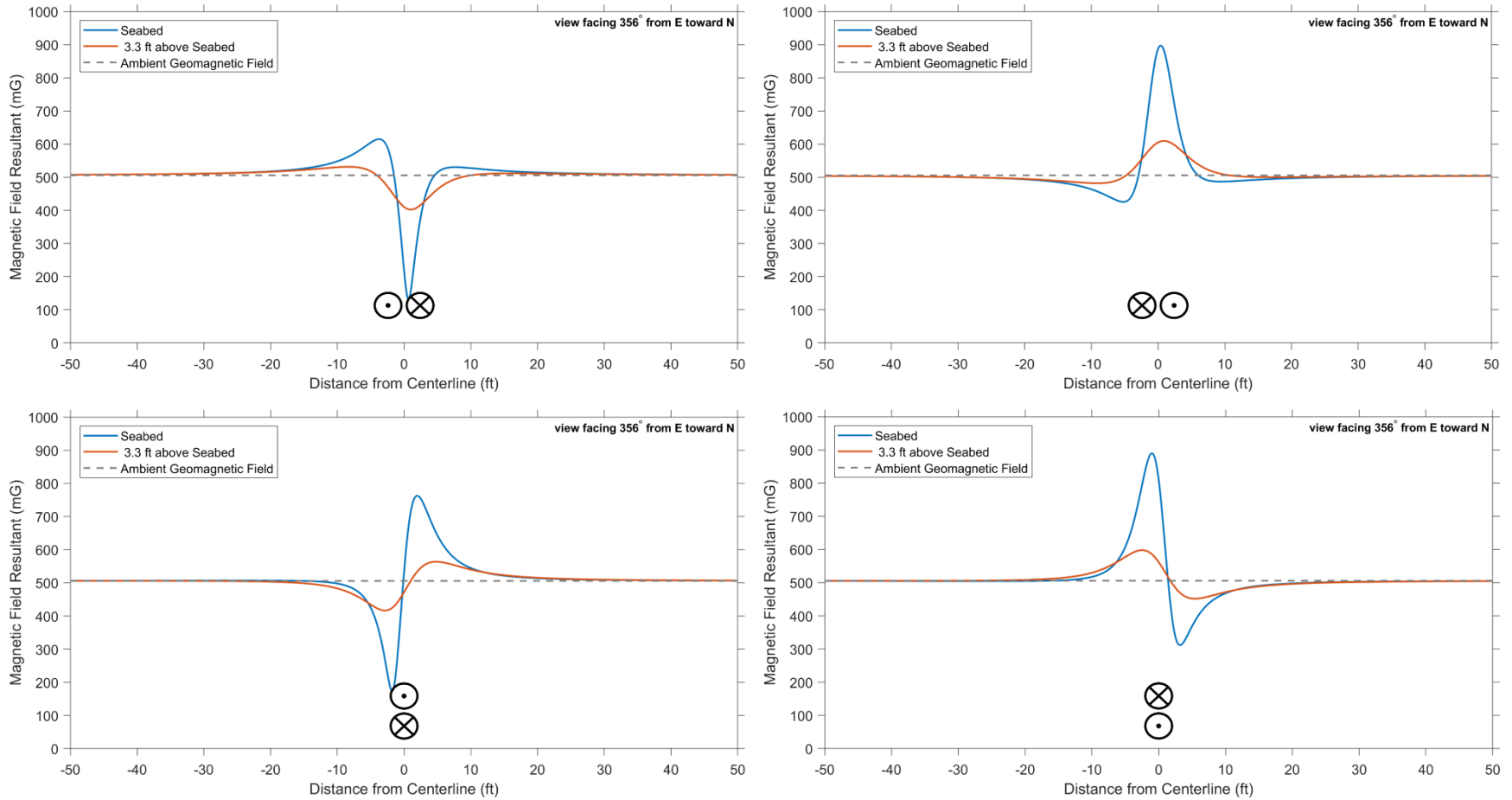
Figure C-2.   Total DC magnetic field at peak loading on the seabed (blue line) and 3.3 ft (1 m) above the seabed (orange line) for four different installation scenarios, indicated by the figure at the bottom center of each plot. In all four plots the cable is oriented 30° north of east.

Figure C-3.   Total DC magnetic field at peak loading on the seabed (blue line) and 3.3 ft (1 m) above the seabed (orange line) for four different installation scenarios, indicated by the figure at the bottom center of each plot. In all four plots the cable is oriented 161° north of east.
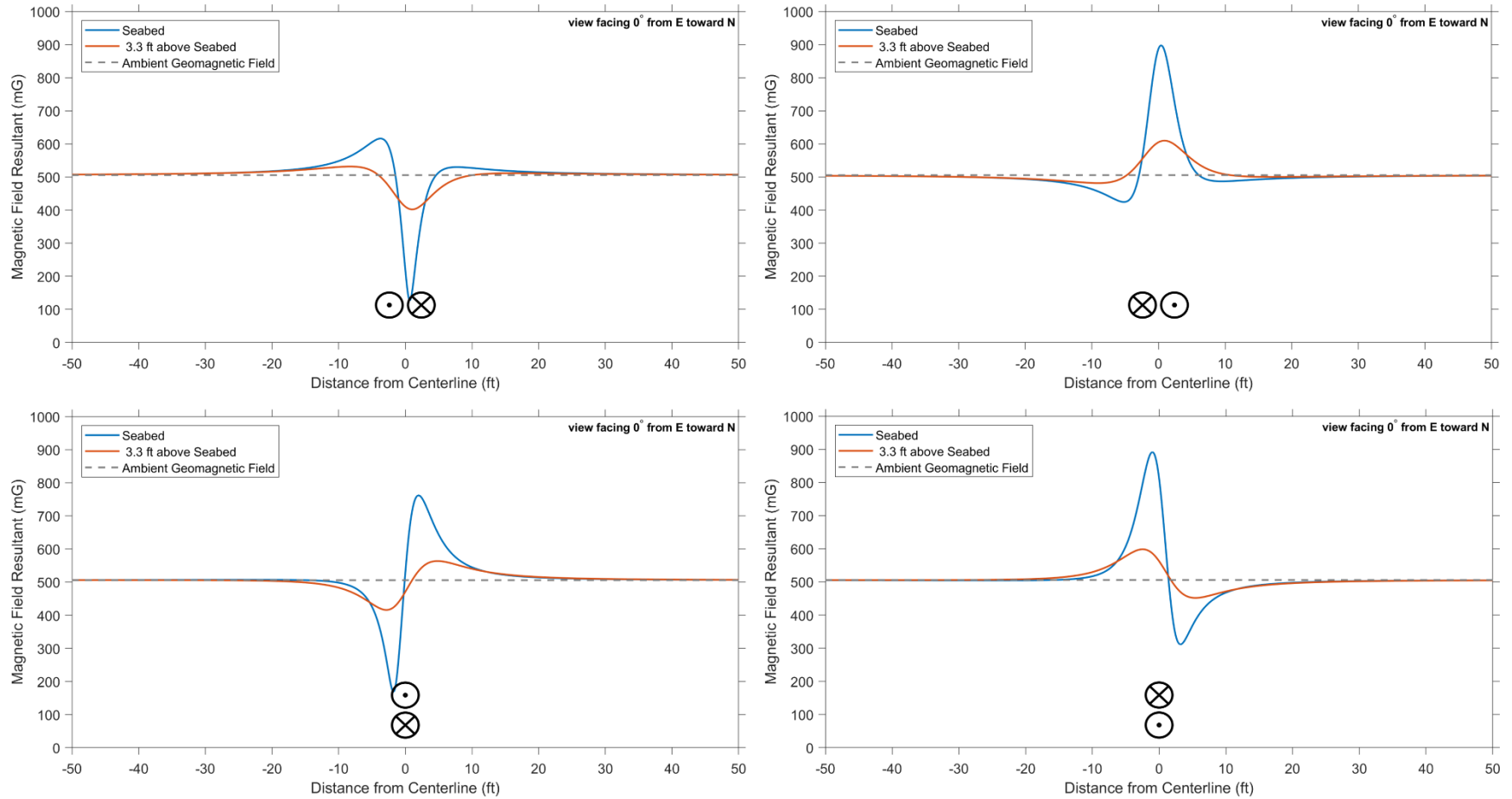
Figure C-4.   Total DC magnetic field at peak loading on the seabed (blue line) and 3.3 ft (1 m) above the seabed (orange line) for four different installation scenarios, indicated by the figure at the bottom center of each plot. In all four plots the cable is oriented 356° north of east.

Figure C-5.   Total DC magnetic field at peak loading on the seabed (blue line) and 3.3 ft (1 m) above the seabed (orange line) for four different installation scenarios, indicated by the figure at the bottom center of each plot. In all four plots the cable is aligned along the east-west axis.
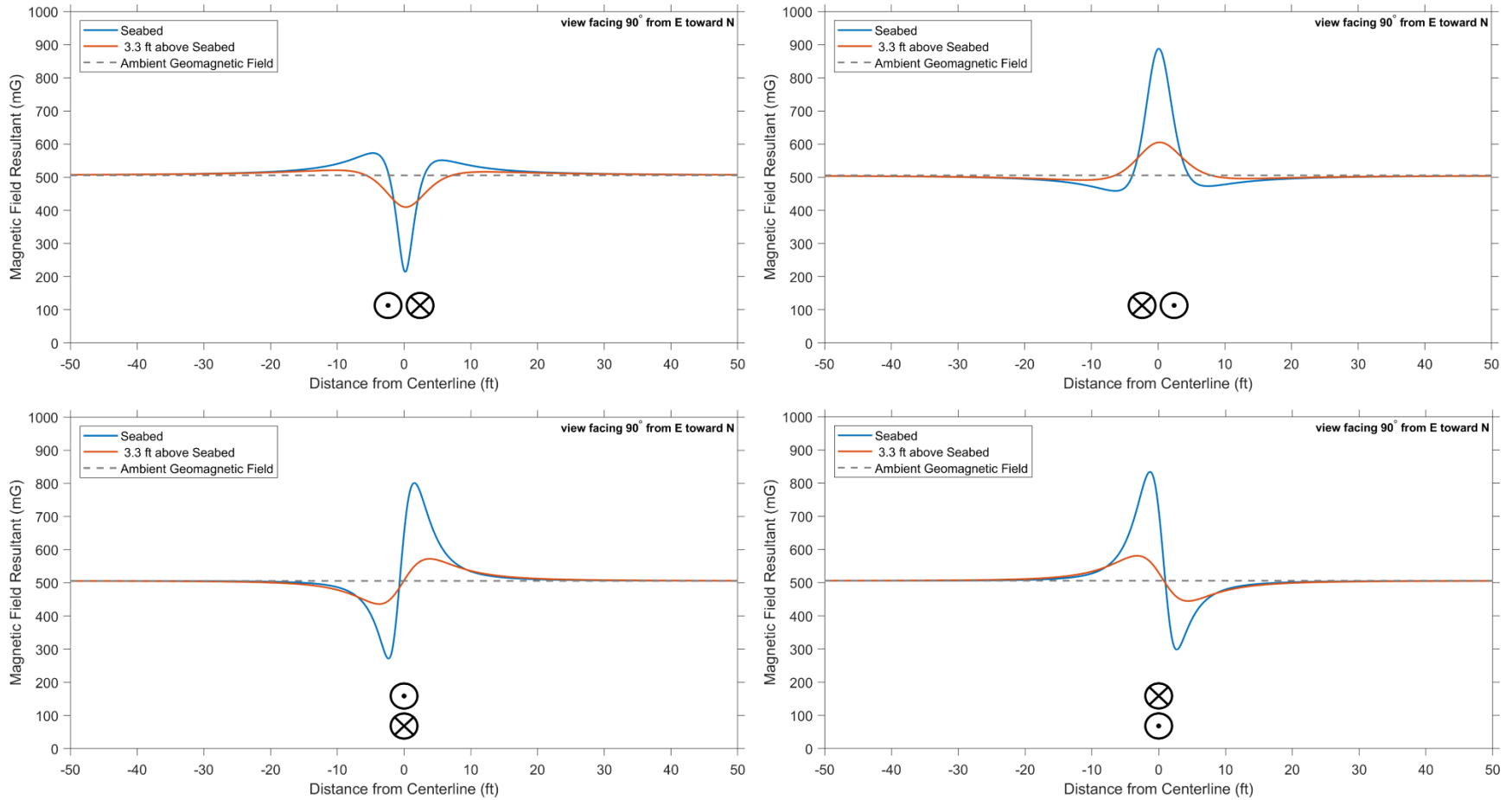
Figure C-6. Total DC magnetic field at peak loading on the seabed (blue line) and 3.3 ft (1 m) above the seabed (orange line) for four different installation scenarios, indicated by the figure at the bottom center of each plot. In all four plots the cable is aligned along the north-south axis.
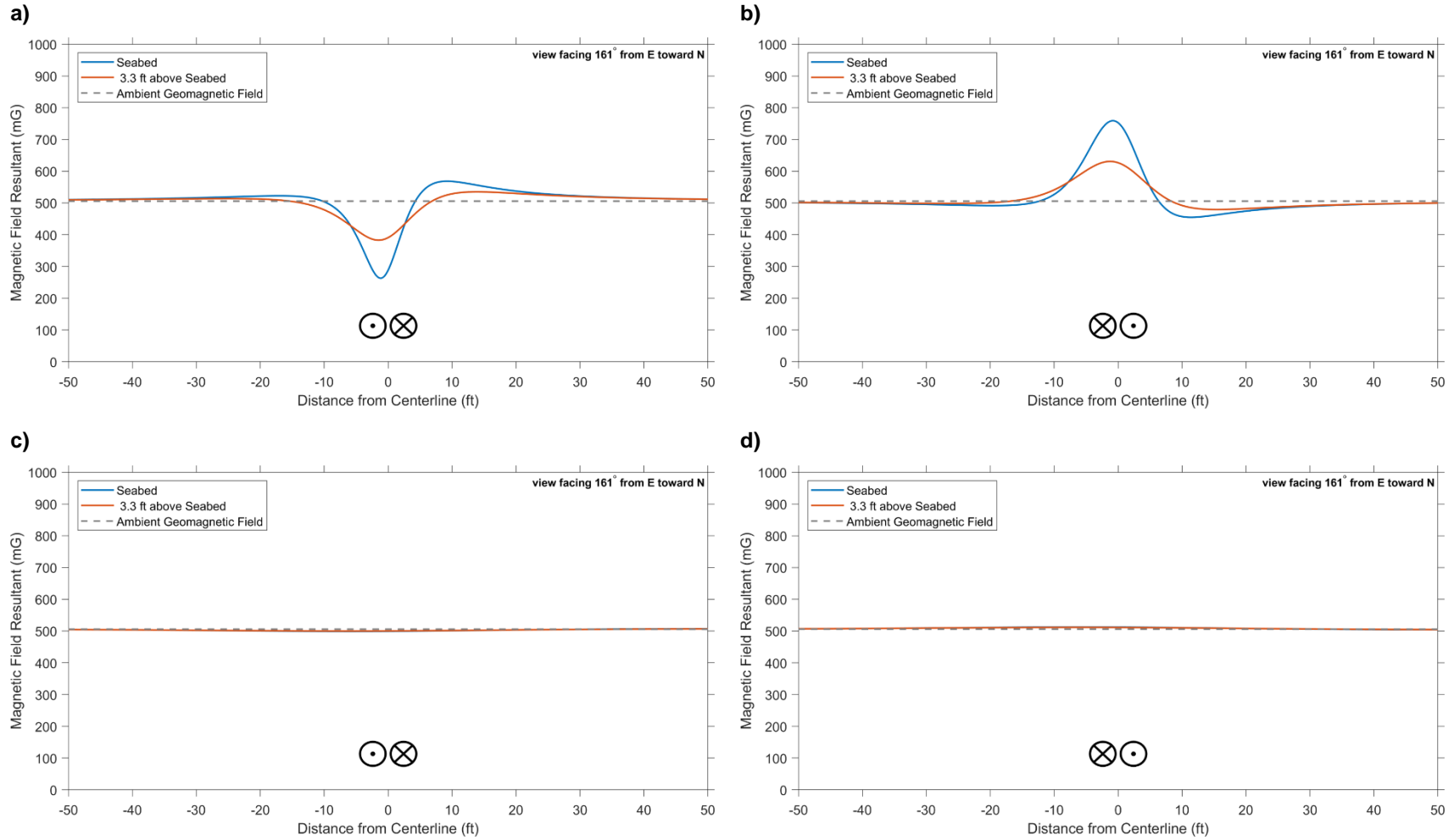
Figure C-7.   Total DC magnetic field for Landfall HDD for a 6 ft (1.8 m) burial depth (plots a and b) and a 46 ft (14 m) burial depth (plots c and d) at peak loading and evaluated both at seabed (blue line) and at 3.3 ft (1 m) above the seabed (orange line) oriented 161° north of east for two different installation scenarios, indicated by the figure at the bottom center of each plot.

DC Electric Fields

The SRWEC produces a static DC magnetic field but does not produce a DC electric field in the marine environment. There is, however, an electric field related to the movement of electric charges through the static magnetic field generated by the SRWEC, assessed by applying the Lorentz force equation (discussed in Attachment B). This electric field depends on the speed and direction of charge movement of the water (or a fish) over the cable. In the following analysis, the speed of the water or a fish (in cm/s) is substituted for the magnitude of the (assumed perpendicular) velocity vector **v** in Lorentz's law.

At a water velocity of 2 ft/s (60 cm/s) (Oliver et al., 2012), the induced electric field from the ambient geomagnetic field alone is approximately 0.030 mV/m. For this water velocity directly over the buried SRWEC, the induced electric-field level will increase near the cables to 0.059 mV/m. At a horizontal distance of ±10 ft (±3 m) from the SRWEC along the seabed, the electric-field level drops to 0.034 mV/m or less (to within approximately 0.004 mV/m of the induced electric field from the earth's ambient geomagnetic field alone). At a height of 3.3 ft (1 m) above the seabed, the calculated electric-field levels are lower. The electric field in electrosensitive fish of different sizes and swimming speeds also were calculated including dogfish at ~0.7 ft/s (21 cm/s) (Fish and Shannahan 2000), and sturgeon at 1 ft/s (30 cm/s).[29] At these slower velocities, the electric field also will be lower than for the 2.0 ft/s (60 cm/s) ocean currents, summarized in Table C-13.

Table C-13. Calculated DC induced electric-field levels (mV/m) at various horizontal distances 3.3 ft (1 m) above the seabed due to water movement or movement of electrosensitive species through the DC field produced by cables buried (3.3 ft [1 m]) at peak loading

Evaluation Case	Velocity (ft/s)	Height above Seabed	Induced Electric Field (mV/m) in Electrosensitive Species			
			Max	±5 ft (±1.5 m)	±10 ft (±3 m)	Ambient*
Ocean Current	2.0	0 ft	0.054	0.039	0.033	0.030
		3.3 ft	0.037	0.035	0.032	
Sturgeon	0.98	0 ft	0.027	0.019	0.016	0.015
		3.3 ft	0.018	0.017	0.016	
Dogfish	0.66	0 ft	0.019	0.014	0.012	0.011
		3.3 ft	0.013	0.012	0.011	

* Induced by ocean current flow and species-specific swimming velocity.

---

[29] http://www.fsl.orst.edu/geowater/FX3/help/9_Fish_Performance/Fish_Length_and_Swim_Speeds.htm

Compass Deflection

A compass needle responds to the horizontal component of the earth's geomagnetic field by pointing along the direction of this vector and a change in the compass direction is sometimes called a compass deflection. Some marine species are known to use the earth's geomagnetic field for navigation and mariners have historically used a compass to visualize the alignment of the horizontal component of the earth's geomagnetic field for navigation. Traditional compasses that rely on the earth's geomagnetic field may detect a small effect on compass readings above the cables in shallow water that will diminish quickly with distance. Modern navigational instruments that obtain compass readings and locations from global positioning system receivers would not be affected by the Project cables.

To assess the effect of the DC cables on potential biological compass readings, the deflections of the horizontal component of the total magnetic field from that of the earth's geomagnetic field were calculated. As an illustrative representation of the results, the plotted data below show the calculated compass deflection for each of the four DC cable configurations when the cables are oriented 30° north of east at a 3.3-ft (1-m) burial depth. These results in Figure C-8 and Table C-14 and Table C-15, are presented in a similar manner as Figure C-1, Table C-1, and Table C-2, discussed above, and show that within 10 ft (3 m) of the SRWEC centerline, compass deviations are approximately 3.6 degrees or less along the cable route. Detailed results of the compass deviation for every configuration and geographic orientation are presented in Table C-14 to Table C-23 and graphical results of buried cables are shown in Figure C-9 to Figure C-13. Given the large habitats traversed by migrating fish, and the importance of other senses, a local deviation of a few degrees for such a short distance would not interfere with these species' use of the earth's geomagnetic field for navigational purposes.
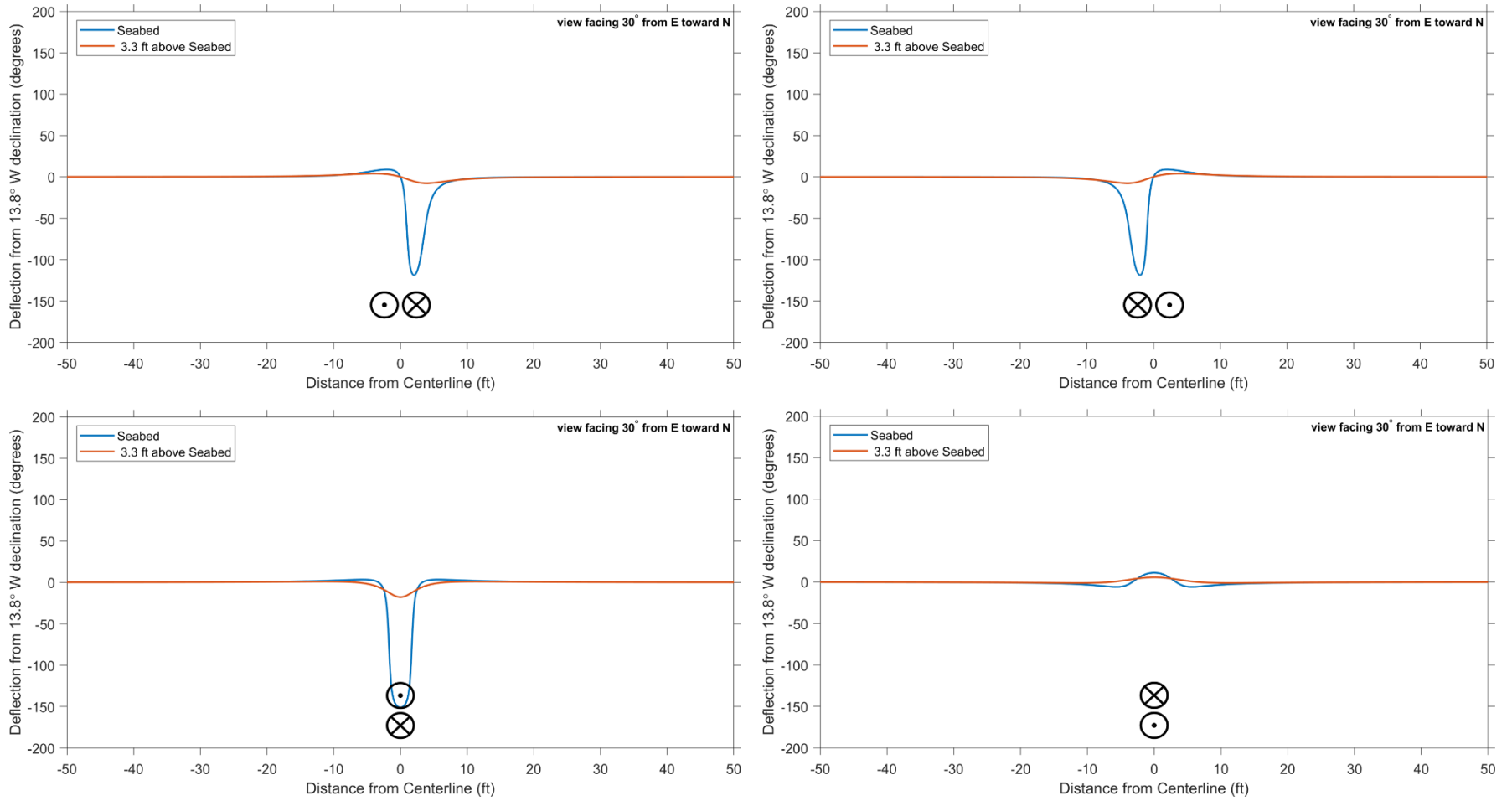
Figure C-8.   Compass deflection (degrees) from magnetic north for DC cables oriented 30° north of east, calculated at the seabed (blue line) and 3.3 ft (1 m) above the seabed (orange line) for each of the four DC cable configurations—depicted in the bottom center inset of each plot—installed at a 3.3-ft (1-m) burial depth.

Table C-14. Compass deflection (degrees) for a 30° north of east cable orientation at various horizontal distances 3.3 ft (1 m) above the seabed and peak loading

Installation Type	Configuration	Compass deflection (degrees)			
		−10 ft (−3 m)	(+) Max	(−) Max	+10 ft (+3 m)
Buried (3.3 ft [1 m])	⊙ ⊗	2.1	4.0	-7.7	-2.8
	⊗ ⊙	-2.8	4.0	-7.7	2.1
	⊙ over ⊗	-1.1	5.7	-1.2	-1.1
	⊗ over ⊙	1	1	-18	1
	30° North of East Summary	-2.8 to 2.1	1 to 5.7	-18 to -1.2	-2.8 to 2.1

Table C-15. Compass deflection (degrees) summary for the four cable orientations at various horizontal distances 3.3 ft (1 m) above the seabed and peak loading

Installation Type	Cable Route	Compass deflection (degrees)			
		−10 ft (−3 m)	(+) Max	(−) Max	+10 ft (+3 m)
Buried (3.3 ft [1 m])	30° north of east	-2.8 to 2.1	1 to 5.7	-18 to -1.2	-2.8 to 2.1
	161° north of east	-4.1 to 5.3	2.2 to 29	-11 to -2	-4.1 to 5.3
	356° north of east	-2.3 to 3	1.3 to 19	-6.3 to -1.1	-2.3 to 3
	east-west	-1.8 to 2.4	1 to 16	-4.9 to -0.9	-1.8 to 2.4
	north-south	-8.5 to 8	3.7 to 25	-31 to -3.8	-8.5 to 8

Compass Deflection Results

Calculated change (i.e., deflection) in the horizontal component of earth's ambient magnetic field as a result of the SRWEC are provided in Table C-16 to Table C-20 below, indicating the maximum range of the variation in compass deflection for any of the four DC cable-pair configurations evaluated. Table C-22 and Table C-23 provide summaries of calculated magnetic-field deviations from Earth at peak loading for buried (Table C-22) and mattress-covered (Table C-23) for all cable configurations and orientations Results are evaluated for four orientations at peak loading for buried cables.

The plots in Figure C-9 to Figure C-13 below show the compass deflection in the vicinity of the SRWEC for buried cables at peak loading with each of the four DC cable-pair configurations.

Table C-16.   Compass deflection (degrees) summary for a 30° north of east cable orientation at various horizontal distances above buried (3.3 ft [1 m]) cables and peak loading

Location	Compass deflection (degrees)			
	−10 ft (−3 m)	(+) Max	(−) Max	+10 ft (+3 m)
Seabed	-3.3 to 2.3	3.5 to 11	-151 to -5.9	-3.3 to 2.3
3.3 ft (1 m) Above Seabed	-2.8 to 2.1	1 to 5.7	-18 to -1.2	-2.8 to 2.1

Table C-17.   Compass deflection (degrees) summary for a 161° north of east cable orientation at various horizontal distances above buried (3.3 ft [1 m]) cables and peak loading

Location	Compass deflection (degrees)			
	−10 ft (−3 m)	(+) Max	(−) Max	+10 ft (+3 m)
Seabed	-4.6 to 6.2	11 to 125	-23 to -6.9	-4.6 to 6.2
3.3 ft (1 m) Above Seabed	-4.1 to 5.3	2.2 to 29	-11 to -2	-4.1 to 5.3

Table C-18.   Compass deflection (degrees) summary for a 356° north of east cable orientation at various horizontal distances above buried (3.3 ft [1 m]) cables and peak loading

Location	Compass deflection (degrees)			
	−10 ft (−3 m)	(+) Max	(−) Max	+10 ft (+3 m)
Seabed	-2.6 to 3.6	6.4 to 148	-12 to -3.8	-2.6 to 3.6
3.3 ft (1 m) Above Seabed	-2.3 to 3	1.3 to 19	-6.3 to -1.1	-2.3 to 3

Table C-19.   Compass deflection (degrees) summary for east-west orientation at various horizontal distances above buried (3.3 ft [1 m]) cables and peak loading

Location	Compass deflection (degrees)			
	−10 ft	(+) Max	(−) Max	+10 ft
Seabed	-2 to 2.8	5.1 to 155	-9.5 to -2.9	-2 to 2.8
3.3 ft (1 m) Above Seabed	-1.8 to 2.4	1 to 16	-4.9 to -0.9	-1.8 to 2.4

Table C-20.   Compass deflection (degrees) summary for north-south orientation at various horizontal distances above buried (3.3 ft [1 m]) cables and peak loading

Location	Compass deflection (degrees)			
	−10 ft	(+) Max	(−) Max	±10 ft
Seabed	-9.8 to 9	14 to 54	-77 to -16	-9.8 to 9
3.3 ft (1 m) Above Seabed	-8.5 to 8	3.7 to 25	-31 to -3.8	-8.5 to 8

Table C-21.   Compass deflection (degrees) from the 506 mG geomagnetic field, at a height of 3.3 ft (1 m) above seabed and offset from the centerline of the SRWEC evaluated for peak loading at the Landfall HDD along a geographic direction of 161° north of east.

Configuration	Cable Orientation	DC Magnetic-Field Deviation (mG)			
		-10 ft (-3 m)	(+) Max	(−) Max	+10 ft (+3 m)
Landfall HDD (6-ft [1.8-m] burial depth)		14	18	-9.2	-8.1
		-8.1	18	-9.2	14
	161° north of east Summary	-8.1 to 14	18	-9.2	-8.1 to 14
Landfall HDD (46 ft [14-m] burial depth)		0.3	0.6	-0.6	-0.3
		-0.3	0.6	-0.6	0.3
	161° north of east Summary	-0.3 to 0.3	0.6	-0.6	-0.3 to 0.3

Table C-22. Summary of compass deflection (degrees) at various horizontal distances and 3.3. ft (1 m) burial depth for all cable configurations and orientations at peak loading

Evaluation Height	Compass deflection (degrees)											
	−75 ft (−23 m)	−50ft (−15 m)	−25 ft (−18 m)	−10ft (−3 m)	−5 ft (−1.5 m)	(+) Max	(−) Max	+5 ft (+1.5 m)	+10 ft (+3 m)	+25 ft (+18 m)	+50 ft (+15 m)	+75 ft (+23 m)
At seabed	-0.2 to 0.2	-0.5 to 0.5	-2 to 2	-9.8 to 9	-34 to 33	3.5 to 155	-151 to -2.9	-34 to 33	-9.8 to 9	-2 to 2	-0.5 to 0.5	-0.2 to 0.2
At 3.3 ft (1 m) above seabed	-0.2 to 0.2	-0.5 to 0.5	-1.7 to 1.7	-8.5 to 8	-18 to 16	1 to 29	-31 to -0.9	-18 to 16	-8.5 to 8	-1.7 to 1.7	-0.5 to 0.5	-0.2 to 0.2

Table C-23. Summary of compass deflection (degrees) at various horizontal distances and 1-ft (0.3-m) mattress-covering for all cable configurations and orientations at peak loading

Evaluation Height	Compass deflection (degrees)											
	−75 ft (−23 m)	−50ft (−15 m)	−25 ft (−18 m)	−10ft (−3 m)	−5 ft (−1.5 m)	(+) Max	(−) Max	+5 ft (+1.5 m)	+10 ft (+3 m)	+25 ft (+18 m)	+50 ft (+15 m)	+75 ft (+23 m)
At seabed	-0.2 to 0.2	-0.5 to 0.5	-2.1 to 2.1	-13 to 12	-49 to 56	12 to 166	-163 to -10	-49 to 56	-13 to 12	-2.1 to 2.1	-0.5 to 0.5	-0.2 to 0.2
At 3.3 ft (1 m) above seabed	-0.2 to 0.2	-0.5 to 0.5	-1.9 to 1.9	-8.4 to 7.8	-30 to 26	2.2 to 129	-123 to -1.9	-30 to 26	-8.4 to 7.8	-1.9 to 1.9	-0.5 to 0.5	-0.2 to 0.2

Table C-24.   Summary of compass deflection (degrees) from Landfall HDD at 6 ft (1.8 m) burial depth and at peak loading.

Evaluation Height	Compass deflection (degrees)											
	−75 ft (−23 m)	−50ft (−15 m)	−25 ft (−18 m)	−10ft (−3 m)	−5 ft (−1.5 m)	(+) Max	(−) Max	+5 ft (+1.5 m)	+10 ft (+3 m)	+25 ft (+18 m)	+50 ft (+15 m)	+75 ft (+23 m)
At seabed	-0.1 to 0.1	-0.3 to 0.3	-1.8 to 2.1	-10 to 22	-15 to 53	54 to 54	-15 to -15	-15 to 53	-10 to 22	-1.8 to 2.1	-0.3 to 0.3	-0.1 to 0.1
At 3.3 ft (1 m) above seabed	-0.1 to 0.1	-0.4 to 0.4	-2.2 to 2.5	-8.1 to 14	-9 to 17	18 to 18	-9.2 to -9.2	-9 to 17	-8.1 to 14	-2.2 to 2.5	-0.4 to 0.4	-0.1 to 0.1

Table C-25.   Summary of compass deflection (degrees) from Landfall HDD at 46 ft (14 m) burial depth and at peak loading.

Evaluation Height	Compass deflection (degrees)											
	−75 ft (−23 m)	−50ft (−15 m)	−25 ft (−18 m)	−10ft (−3 m)	−5 ft (−1.5 m)	(+) Max	(−) Max	+5 ft (+1.5 m)	+10 ft (+3 m)	+25 ft (+18 m)	+50 ft (+15 m)	+75 ft (+23 m)
At seabed	-0.3 to 0.3	-0.5 to 0.5	-0.7 to 0.7	-0.4 to 0.4	-0.2 to 0.2	0.7 to 0.7	-0.7 to -0.7	-0.2 to 0.2	-0.4 to 0.4	-0.7 to 0.7	-0.5 to 0.5	-0.3 to 0.3
At 3.3 ft (1 m) above seabed	-0.3 to 0.3	-0.5 to 0.5	-0.6 to 0.6	-0.3 to 0.3	-0.2 to 0.2	0.6 to 0.6	-0.6 to -0.6	-0.2 to 0.2	-0.3 to 0.3	-0.6 to 0.6	-0.5 to 0.5	-0.3 to 0.3

Figure C-9. Compass deflection (degrees) from magnetic north for DC cables oriented 30° north of east, calculated at seabed (blue line) and 3.3 ft (1 m) above seabed (orange line) for each of the four DC cable configurations depicted in bottom center inset of each plot.
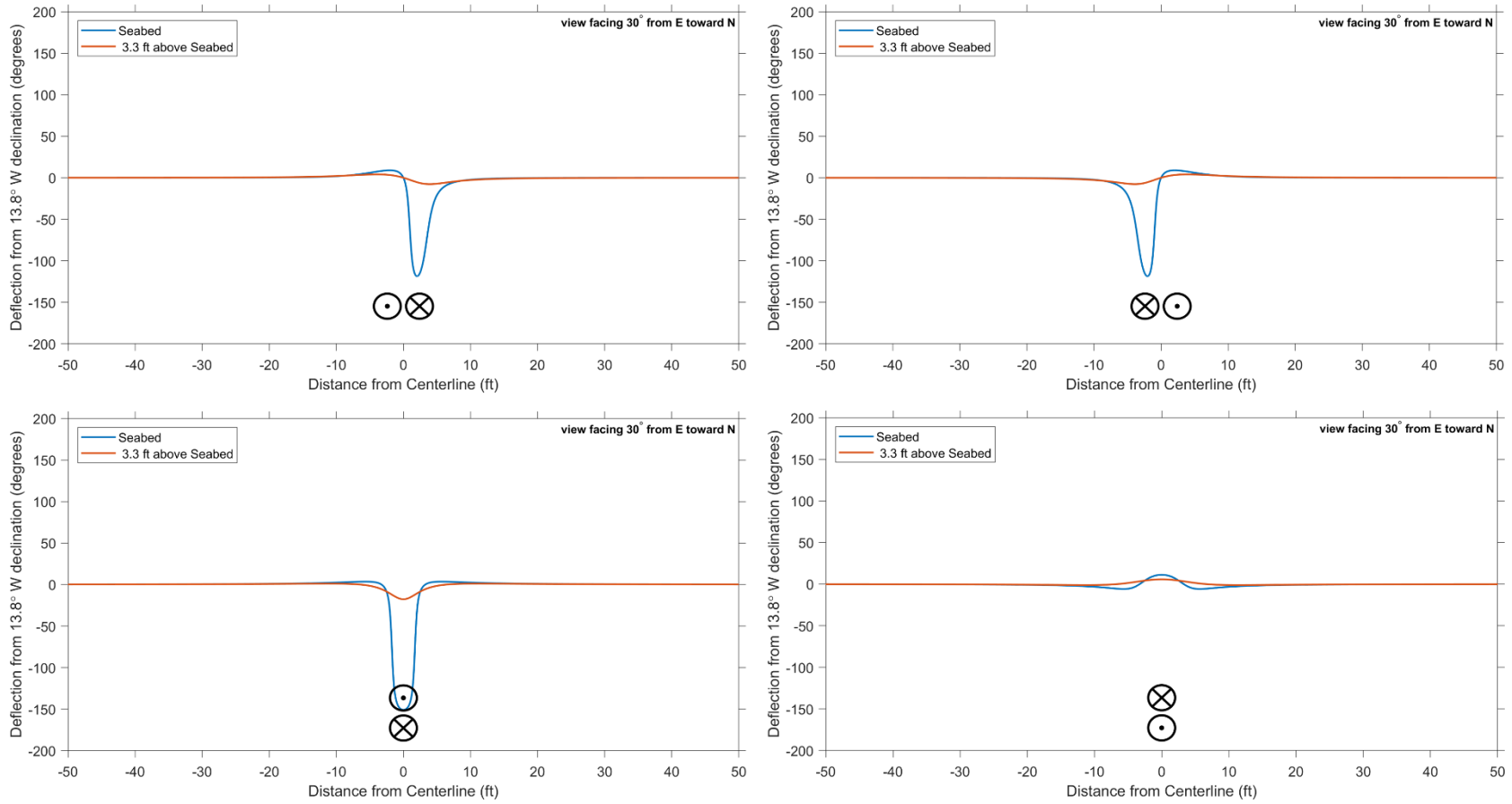
Figure C-10.   Compass deflection (degrees) from magnetic north for DC cables oriented 161° north of east, calculated at seabed (blue line) and 3.3 ft (1 m) above seabed (orange line) for each of the four DC cable configurations depicted in bottom center inset of each plot.
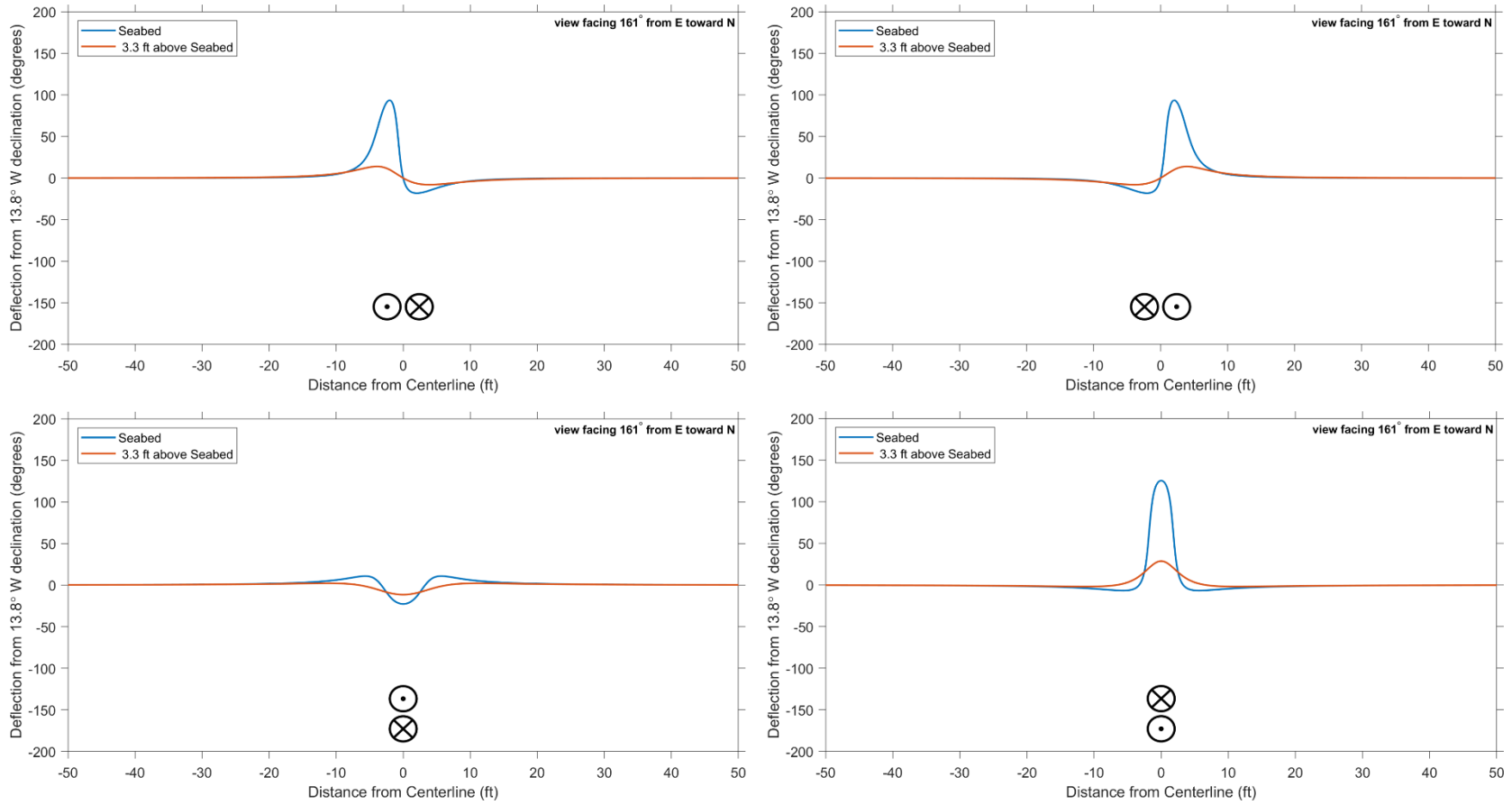
Figure C-11.   Compass deflection (degrees) from magnetic north for DC cables oriented 356° north of east, calculated at seabed (blue line) and 3.3 ft (1 m) above seabed (orange line) for each of the four DC cable configurations depicted in bottom center inset of each plot.
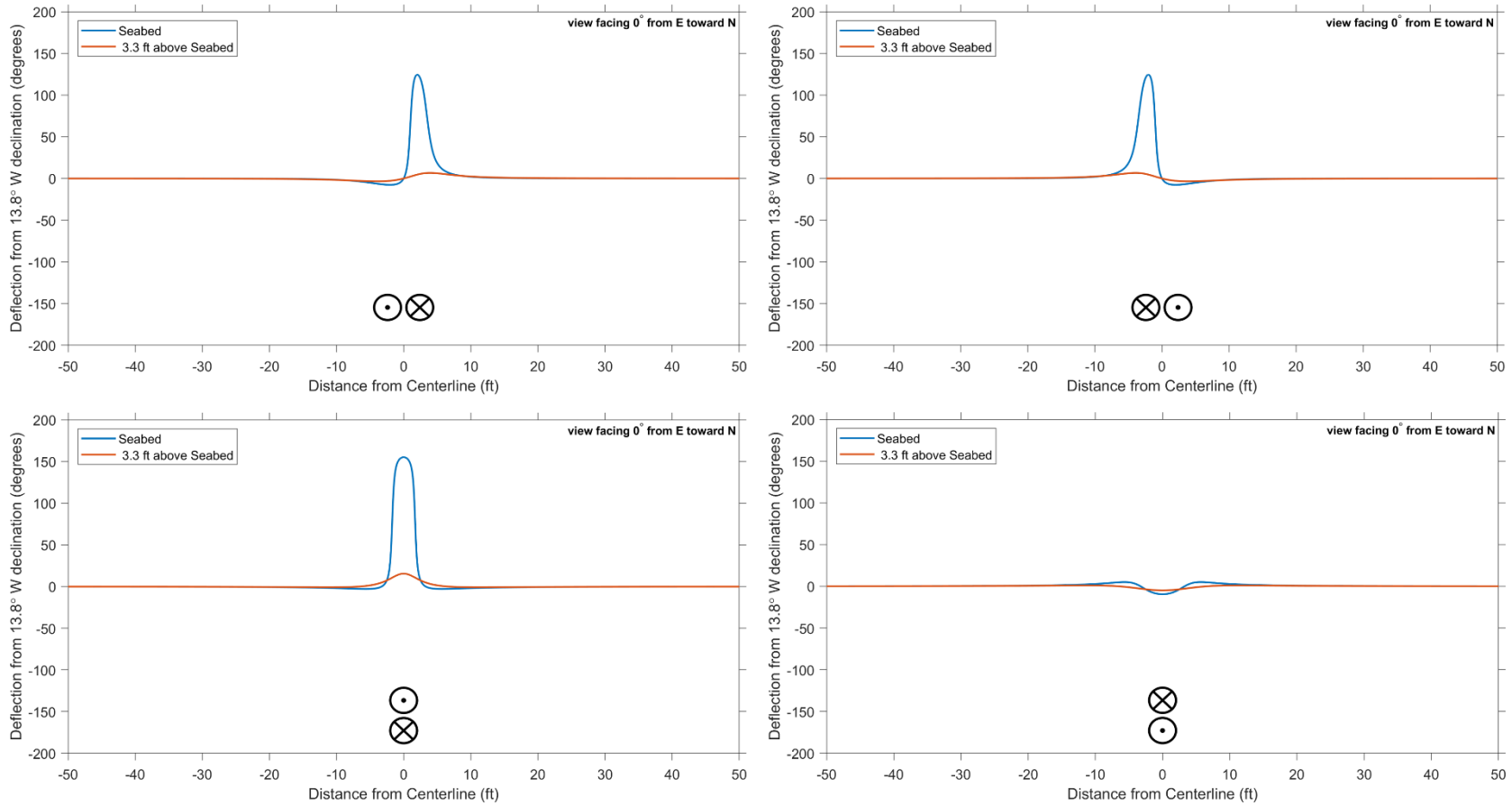
Figure C-12. Compass deflection (degrees) from magnetic north for DC cables oriented along an east-west axis, calculated at seabed (blue line) and 3.3 ft (1 m) above seabed (orange line) for each of the four DC cable configurations depicted in bottom center inset of each plot.
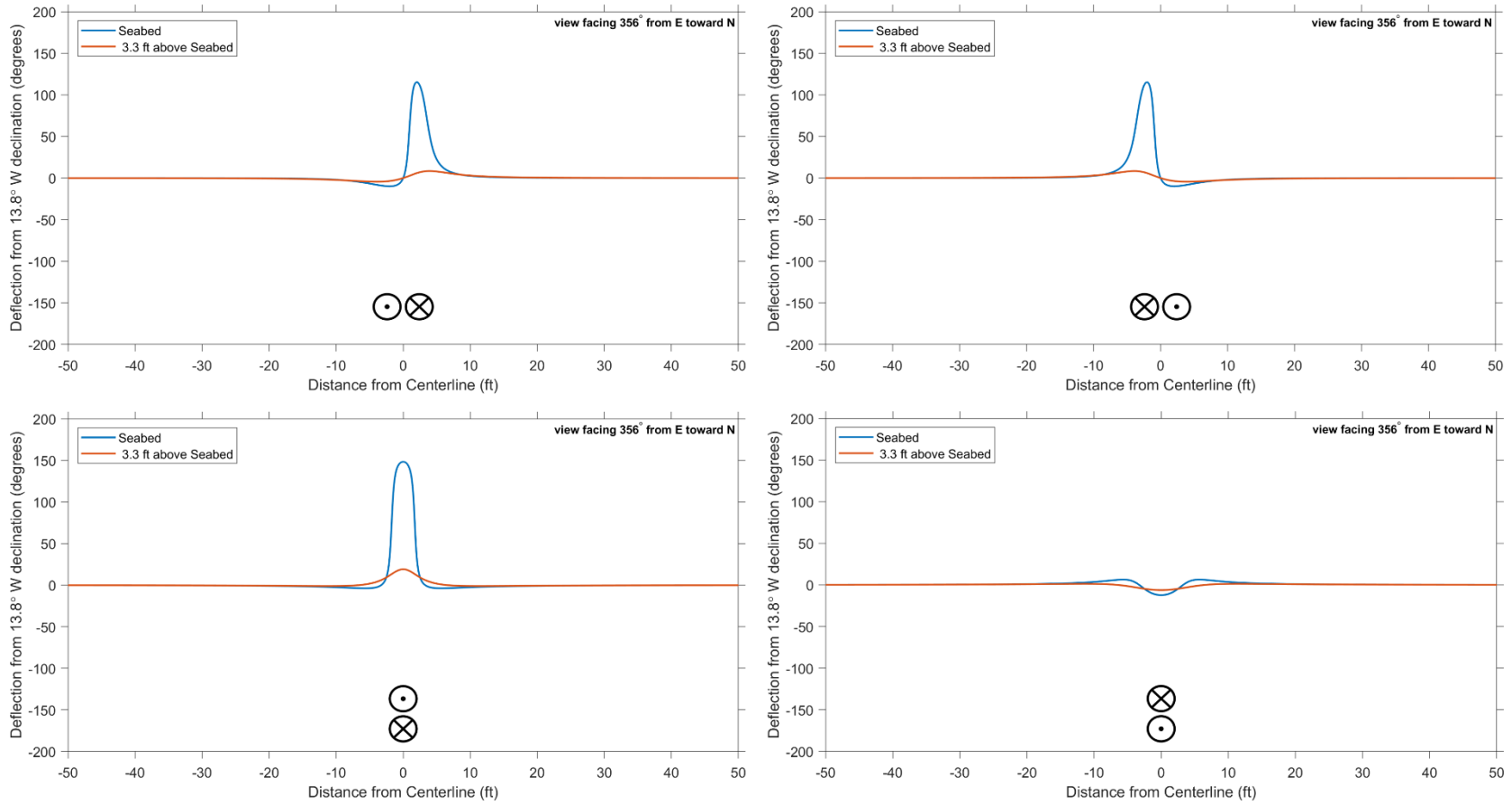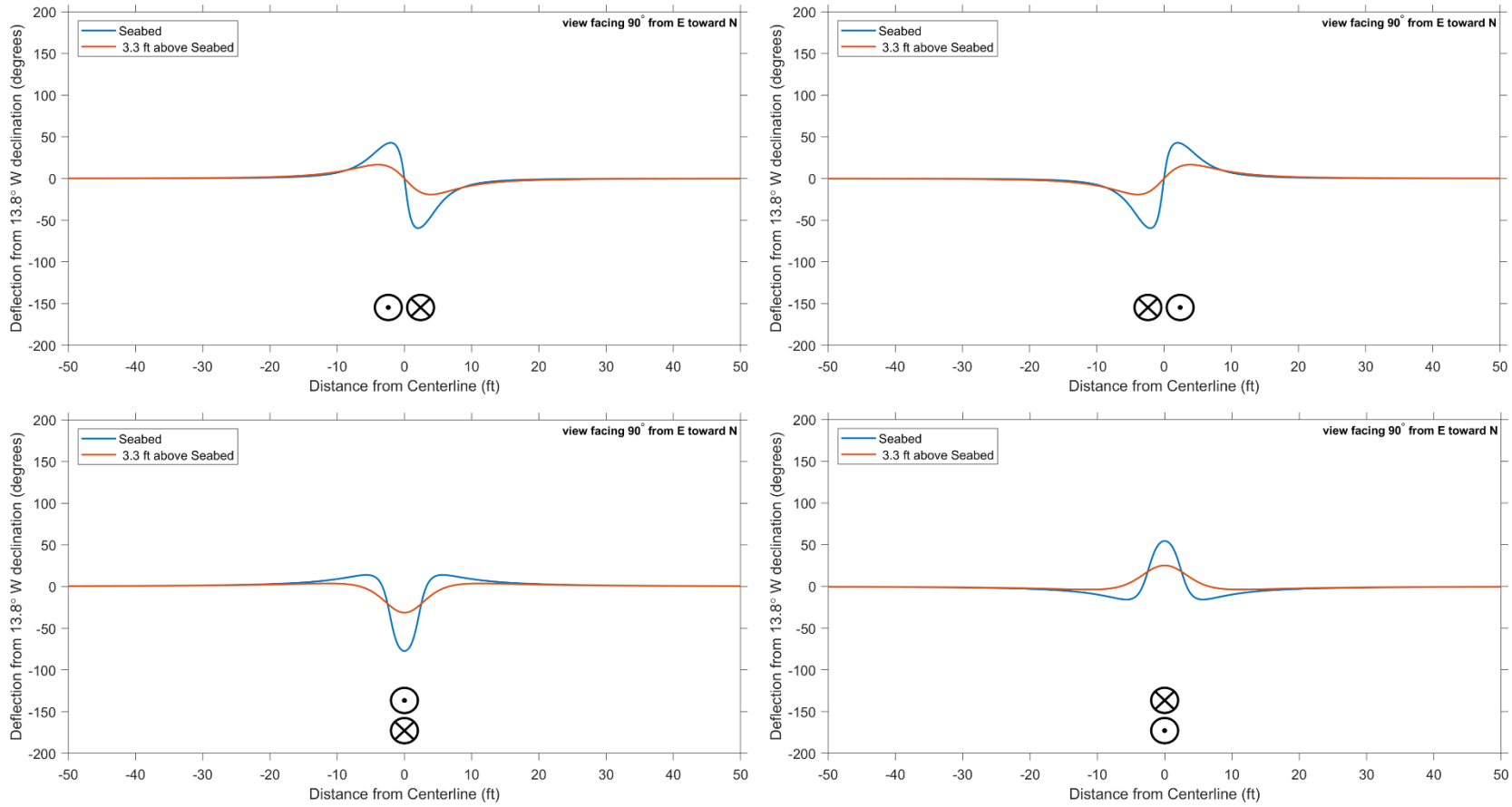
Figure C-13.   Compass deflection (degrees) from magnetic north for DC cables oriented along a north-south axis, calculated at seabed (blue line) and 3.3 ft (1 m) above seabed (orange line) for each of the four DC cable configurations depicted in bottom center inset of each plot.
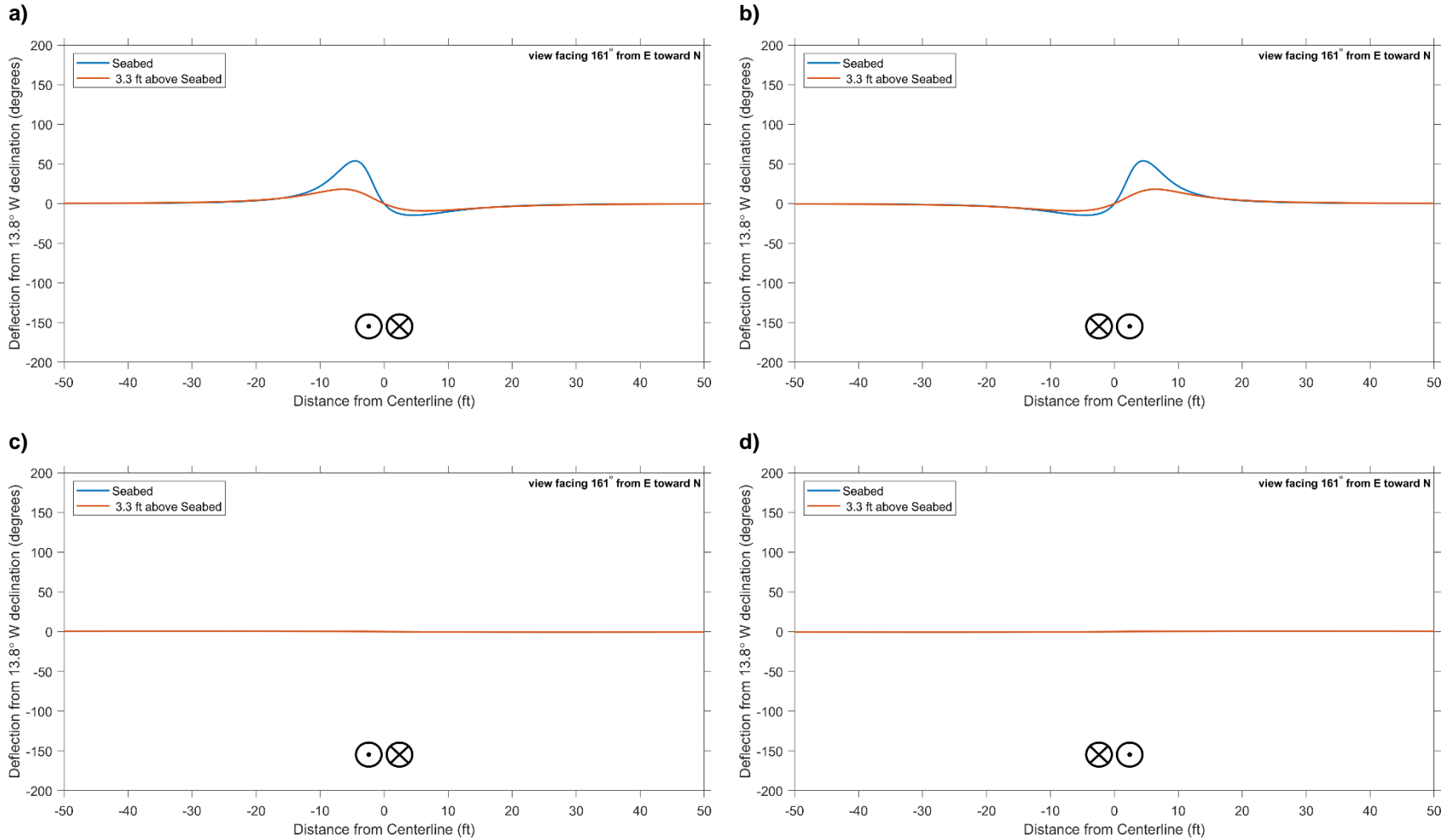
Figure C-14. Compass deflection (degrees) from magnetic north for Landfall HDD for a 6 ft (1.8 m) burial depth (plots a and b) and a 46 ft (14 m) burial depth (plots c and d) at peak loading and evaluated both at seabed (blue line) and at 3.3 ft (1 m) above the seabed (orange line) oriented 161° north of east for two different installation scenarios, indicated by the figure at the bottom center of each plot.

AC Cables

The magnetic-field and induced electric-field levels were calculated for IACs at two effective burial depths. Details of the modeled cables are presented in Attachment A, Table A-2. The calculated field levels for 66-kV IACs at a height of 3.3 ft (1 m) above the seabed with a 3.3-ft (1 m) burial depth and peak loading are summarized below. In general, loading is evaluated for anticipated average loading, as well as for the peak loading.

AC Magnetic-Field Levels

The calculated magnetic-field levels above the 66-kV IACs for a 3.3-ft (1 m) burial depth and peak loading are plotted in Figure C-15. The calculated magnetic field at a height of 3.3 ft (1 m) above the seabed is highest directly above the buried cables (4.6 mG) and decreases rapidly with distance. All calculated field levels are well below the ICNIRP reference level of 2,000 mG and the ICES reference level of 9,040 mG for exposure of the general public.
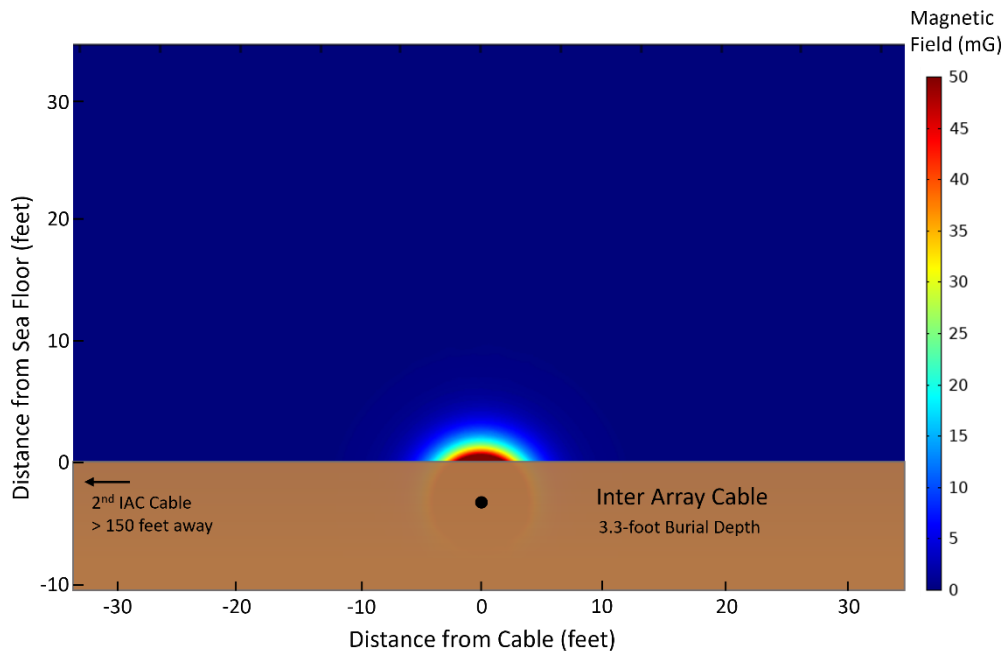
Figure C-15.   Calculated magnetic-field levels in seawater above the 66-kV IAC for a 3.3-ft (1 m) burial depth and peak loading. The filled black circle indicates the position of the center of the cable.

Calculated magnetic-field levels above the IAC at a 3.3-ft (1-m) burial depth and peak loading is 61 mG at seabed and 4.6 mG at 3.3-ft (1-m) above the seabed, as shown in Table C-26. Where the cables may be laid on the seabed for short distances and covered by protective concrete mattresses, the field levels would be higher, but also will decrease very rapidly with distance. For horizontal distances beyond 10 ft (3 m) from the cables (including where covered by protective mattresses), the magnetic-field levels are calculated to be 0.3 mG or less for average loading, and 0.5 mG or less for peak loading.[30]

---

[30]   At the seabed, the highest calculated AC magnetic field was 416 mG at average loading and 770 mG at peak loading. At a height of 3.3 feet (1 m) above the seabed, the highest calculated AC magnetic-field was 14 mG at average loading and 27 mG at peak loading. All these maxima occurred directly above the IACs where, for limited distances, the cables may be laid on the seabed and covered by protective concrete mattresses or rock berms. These highest calculated levels are still well below the ICNIRP and ICES limits for exposure of the general public.

Table C-26.   Calculated AC magnetic-field levels (mG) at various horizontal distances at seabed and at 3.3 ft (1m) above the seabed for a 3.3-ft (1 m) burial depth and peak loading

66-kV IAC Evaluation Height	AC Magnetic Fields (mG)		
	Max	±5 ft (±1.5 m)*	±10 ft (±3 m)*
At seabed	61	7.8	0.3
At 3.3 ft (1m) above seabed	4.6	1.4	0.1

* One cable is modeled for the IACs. The horizontal distance is measured from the center of the IAC.

AC Electric-Field Levels Induced in Seawater

The calculated electric fields induced in seawater at the seabed and at a height of 3.3 feet (1 m) above the seabed for the IAC at a 3.3-ft (1-m) burial depth and peak loading are shown in Table C-27. Induced electric-field levels in seawater were calculated to be 1.0 mV/m at seabed, decreasing rapidly to 0.09 mV/m at 3.3 feet (1 m) above the seabed. For short distances where the cables potentially may be laid on the seabed and covered by protective concrete mattresses or rock berms, the field levels would be higher, but also will decrease very rapidly with distance. For horizontal distances beyond 10 ft (3 m) from the buried cables, the induced electric-field levels for all configurations were calculated to be <0.01 mV/m for average and peak loading.[31]

Table C-27.   Calculated induced AC electric-field levels (mV/m) at various horizontal distances at seabed and at 3.3 ft (1 m) above the seabed for a 3.3-ft (1 m) burial depth and peak loading

66-kV IAC Evaluation Height	Induced AC Electric Fields (mV/m) in Seawater*		
	Max	±5 ft (±1.5 m)	±10 ft (±3 m)
At seabed	1.0	0.15	<0.01
At 3.3 ft (1m) above seabed	0.09	0.03	<0.01

* One cable is modeled for the IACs. The horizontal distance is measured from the center of the IAC.

AC Electric-Field Levels Induced in Marine Organisms

The calculated electric fields induced in marine organisms at the seabed at 3.3 ft (1 m) above seabed are shown in Table C-28 for the IACs at a 3.3-ft (1-m) burial depth and peak loading. At peak loading, the calculated electric-field levels induced in sturgeon are 0.74 mV/m at seabed and 0.06 mV/m at 3.3-ft (1 m) above seabed. The electric field calculated to be induced in marine organisms scales linearly with the magnetic-field levels and thus, like the magnetic field, also will decrease rapidly with distance from the cables.

---

[31]   At the seabed, the highest induced AC electric field was calculated to be 4.1 mV/m at average loading and 7.7 mV/m at peak loading. At a height of 3.3 feet (1 m) above the seabed, the highest induced AC electric-field level was calculated to be 0.3 mV/m at average loading and 0.5 mV/m at peak loading. All these maxima occurred directly above the IACs where the cables may potentially be laid on the seabed for short distances and covered by a protective concrete mattress or rock berms. These highest calculated levels are still well below the ICNIRP and ICES limits for exposure of the general public.

Table C-28.   Calculated AC electric-field levels (mV/m) induced in marine organisms at seabed and at 3.3 ft (1 m) above the seabed for a 3.3-ft (1-m) burial depth and peak loading

66-kV IAC Evaluation Height	Induced AC Electric Fields (mV/m) in Electrosensitive Species	
	Dogfish	Sturgeon
At seabed	0.39	0.74
At 3.3 ft (1m) above seabed	0.03	0.06

Calculated AC Cable Electric and Magnetic Fields

Calculated AC magnetic and induced electric fields in seawater are provided below for the IACs, with parameters presented in Attachment A, Table A-2. Figures are shown for an isolated IAC at a 3.3-ft (1 m) burial depth and both peak and average loading. The IACs are proposed to be separated by a large distance in regions away from WTGs and OCS–DC, and so were modeled in isolation from one another to characterize the associated field levels. In the figures and tables below, field levels are presented as a function of horizontal distance from the center of an IAC.

Calculated magnetic-field levels from IACs in seawater are summarized in Table C-29 and Table C-30 for transects at the seabed and at a height of 3.3 ft (1 m) above the seabed, for average and peak loading, respectively. Calculated electric-field levels from IACs induced in seawater are summarized in Table C-31 and Table C-32 for transects at the seabed and at a height of 3.3 ft (1 m) above the seabed for both average and peak loading.

The calculated electric-field levels induced in representative electrosensitive species are summarized for the 66-kV IACs at the seabed and at 3.3 ft (1 m) above the seabed in Table C-33 and Table C-34. Where covered by protective concrete mattresses or rock berms, field levels are reported at the top of the protective cover and at 3.3 ft (1 m) above the protective cover.

Calculated field levels at average loading are plotted as a function of horizontal distance from the circuit centerline in Figure C-16 (magnetic-field levels) and Figure C-17 (induced electric-field levels). Similarly, calculated field levels at peak loading are plotted in Figure C-18 (magnetic-field levels) and Figure C-19 (electric-field levels). All figures present results for calculations of cables installed at a 3.3-ft (1 m) burial depth. Results for this installation type are expected to be representative of those encountered along most of the proposed cable.

Table C-29.   Calculated AC magnetic-field levels (mG) at various horizontal distances from AC cables for average loading

Cable	Voltage	Installation Type	Location	AC Magnetic Field (mG)*		
				Max	±5 ft (±1.5 m)	±10 ft (±3 m)
IACs	66-kV	Buried (3.3 ft [1m])	Seabed	33	4.2	0.2
			3.3 ft (1 m) above seabed	2.5	0.8	< 0.1
		Mattress-Covered (1 ft [0.3m])	Top of protective cover	416	9.0	0.3
			3.3 ft (1 m) above protective cover	14	2.7	0.1

* IACs are modeled as isolated cables. The horizontal distance is measured from the center of the IACs.

Table C-30.   Calculated AC magnetic field levels (mG) at various horizontal distances from AC cables for peak loading

Cable	Voltage	Installation Type	Location	AC Magnetic Field (mG)*		
				Max	±5 ft (±1.5 m)	±10 ft (±3 m)
IACs	66-kV	Buried (3.3 ft [1m])	Seabed	61	7.8	0.3
			3.3 ft (1 m) above seabed	4.6	1.4	0.1
		Mattress-Covered (1 ft [0.3m])	Top of protective cover	770	17	0.5
			3.3 ft (1 m) above protective cover	27	4.9	0.3

*   IACs are modeled as isolated cables. The horizontal distance is measured from the center of the IACs.

Table C-31.   Calculated AC electric-field levels (mV/m) at various horizontal distances from AC cables for average loading

Cable	Voltage	Installation Type	Location	Induced AC Electric Fields in Seawater (mV/m)*		
				Max	±5 ft (±1.5 m)	±10 ft (±3 m)
IACs	66-kV	Buried (3.3 ft [1m])	Seabed	0.5	0.1	< 0.01
			3.3 ft (1 m) above seabed	< 0.01	< 0.01	< 0.01
		Mattress-Covered (1 ft [0.3m])	Top of protective cover	4.1	0.2	< 0.01
			3.3 ft (1 m) above protective cover	0.3	< 0.01	< 0.01

*   IACs are modeled as isolated cables. The horizontal distance is measured from the center of the IACs.

Table C-32.   Calculated AC electric-field levels (mV/m) at various horizontal distances from AC cables for peak loading

Cable	Voltage	Installation Type	Location	Induced AC Electric Fields (mV/m) in Seawater*		
				Max	±5 ft (±1.5 m)	±10 ft (±3 m)
IACs	66-kV	Buried (3.3 ft [1m])	Seabed	1.0	0.15	< 0.01
			3.3 ft (1 m) above seabed	0.09	0.03	< 0.01
		Mattress-Covered (1 ft [0.3m])	Top of protective cover	7.7	0.31	0.01
			3.3 ft (1 m) above protective cover	0.47	0.1	< 0.01

*   IACs are modeled as isolated cables. The horizontal distance is measured from the center of the IACs.

Table C-33. Calculated AC electric-field levels (mV/m) induced in electrosensitive species for average loading

Cable	Voltage	Installation Type	Location	Induced AC Electric Fields (mV/m) in Electrosensitive Species	
				Dogfish	Sturgeon
IACs	66-kV	Buried (3.3 ft [1m])	Seabed	0.21	0.40
			3.3 ft (1 m) above seabed	0.02	0.03
		Mattress-Covered (1 ft [0.3m])	Top of protective cover	2.7	5.1
			3.3 ft (1 m) above protective cover	0.09	0.18

Table C-34. Calculated AC electric-field levels (mV/m) induced in electrosensitive species for peak loading

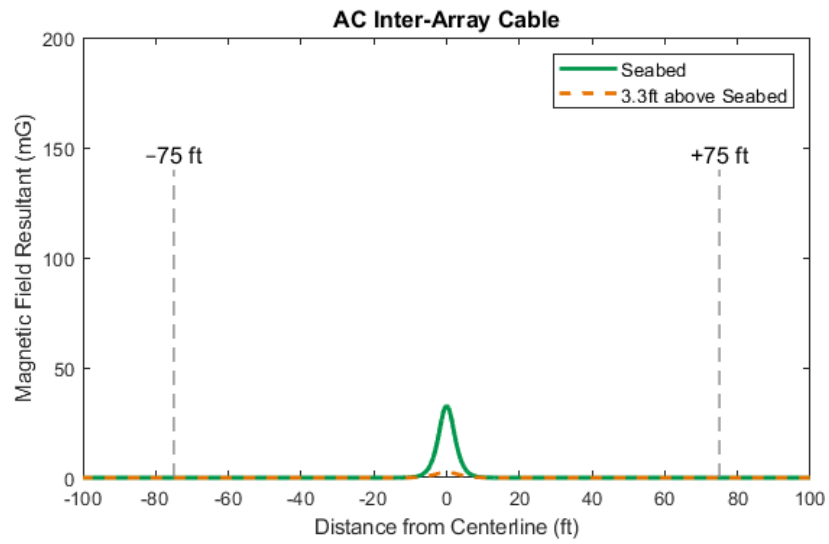| Cable	Voltage	Installation Type	Location	Induced AC Electric Fields (mV/m) in Electrosensitive Species	
				Dogfish	Sturgeon
IACs	66-kV	Buried (3.3 ft [1m])	Seabed	0.39	0.74
			3.3 ft (1 m) above seabed	0.03	0.06
		Mattress-Covered (1 ft [0.3m])	Top of protective cover	5.0	9.4
			3.3 ft (1 m) above protective cover	0.17	0.33

Figure C-16.   Calculated AC magnetic-field levels in seawater above the 66-kV IACs for a 3.3-ft (1-m) burial depth and average loading.

Figure C-17.   Calculated AC induced electric-field levels in seawater above the IACs for a 3.3-ft (1-m) burial depth and average loading.

Figure C-18. Calculated AC magnetic-field levels in seawater above the 66-kV IACs for a 3.3-ft (1-m) burial depth and peak loading.
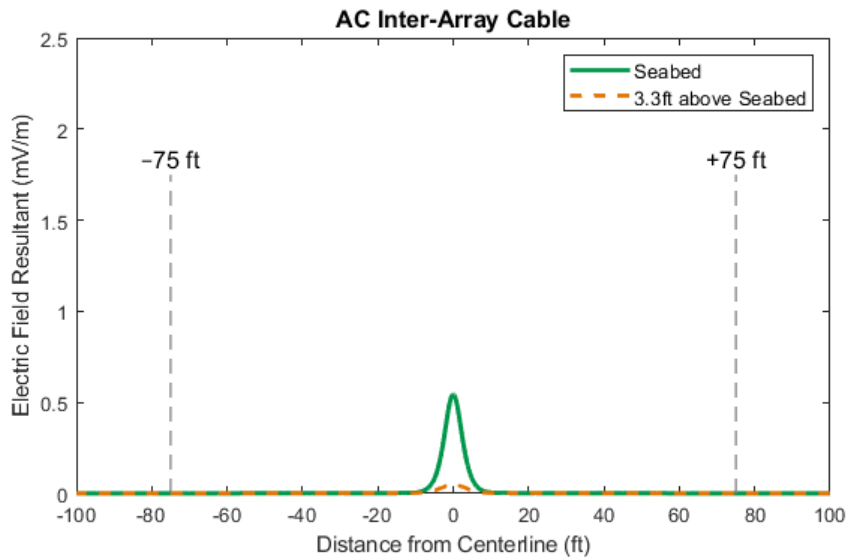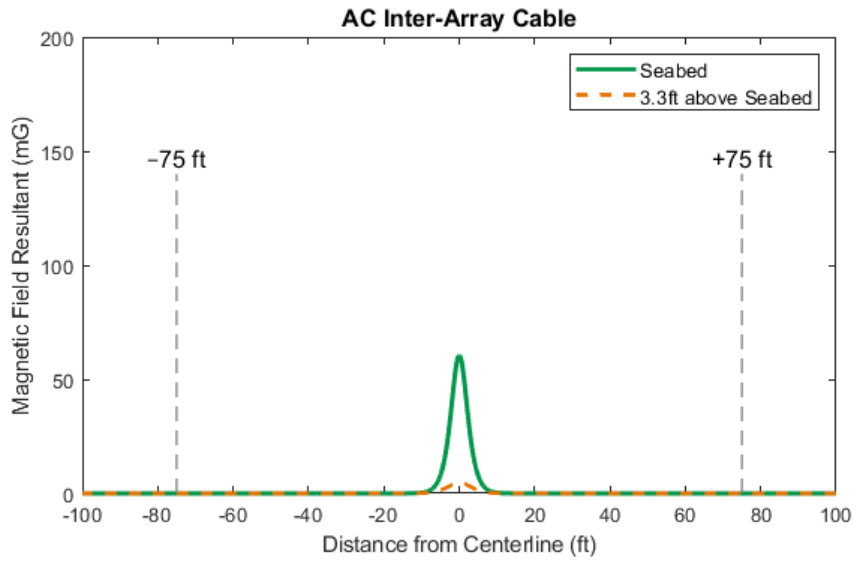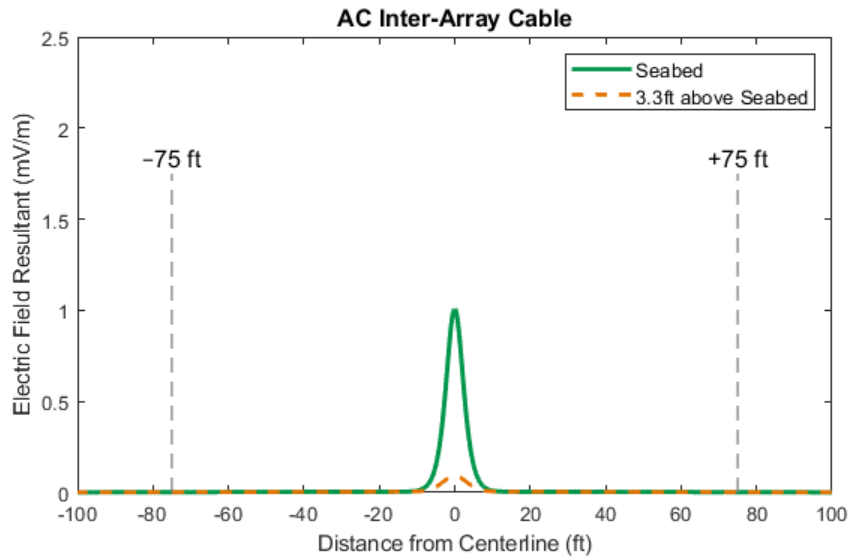

Figure C-19. Calculated AC induced electric-field levels in seawater above the IACs for a 3.3-ft (1-m) burial depth and peak loading.

Attachment D

Calculated EMF Levels for WTG, OCS–DC, Cables with Protective Coverings and at Landfall

At locations where WTG and OCS-DC foundations will introduce a new vertical habitat and at the protective mattresses or rock berms covering surface-laid cable, average magnetic- and induced electric-fields around the offshore installations were evaluated for various volumes of seawater where different marine species might spend more time.

Cables with Protective Covering

The results of both DC and AC magnetic and induced electric fields for the bulk of the cables that are wholly buried were reported in Attachment C. However, to address the fact that some marine organisms may congregate in the area over hard ground provided by protective coverings, such as protective mattresses or rock berms covering isolated surface laid cables, volume-averaged magnetic fields and induced electric fields were calculated. The volume over which these calculations were averaged corresponds to a region within a 3.3-ft (1-m) cube, extending vertically from the top of the protective covering. The volume averaged calculations are shown in Table D-1.

Table D-1. Calculated volume-averaged DC and AC magnetic-fields (mG) and electric-fields (mV/m) above cables covered by protective mattresses

Volume of Water	Field Type	Average Loading		Peak Loading	
		Magnetic-Field (mG)	Electric Field (mV/m)*	Magnetic-Field (mG)	Electric Field (mV/m)
SRWEC	DC	832	0.05	1173	0.07*
IAC	AC	79	1.1	147	2.0

* Assuming an ocean current velocity of 2 ft/s (60 cm/s)

OCS–DC and WTG

The calculated magnetic field and induced electric fields in the previous sections represent the fields over the vast majority of the Project Area where the SRWEC and the individual IAC carry power between other project elements (i.e., WTGs, OCS–DC, and the shore landing). At the WTG and OCS–DC installations, depicted in figures below, multiple cables converge, and thus the combined effects of multiple cables on field levels were assessed by FEA modeling both at the seabed (monopile foundation) and in the water column (jacket foundations). The locations in which volume averages have been calculated for each structure configuration is provided below along with computed average field levels.

OCS–DC at the Seabed

The DC and AC magnetic and induced electric fields around the OCS–DC at the seabed were modeled using a monopile configuration which results in both the minimum cable-cable distance and minimum volume-averaging area, thus conservatively overestimating results. Both magnetic and induced electric fields have been assessed as volume averages within regions representative of various marine habitats. With reference to Figure D-1, the pink region represents marine life swimming or crawling on top of the scour protection layer in the vicinity of the SRWEC. The volume over which calculated field values have been averaged corresponds to the region extending vertically from the top of the scour protection to a height 1.6-ft (0.5-m) above the CPS, and extending radially from outer perimeter of the respective skirt to a distance 49-ft (15-m) from the monopile. The region representative of life that shelters beneath the artificial skirt created between the SRWEC and the monopile is shown in Figure D-1 in green. The volume over which calculated field values have been averaged correspond to the region, with a roughly triangular cross-section, bounded by the top of the scour protection, the edge of the monopile, and a line 3.3-ft (1-m) above the CPS.

The DC magnetic field is computed as the vector addition of the earth's geomagnetic field and the DC field generated by each SRWEC. The DC magnetic field was computed with the midpoint between each SRWEC aligned towards the expected SRWEC route, which travels towards the OCS–DC with a direction of approximately 30° north from east. Since the direction of DC current within each SRWEC is currently unknown, both possible polarity configurations were assessed. The maximum calculated volume average for the static magnetic field for the skirt region (green) and the region above the scour protection (pink) are indicated in Figure D-1 below. The maximum volume average DC magnetic field around the foundation of the OCS–DC was 3,961 mG. At this field, the corresponding induced volume averaged electric field due to the movement of seawater (2 ft/s [0.6 m/s]) is 0.238 mV/m.
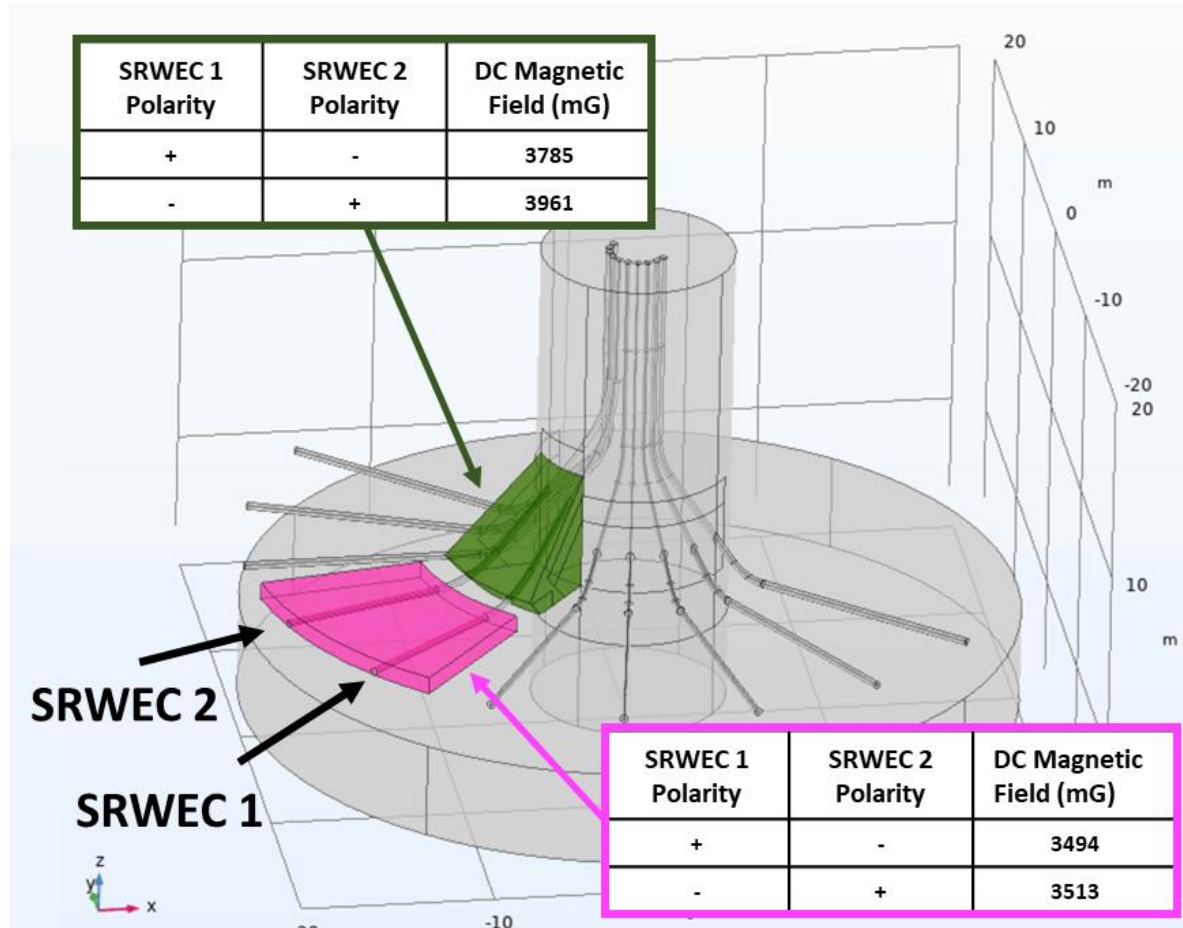

SRWEC 1 Polarity	SRWEC 2 Polarity	DC Magnetic Field (mG)
+	-	3785
-	+	3961

SRWEC 1 Polarity	SRWEC 2 Polarity	DC Magnetic Field (mG)
+	-	3494
-	+	3513

Figure D-1.   Volume average DC magnetic-field levels at seabed near the OCS–DC. [32]

Volume averages are calculated for analogous scour protection and skirt regions corresponding to the fields generated by the IACs. The purple region in the Figure D-2 below represents marine life swimming or crawling on top of the scour protection layer in the vicinity of the IAC, and the orange region is representative of life that shelters beneath the artificial skirt created between the IACs and the monopile. The maximum

---

[32]   The PDE for the maximum capacity loading of the SRWEC has decreased by approximately 10% since these calculations were performed. However, since a lower loading will result in overall lower magnetic field levels, the complex models required for the 3D calculations of the DC magnetic field at the OCS–DC were not remodeled. The values in this paragraph therefore represent a conservative upper bound to the fields from the current design. Actual field levels are likely to be approximately 10% lower than these calculated values.

volume average AC magnetic and induced electric fields resulting from the IAC are indicated in the Figure D-2 below for the skirt region (orange) and the region above the scour protection (purple).
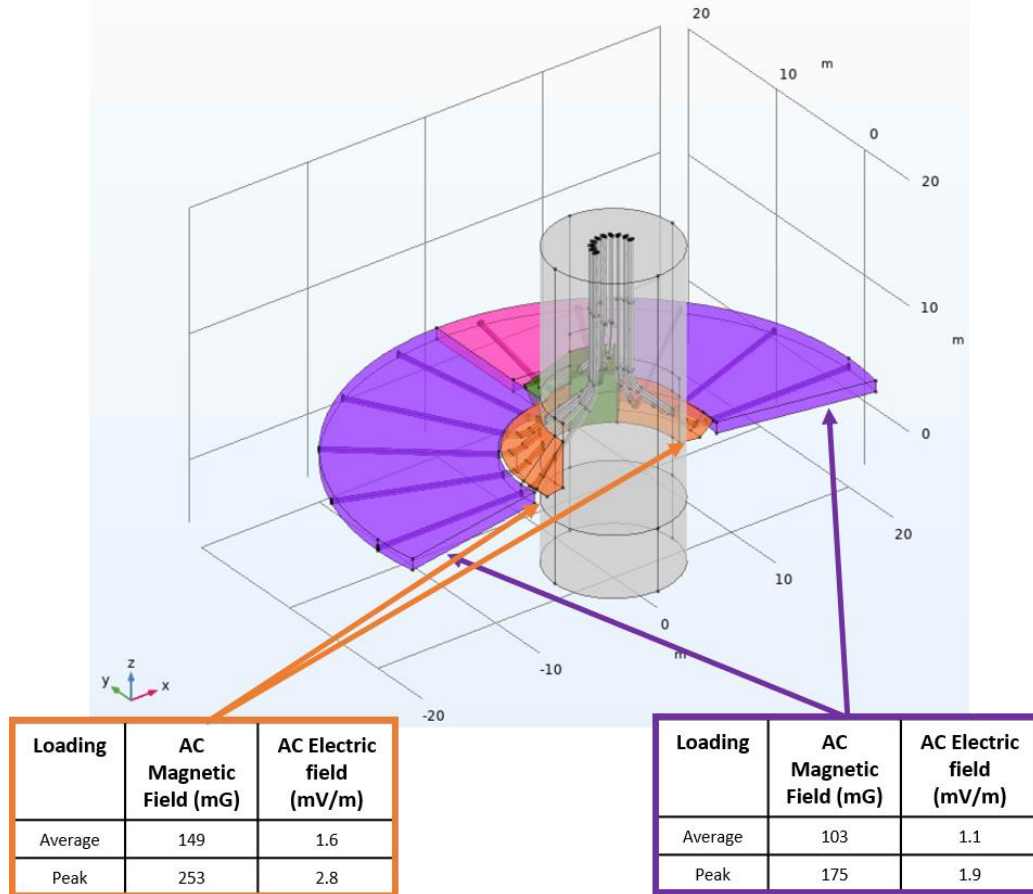

Loading	AC Magnetic Field (mG)	AC Electric field (mV/m)
Average	149	1.6
Peak	253	2.8

Loading	AC Magnetic Field (mG)	AC Electric field (mV/m)
Average	103	1.1
Peak	175	1.9

Figure D-2.   Volume average AC magnetic- and induced-electric field levels at the OCS–DC monopile foundation. [33]

---

[33]   The PDE for the maximum size and maximum loading of the IAC have both increased incrementally since these calculations were performed. Additional analyses summarized in Section 3.2 show that these design changes to the IAC increase AC magnetic and induced electric field levels by approximately 3%. Since the change in field level resulting from this change is so small, the complex models required for the 3D calculations of the AC magnetic field at the WTG and OCS–DC were not remodeled. The values in this paragraph may therefore be approximately 3% higher than reported above.

OCS–DC in the Water Column

The DC and AC magnetic field in the water column around the OCS–DC, modeled using a jacket configuration, were assessed as volume averages within regions representative of marine life swimming among the cables on the structure. The DC field is computed as the vector addition of the earth's geomagnetic field and the DC field generated by the SRWEC. The DC magnetic field was computed with the plane of two SRWEC perpendicular to the expected SRWEC route, which travels towards the OCS–DC with a direction of 30° north from east. Since the polarity of the DC current within each SRWEC is unknown, both possible polarity configurations were assessed. With reference to Figure D-3, the DC magnetic field was evaluated within the darker shaded region, which encloses the volume approximately within 3.3 ft (1 m) of the J-tubes surrounding the two SRWEC. The maximum volume average DC magnetic field in the water column of the OCS–DC was 4,333 mG. At this field, the corresponding induced volume averaged electric field due to the movement of seawater (2 ft/s [0.6 m/s]) is 0.26 mV/m.
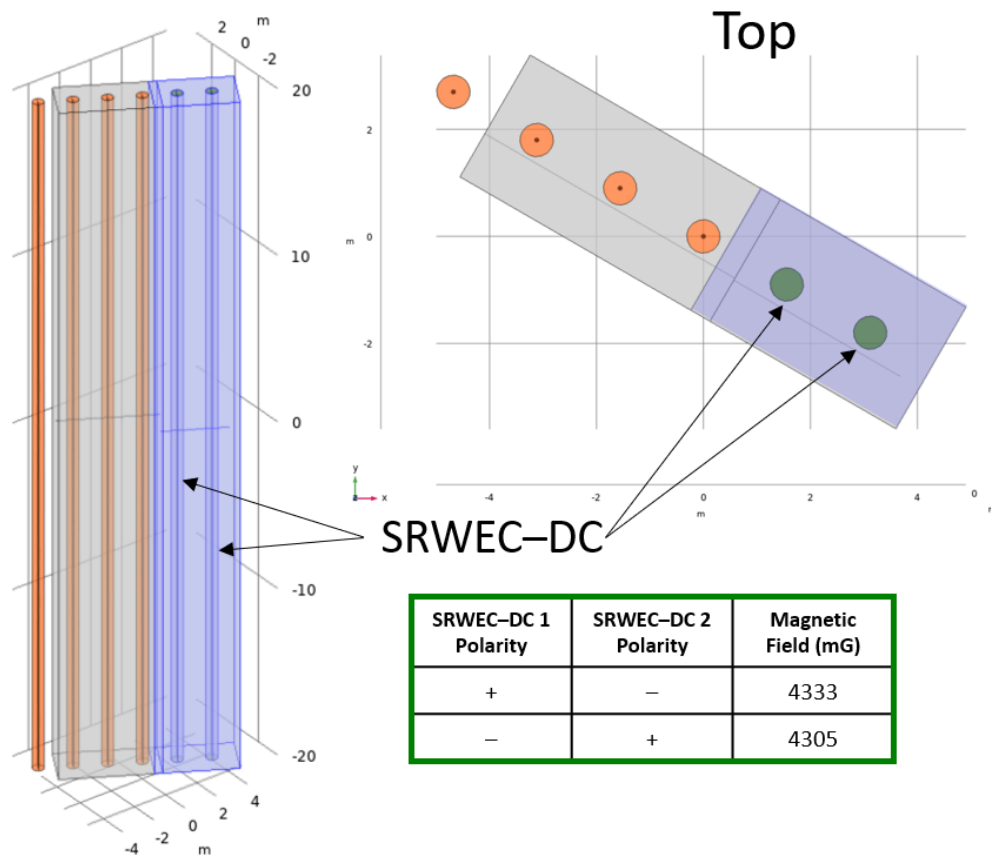

SRWEC–DC 1 Polarity	SRWEC–DC 2 Polarity	Magnetic Field (mG)
+	−	4333
−	+	4305

Figure D-3.   Volume average DC magnetic-field levels at the OCS–DC jacket foundation. The representative volume encompasses both SRWEC.[32]

The AC magnetic and electric fields in the water column around the OCS–DC, generated by the IACs, were also assessed as volume averages within a region representative of where marine life may be exposed to the fields from the cables. With reference to Figure D-4, below, the AC magnetic field was evaluated within the darker shaded region, which encloses the volume approximately within 3.3 ft (1 m) of the J-tubes surrounding three of the IAC. The calculated volume average results would not be impacted by including the fourth IAC shown in the figure.
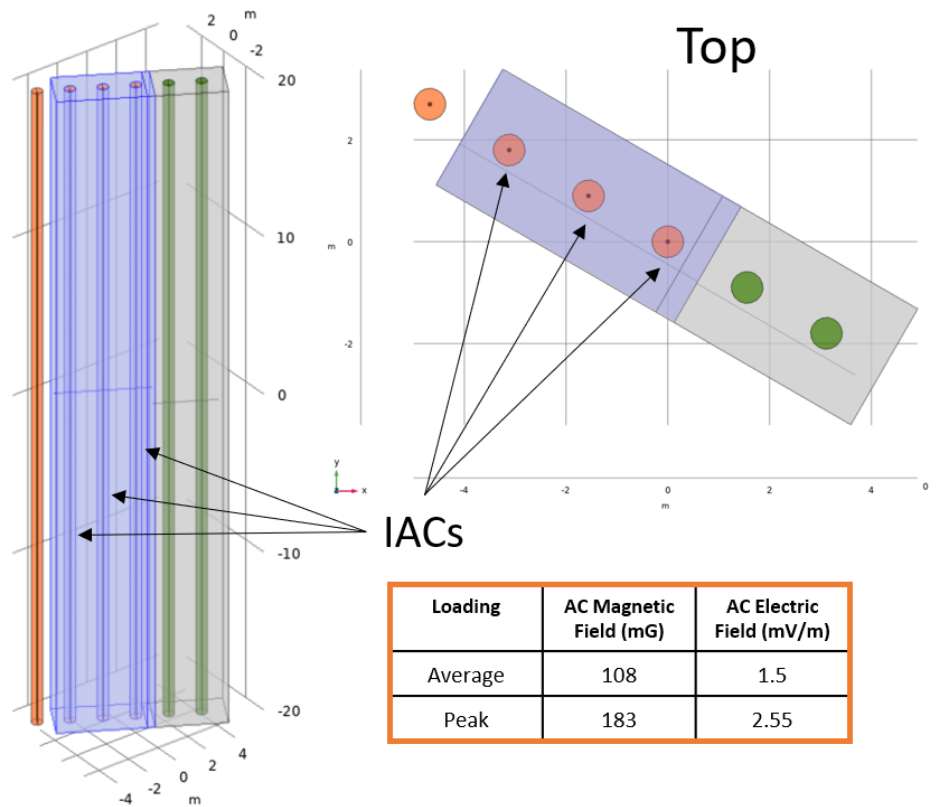
Loading	AC Magnetic Field (mG)	AC Electric Field (mV/m)
Average	108	1.5
Peak	183	2.55

Figure D-4.   Volume average AC magnetic- and induced-electric field levels in the water column at the OCS–DC jacket foundation. The representative volume encompasses three IAC.[33]

WTG Monopile Configuration

The AC magnetic and electric fields around the WTG monopile structure were assessed as volume averages within regions representative of various marine habitats. With reference to Figure D-5, below, the regions extending vertically from the top of the scour protection to a height 1.6-ft (0.5-m) above the CPS of the IACs are shown in purple, and represent marine life swimming or crawling on top of the scour protection layer; the regions representative of life that shelters beneath the artificial skirt/canopy created between the IACs and the monopile are shown in orange. The volume-averaged magnetic-field and induced electric-field level around the WTG monopiles are summarized in Table D-2.

Table D-2.   Calculated volume-averaged AC magnetic fields (mG) and electric fields (mV/m) around the WTG monopile foundation

Volume of Water	Average Loading		Peak Loading	
	AC Magnetic-Field (mG)	AC Electric Field (mV/m)	AC Magnetic-Field (mG)	AC Electric Field (mV/m)
IAC – Above scour protection	~31	~0.3	~52	~0.6
IAC – Skirt to 3.3 ft (1 m) above cables	~48	~0.5	~81	~0.9

Loading	AC Magnetic Field (mG)	AC Electric field (mV/m)
Average	31	0.3
Peak	52	0.6

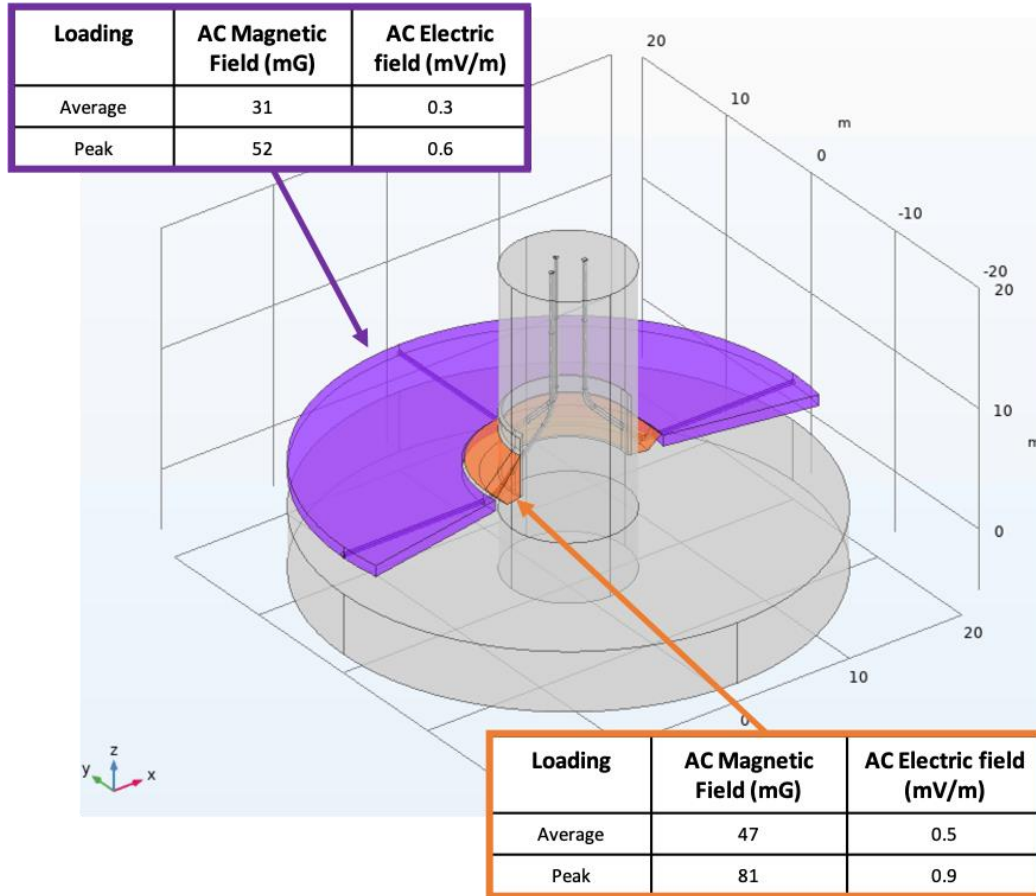| Loading	AC Magnetic Field (mG)	AC Electric field (mV/m)
Average	47	0.5
Peak	81	0.9

Figure D-5.   Volume average AC magnetic- and induced-electric field levels at the WTG monopile foundation. [33]